NISTIR 6041

Gasification of Silicone Fluids Under External Thermal Radiation

Philip J. Austin, Robert R. Buch and Takashi Kashiwagi

United States Department of Commerce
Technology Administration
National Institute of Standards and Technology

NISTIR 6041

Gasification of Silicone Fluids Under External Thermal Radiation

Philip J. Austin, Robert R. Buch and Takashi Kashiwagi

July 1997
Building and Fire Research Laboratory
National Institute of Standards and Technology
Gaithersburg, MD 20899

U.S. Department of Commerce
William M. Daley, *Secretary*
Technology Administration
Gary R. Bachula, *Acting Under Secretary for Technology*
National Institute of Standards and Technology
Robert E. Hebner, *Acting Director*

TABLE OF CONTENTS

Gasification of Silicone Fluids Under External Thermal Radiation

Philip J. Austin, Robert R. Buch[1], and Takashi Kashiwagi

Building and Fire Research Laboratory, National Institute of Standards and Technology, Gaithersburg, MD 20899

ABSTRACT

Transient gasification rate and fluid temperatures were measured for polydimethylsiloxanes having fluid viscosity from 0.65 cS to 60,000 cS in a nitrogen atmosphere at external radiant fluxes from 20 kW/m^2 to 70 kW/m^2. Trapped volatile products and fluid residues collected at different gasification stages were analyzed to determine their chemical structure using various analytical methods. Detailed energy balance of fluid samples was conducted to determine global heat of vaporization including absorption of incident radiation by the volatile products, reradiation loss from heated fluids and heat loss to the substrate. The measured average gasification rate of all siloxanes studied in this work increases linearly with an increase in external radiant flux. The global heat of vaporization per unit mass of siloxane increases with an increase in the molecular weight of the siloxanes up to a 50 cS fluid and its value remains constant at about 1,200 J/g for all higher molecular weight dimethylsiloxanes. The gasification of siloxanes occurs via two modes or regimes or combinations thereof: 1) volatilization of molecular species native to the polymer, and 2) volatilization of cyclic molecules which result from the thermally induced degradation of the polymer via siloxane bond rearrangement. The former process dominates for low molecular weight siloxanes (< 10 cS) and the latter process dominates for high molecular weight siloxanes (> 1,000 cS). For the intermediate molecular weight siloxanes, both volatilization and degradation processes occur.

1. INTRODUCTION

Silicones encompass a wide variety of novel materials, e.g. fluids, foams, sealants, resins and elastomers. Currently, these silicon-based materials are utilized in virtually every major industry sector ranging from cosmetics to electronics to defense/aerospace to automotive. New potential applications include their use as precision cleaning solvents, fire resistant communication cable components, fire retardant additives for thermoplastics, and other fire-related applications. Most commonly used silicone is a series of trimethylsiloxy end-blocked polydimethylsiloxane (PDMS), $[(CH_3)_3Si\text{-}O[\text{-}Si(CH_3)_2\text{-}O]_n\text{-}Si(CH_3)_3]$, where n indicates *average* degree of polymerization, i.e. the number of siloxane monomer units in the molecule. Incorporation of appropriate functional backbone substituents or end-groups provides a variety of cure chemistries for formulating a broad range of product forms (coatings, gels, foams, sealants, rubbers). Since

[1] Research associate from Dow Corning Corporation, Auburn Michigan 48611.

all commercially available oligomer/homopolymer silicones from the shortest chain length to the long chain polymers are fluids (due to the exceptional flexibility of the Si-O-Si bond), these fluids/polymers are typically referred to by their viscosity in centistoke [cS][2], which is directly related to n. In addition to their unique surface, physical, and chemical properties, several current applications of these materials, e.g. dielectric coolants, firestop foams, rely to a large extent on the unique fire properties of silicones.

The observed combustion of long-chain PDMS shows a low heat release rate and the unique characteristic that the heat release rate does not increase significantly with an increase in external applied thermal radiant flux [1] or pool size [2-4] . This is in sharp contrast to most hydrocarbon materials whose heat release rates increase substantially with an increase in external thermal radiant flux [1]. The burning rates of large pool fires of PDMS are much lower than hydrocarbons. One of the causes of the lower burning rate is attributed to the accumulation of the silica ash layer at the silicone fuel surface [2,3]. This accumulation of amorphous silica ash at the surface results from the deposition of silica particles, one of the major combustion products of silicone oligomers (cyclic and or linear structures) in the gas phase. Early studies by Lipowitz, et.al. resulted in a proposed model for the combustion of these materials [6,7]. Insight into the burning behavior of polydimethylsiloxane (PDMS) is evident from the complete combustion stoichiometry:

$$(CH_3)_3Si\text{-}O[\text{-}Si(CH_3)_2\text{-}O]_n\text{-}Si(CH_3)_3 + (12+4n)O_2 \rightarrow$$

$$(2+n)SiO_2 + (6+2n)CO_2 + (9+3n)H_2O$$

$$\Delta H_{comb}(\text{Gross}) = 26.5 \text{ MJ/kg}$$

$$\Delta H_{comb}(\text{Net}) = 24.8 \text{ MJ/kg}$$

where, for example, the combustion of 1 mole of MD_1M leads to the formation of 3 moles of SiO_2, an amorphous, white particulate ash. The deposition rate of silica on to the fuel surface increases with an increase in PDMS chain-length [1,5] for low viscosity fluids and reaches a limiting rate at fluid viscosities of approximately 50 cS. In contrast to longer chain silicones, the burning rate of short-chain cyclic and linear oligomers increases significantly with an increase in external thermal radiant flux and no significant accumulation of silica ash layer is observed for these materials [1, 5]. Removal of the particulate silica results from the fire plume buoyancy, i.e., high mass vaporization rate of the fuel and strong convective combustion product flow rates.

Cyclic siloxanes assume an exceptionally prominent role within the silicone industry. These compounds are both end-products and key intermediates used for the manufacture of most commercial silicones. A review of the chemistry of these materials is given in [8]. Cyclic

---

[2] cS is used as a part of silicone designation in silicone industry

silicone oligomers [D_n], i.e. "cyclics", are the major products formed as a result of thermal degradation of silicones. Many studies have documented the dominant role of cyclics as the key rearrangement products resulting from thermally induced degradation of silicones [9,10,11]. The dominant cyclic is typically D_3 although a wide spectrum of molecular weights has been observed and documented.

The fire behavior (ease of ignition, heat release rate) of a material results from the dominant gasification processes which occur as a result of the thermal energy imposed on the material. An understanding of the gasification process, i.e. the dominant mechanisms, characteristic energies, and ensuing volatile products, is relevant and perhaps essential for modeling systems in which these materials are used. For short chain-length PDMS fluids, it is expected that vaporization will be the dominant gasification process because of their low boiling temperatures (high vapor pressure) and comparatively low heats of vaporization. Intermediate viscosity PDMS fluids consist of a broad distribution of different chain-length components: short chain-length species will vaporize while longer chain-length components may thermally decompose resulting in the formation of cyclic oligomers. Gasification of high viscosity fluids perhaps occurs almost exclusively via thermal degradation to volatile cyclic oligomers. Thus, the gasification process of PDMS fluids under fire conditions might involve several gasification mechanisms. The global heat of gasification of PDMS might depend strongly on the composition of the fluid, i.e. the distribution of structures and their respective molecular sizes or chain-lengths. Furthermore for silicones, the transport of radiant thermal energy to the material perhaps is mediated by the accumulation of the silica ash layer on the sample surface.

It is of interest to understand the gasification process of PDMS for a wide range of chain lengths and compositions under external thermal radiant fluxes relevant to fire. Limited data are available on the global heat of gasification of PDMS. Two previous studies measured the gasification rate of 50 cS PDMS in nitrogen or reduced oxygen (volume fraction of 7%) atmospheres under various external radiant fluxes[2,4]. A small increase in the gasification rate with an increase in external radiant flux was observed from 26 kW/m^2 up to 56 kW/m^2 in volume fraction of 7 % oxygen atmosphere [2] and up to 37 kW/m^2 in nitrogen [4]. Above these fluxes, the rate of increase of the gasification rate increased substantially. It was speculated that there were two regimes of gasification, perhaps the result of different thermal decomposition mechanisms and rates. Subsequent to these earliest studies, Steciak and Tewarson [12] measured a range of key fire parameters for both organic and silicone dielectric coolant fluids and several resin compounds. A unique apparatus and novel approach was developed in an attempt to eliminate the influence of the silica ash layer on the gasification behavior of the silicone fluid. The "dual regime" gasification behavior of silicone fluid was observed and heats of gasification were reported for the respective regimes (1.8kJ/g and 3.9 kJ/g).

To understand the gasification processes of PDMS under conditions similar to those experienced in fires, in the current study a wide range of PDMS fluids (0.65 cS to 60,000 cS) were exposed to various external radiant fluxes, up to 70 kW/m^2 in a nitrogen atmosphere. Gasification rates and

fluid temperatures were measured. Since oxygen cannot reach the gasifying fluid surface in a pool burning configuration due to highly efficient oxygen-consuming gas phase oxidation reactions, a nitrogen atmosphere was used to avoid any oxidative degradation. Evolved gaseous products and fluids residues were collected at different times during the experiments and their chemical compositions were measured to determine the extent of thermal degradation of the fluids. A knowledge of their formation and composition is of considerable relevance to modeling of ignition, flame spread, and general burning behavior of methylated siloxanes. Therefore, the identification and quantitation of the specific molecular species resulting from the pyrolysis of these polymers was also addressed in this investigation. Volatile products analyses were previously conducted by grab sampling inside of a small D_4 flame and also by pyrolysis of a 1000 cS PDMS in a helium atmosphere using a heated platinum ribbon [6]. The effect of a sample-container material on gasification rate and the extent of absorption of the external radiation by the evolved gaseous products above the sample surface during gasification were quantified and their effects on understanding of the gasification process of PDMS will be discussed.

2. EXPERIMENTAL APPARATUS

2.1 Materials

The fluids, oligomers and polymers, used in this investigation were commercial-grade materials supplied by Dow Corning Corporation. PDMS fluids/polymers are typically referred to by their viscosity which increases with the average chain length as shown in Table 1. A convenient shorthand notation for PDMS molecules is: MD_nM where $M=(CH_3)_3SiO_{1/2}$, $D=(CH_3)_2SiO_{2/2}$, and n is the chain length for pure oligomeric cyclics or linears and is the average chain length for polydisperse polymers. Other structural siloxane units are represented by: $T=(CH_3)SiO_{3/2}$, and $Q=SiO_{4/2}$. The fluids studied were octamethylcyclotetrasiloxane, $[(CH_3)_2SiO]_4$, and a series of trimethylsiloxy end-blocked polydimethylsiloxane (PDMS) fluids, $[(CH_3)_3Si\text{-}O[\text{-}Si(CH_3)_2\text{-}O]_n\text{-}Si(CH_3)_3]$, where n indicates the average chain length, i.e., the number of siloxane units in the molecule. A "monodisperse model" fluid was synthesized using a specific monomer, catalyst and polymerization conditions to ensure a narrow distribution polymer and to minimize formation of oligomeric cyclics and linears. Solvents were purchased from Aldrich Chemical Company and used as received[3].

2.2 Gasification Apparatus

For these experiments, a radiant gasification apparatus, somewhat similar in design to a Cone

---

[3] Certain trade names and company products are mentioned in the text or identified in an illustration in order to specify adequately the experimental procedure and equipment used. In no case does such identification imply recommendation or endorsement by NIST, nor does it imply that the products are necessarily the best available for the purpose.

Calorimeter, was constructed. The "gasification apparatus," as it is called, is designed to allow exposure of a solid or liquid sample to a uniform heat flux in a non-oxidizing or partially oxidizing atmosphere. As with a Cone Calorimeter, samples to be studied are placed underneath a cone-shaped heater and are then exposed to a controlled, uniform radiant heat flux when a shutter is removed. The primary difference between the gasification apparatus and a typical cone calorimeter is that, in the gasification apparatus, the radiant exposure of the sample occurs in a sealed cylindrical chamber which is continuously purged with a controlled gas mixture typically nitrogen, rather than in the open air. As a result, the gasification apparatus was designed for studying the gasification processes of polymeric samples by measuring mass loss rate and temperatures of the sample rather than for calorimetry.

A drawing of the gasification apparatus is provided in Figure 1. The apparatus consists of a stainless-steel cylindrical chamber that is 1.70 m tall and 0.61 m in diameter. In order to maintain a negligible background heat flux, the interior walls of the chamber are painted black and the chamber walls are water-cooled to 25 °C. Purge gases are introduced into the chamber via an annulus at the bottom of the chamber. This annulus, which contains a layer of glass beads, was designed to ensure flow uniformity. Purge gases, in addition to any gases produced by the sample, are vented through the top of the chamber through an exhaust duct. The bottom of the chamber is sealed with a removable base plate which is used to introduce the sample into the chamber.

A 30 cm diameter cone-shaped heater is suspended in the middle of the chamber, facing downwards. This heater, which contains three coiled elements, is considerably larger than that used in a typical cone-calorimeter which has a single coiled element. Its design allows for a more uniform planar heat flux distribution over a wide range of distances from the heater. The sample is held in place underneath the center of the heater using a block of Foamglas® insulation on which the sample, or a dish containing the sample (for liquids), is placed. This block of insulation, rests on a thin aluminum plate which is supported by a thin walled aluminum cylinder. The cylinder, in turn, is connected to the weighing mechanism of the load cell, which is anchored to the removable base plate. With this sample holder and heater configuration, the incident flux to which the sample is exposed is controlled by keeping the heating coil temperature fixed at an average temperature of 750 °C while adjusting the distance between the sample and the heater. This is accomplished by varying the length of the aluminum support cylinder. This is one way in which the gasification apparatus differs from a cone calorimeter, because, in a typical cone calorimeter, the flux is varied by changing the temperature of the heating coil. The advantage to the gasification apparatus design is that because the coil temperature is constant, the incident flux has the same spectral distribution at all flux levels. In addition, the cone design provides excellent flux uniformity over a typical 10 cm diameter sample. Heat flux measurements made using a 16 mm diameter Gardon-type gauge showed that the minimum flux at the edge of a 10 cm diameter circle was within 91% of the centerline flux for the full range of incident flux exposures (20 kW/m^2 - 70 kW/m^2).

The gasification apparatus is equipped with a retractable water-cooled shutter, which can be inserted between the heater and the sample in order to shield the sample from the heater flux. This shutter is held in place prior to each test, and then retracted to begin the test. The shutter may be closed at

any time during a test to interrupt the gasification process in order to preserve the exposed sample for further chemical analysis.

The chamber's base plate is connected to a hydraulic lifting mechanism which allows it to be lowered from the bottom of the chamber. The lifting mechanism and base plate are connected to a moveable cart which can be pulled out from underneath the chamber. This allows convenient access to the sample and any associated instrumentation when they are outside of the chamber. For this reason, the gasification apparatus is designed such that all data collection associated with the sample, with the exception of visual observations, is done by way of the base plate.

A terminal strip that allows fine-wire thermocouples from the sample to be connected to the data acquisition system rests on an aluminum bridge underneath the sample holder. The bridge, which is supported by two posts that are connected to the base plate, is adjustable to accommodate different sample heights. The bridge is designed such that the support post for the sample holder passes through the bridge without touching it. This configuration allows a minimum of influence by the sample thermocouples on the mass loss measurements.

Two optical ports on the sides of the chamber, just beneath the level of the heater, allow observation of the sample during testing. In addition, a periscope-like system of mirrors is used at one of the optical ports to allow viewing of the sample's top surface during gasification.

2.3 Sample Holder

A drawing of the sample holder is provided in Figure 2. The drawing shows the main components of the sample holder: the sample dish, the insulation block on which it rests, and the support structure which connects the sample holder to the load cell. The insulation block on which the sample dish rests was composed of Foamglas®, a closed-cell glass insulation. Foamglas® was chosen because of its beneficial thermal properties: low thermal mass and low thermal conductivity and its closed-cell nature minimizing the accumulation of moisture and attendant uncertainty in the in the mass-loss measurement. In addition, Foamglas® insulation is a friable material, similar to low density lava rock, which, although fragile, is easily machined. Using this material allows the sample holder to be uniquely designed for the specific type of sample being tested. For the tests of this study, a Foamglas® sample holder that was 13 cm in diameter and 5 cm thick was used. The PDMS fluids were contained in a dish that rested in a 10 cm diameter, 1.5 cm deep cavity in the top surface of the Foamglas®. This cavity was designed to tightly accommodate the dish. The bottom of this cavity was instrumented with a single 0.076 mm diameter type K thermocouple in order to measure the temperature beneath the dish.

Several different dishes, each having unique characteristics, were used to hold the fluids in this study. Preliminary tests were conducted using specially-made lightweight borosilicate glass dishes. Borosilicate glass was chosen because it could be fashioned to support thermocouples inside the fluid containing region of the dish. In addition, borosilicate glass is essentially a non-reactive material with beneficial thermal properties: high melting temperature, low thermal conductivity, and

modest thermal mass. Trace alkali (sodium) on the glass surface was a concern insofar as providing a rearrangement catalyst; however, the dish surface was demonstrated to be chemically passive after two gasification experiments. The height and diameter of these dishes were similar to commercially made petri dishes, 25 mm and 100 mm respectively; however, the wall thickness of these dishes (0.5 mm - 0.7mm) was about one-quarter of that found in commercial dishes. As a result, these dishes had considerably less thermal mass than a sample mass (typically about 100 g), and therefore had negligible influence on the test results.

The first of these glass dishes served as a prototype. It was designed to assess the concept of using a borosilicate glass dish instrumented with thermocouples, to allow simultaneous temperature and mass loss measurements to be made during the gasification process. This dish, which had a mass of 17 g., was instrumented with a single 0.076 mm diameter alumel-chromel thermocouple in the center of the dish at a height of 7 mm to 9 mm above the dish's bottom. In addition, this dish was used for preliminary tests to assess the general gasification behavior of PDMS fluids.

Tests conducted using the first borosilicate glass dish demonstrated that the technique of suspending a thermocouple in the dish effectively allowed measurement of the fluid temperature. From these tests it was established that the mass loss rate and temperature data were quite repeatable for the same experimental conditions. Initial tests comparing the behavior of a wide range of PDMS fluids (0.65 cS to 60,000 cS) at a single, intermediate flux of 40 kW/m^2 revealed significant basic differences in the gasification behavior of the various fluids. These observed differences, which will be discussed later in the report, resulted in the classification or grouping of the fluids by their related behaviors, i.e. gasification mechanisms. In addition, many of the problems associated with these types of measurements were also discovered during these preliminary tests. These are discussed in the "Experimental Sensitivities" section of this report. The knowledge gained from these tests was used in modifying the experimental equipment and method to correct for these problems.

The success of the first dish prompted the development of a second, more sophisticated dish. This dish, which had a mass of 12 g., was instrumented with four thermocouples at heights of 3 mm, 7 mm, 14 mm, and 20 mm above the dish's bottom. This dish was used to measure the transient temperature profile of the 1.5 cS, 5 cS, and 50 cS fluids for a range of fluxes between 30 kW/m^2 and 60 kW/m^2.

Because these borosilicate glass dishes were so fragile and extremely difficult to fashion due to their very thin walls, the majority of the tests, conducted to measure the mass loss rate of the fluids, were conducted in a more durable stainless steel dish. Like the borosilicate glass dishes, the stainless steel dish was designed to minimize its thermal influence on the fluid being tested. The use of 0.051mm thick shim sheet stock for fabrication allowed this dish to have a mass of 7 g, about 3/5 that of the second borosilicate glass dish. Although the use of stainless steel precluded in-situ fluid temperature measurement due to its electric conductive nature which causes shortage of the output of thermocouples installed through the container wall, it did provide the beneficial properties of non-reactivity and low thermal mass. While stainless steel has a higher thermal conductivity than borosilicate glass, it is believed that this higher thermal conductivity did not result in a significant

increase in the heat loss from the fluid due to its extremely thin wall.

2.4 Sampling/Trapping of Volatiles

The gasification apparatus was modified to provide a means for sampling the gaseous species immediately above the surface of the fluid. The sampling system consisted of a 3 mm I.D. copper tube which could be swung into position over the center of the sample dish. The tube was connected to a cold trap immersed in a low temperature bath (dewar filled with dry ice/isopropanol) which was connected to a vacuum pump. The cold trap was filled about midway with 3 mm. glass beads to enhance trapping efficiency of the volatiles. A sketch of the gas sampling assembly is given in Figure 3. The condensed volatiles were removed by adding solvent (o-xylene or pentane) to the cold trap and allowing the glass beads/volatiles /solvent to warm to room temperature prior to their removal from the trap system. A small quantity of dodecane was added to the rinse solvent to provide an appropriate internal standard necessary for quantifying molecular species identified via gas liquid chromatography.

3. EXPERIMENTAL METHOD

3.1 Experimental Procedure

Prior to testing a fluid sample at a given heat flux, the appropriate height of the sample, corresponding to the desired flux, is determined. This is accomplished using a 16 mm diameter, water cooled, Gardon-type heat flux gauge that is connected to an adjustable height stand. The stand is placed on a positioning plate, which is connected to the gasification chamber's removable base plate. The positioning plate allows the gauge to be centered underneath the cone heater. Data from previous heat flux measurements are then used to set the height of the gauge to the level for the desired flux. The heat flux is then verified, and adjustments in the height of the heat flux gauge are made until the appropriate height, corresponding to the desired flux, is found. Once the appropriate height of the sample has been determined, a sample holder post is chosen such that the initial location of the upper sample surface is at the level of the desired flux.

Testing of a fluid sample begins with the preparation of the sample. The sample holder, the aluminum plate on which it rests, and the support post are assembled and connected to the load cell. The sample dish, which has been cleaned with toluene and then thoroughly dried, is then placed in the sample holder. Thermocouples from the sample holder and sample dish are then connected to the terminal strip such that there is no significant tension in the thermocouple wires. The load cell is then zeroed and 100 g of fluid are added to the dish. For fast evaporating fluids, extra fluid was added such that 100 g of fluid would be in the dish at the time the sample was exposed to the heat flux. Typically, these 100 g samples were about 16 mm thick; however, this thickness varied somewhat among the fluids tested due to their different densities.

After the sample is prepared, the sample cart is rolled carefully underneath the gasification chamber, and a hydraulic lifting mechanism is actuated to hoist the base plate into position. The base plate,

which is fitted with an o-ring seal, is then clamped to the bottom of the chamber. At this time, the shutter is covering the heater, protecting the sample. The chamber is then purged with nitrogen at a rate of either 12 l/s (1500 SCFH) or 23 l/s (3000 SCFH) depending on the expected mass loss rate of the fluid sample. For the low viscosity fluids (0.65 cS to 5 cS) a purge rate of 23 l/s (3000 SCFH) was necessary to prevent excessive accumulation of fluid vapor inside the gasification chamber. For the higher viscosity fluids (50 cs. and higher) the 23 l/s (3000 SCFH) purge rate was only necessary when the heat flux level was greater than 40 kW/m^2. After the chamber has been purged for several minutes, the gas composition is then sampled at a location near the fluid sample until the appropriate oxygen levels are reached.

After the oxygen concentration in the chamber has fallen below 0.1%, and the temperature of the nitrogen gas flowing into the chamber has stabilized at 25 °C +/- 0.5 °C, the test is initiated. The data acquisition system automatically actuates (withdraws) the shutter after 100 s have elapsed. Mass loss and temperature data are automatically collected while observations of the sample are made either manually or with the aid of a video camera. The test is terminated manually by actuating (inserting) the shutter to cover the sample. Although this is typically done after the sample has been completely gasified, occasionally tests were terminated at various stages of gasification to allow collection and analysis of the residual fluid samples. For these tests, after the shutter was actuated to cover the sample, the sample was allowed to cool to less than 90 °C before it was exposed to air.

3.2 Analytical Methods-Chromatography(GC,GPC)/Mass Spectroscopy

Extraction Method - The analysis of polymers and residual polymer samples for cyclics and linears contents relied on an "acetone extraction technique". 1 gram of the fluid/polymer was added to a 0.015 *l* vial containing ~0.02 g of internal standard solution (10 g of hexane and 0.01 g of n-dodecane) and ~3 g of acetone (Optima Grade). The vial is vigorously shaken for 5 minutes and then centrifuged so as to produce a clear solvent layer for sampling and analysis. The solvent/extract is analyzed via gas-liquid chromatography, GLC. Typically, 1.0 µl is injected. The chromatograph was equipped with fused silica (30 m x 0.25 mm) columns coated with DB-1HT (0.1 µm film thickness) and a flame ionization detection (FID) system. A typical chromatogram illustrating the various species identified and quantified via this technique is given in Figure 4. This method is limited to those cyclic and linear species which elute from the columns, i.e. less than 21 siloxane units. Note that specific identification and quantitation of cyclic and linear oligomers is readily accomplished.

Internal Standard Method - The analysis of condensible products for specific molecular species identification and quantitation also relied on GLC. Typically, 1.0 µl of the solvent (pentane or o-xylene with internal standard) used to rinse/solvate the condensibles in the cold trap was injected onto the GLC columns. A typical GLC chromatogram is given in Figure 5. It is important to note when viewing GLC chromatograms that "peak areas" provide a more reliable representation of the concentration of each species rather than "peak heights." This is especially important for higher molecular weight eluents; so, although a chromatogram at first glance appears to indicate a reduced

concentration of higher molecular weight species, a careful look at the area of the peak may show that this is not necessarily the case. The flame ionization detector, FID, response was demonstrated to be constant for all species which elute and demonstrated no structural (cyclic vs linear) dependence.

Ethylorthosilicate, EOS, Derivatization - A novel base-catalyzed digestion/derivatization technique was used to assay residual fluids/polymers for end-block and monomethyl substituted siloxane units which presumably result from methyl cleavage during pyrolysis. A large excess of tetraethoxysilane is equilibrated with an organosilicon compound (polymer or residual fluid) in the presence of a base catalyst to yield corresponding organoethoxy derivatives. That is,

$$\text{Polymer} + Si(OC_2H_5)_4 \xrightarrow[\{(\text{Excess})\text{Ethanol},120\ C,1\ \text{Hour}\}]{\text{NaOH or KOH}} X\,(CH_3)_3Si(OC_2H_5) + Y\,CH_3Si(OC_2H_5)_3 + Z\,(CH_3)_2Si(OC_2H_5)_2$$

The resultant solution is analyzed by gas chromatography to yield the levels of the silicon substituents, i.e., the ethoxylated species provide a measure of the M-, T-, and D- sub-units comprising the polymer. An internal standard is used. In this investigation, assays of M- and T- were particularly useful and informative to provide insight into the gasification mechanisms (volatilization or degradation/volatilization) and extent of methyl loss via methyl cleavage during pyrolysis.

Gel Permeation Chromatography (GPC) - Gel permeation chromatography was performed on a Waters system (510 reciprocating pump, 410 differential refractometer, WISP 712 auto-sampler). Toluene was the mobile phase. 3 PL-gel columns (5 um) manufactured by Polymer Laboratories were used to affect separation. Calibration was based on narrow distribution polydimethylsiloxane standards ranging in molecular weight from 1330 g/mol to 852,000 g/mol. Polymers/residual fluids were diluted in HPLC-grade toluene prior to injection; solvated samples from the cold traps (pentane or o-xylene) were injected directly. The latter samples provided an analysis of those samples which did not elute quantitatively from the GC columns. Typical GPC chromatograms and the various ranges of molecular weight species of interest in this investigation are given in Figure 6: high molecular weight polymer (elution time (ET)<15 min), intermediate molecular weight polymer (15 min<ET< 17.5 min), and oligomeric cyclics (17.5 min<ET<19.5 min). Note that the internal standard (dodecane) co-elutes with D_3 (ET=19.1 min) and peaks associated with xylenes(s) are observed but do not interfere since their elution times are displaced from the siloxanes of interest.

GPC analysis complemented the GC procedure providing identification and approximate quantitation of short chain oligomers (ET=17.5 min to 19.5 min) as well as intermediate (ET=15.0 to 17.5 min) and high (ET<15 min) molecular weight materials. Recall that the condensed volatiles in the cold traps were removed via the addition of a suitable solvent such as o-xylene or pentane. A small quantity of dodecane was added to these solvents to provide an internal standard for quantitation of the GC data. Note that in the GPC analysis, the dodecane overlaps with the D_3 and to quantify the oligomeric component of the volatiles, the contribution of the docecane must be eliminated. Utilizing GC analysis, the GPC data were corrected for the "dodecane/D_3 overlap."

Mass Spectroscopy - The mass spectral analytical approach utilized in this study involved direct analysis of pentane solutions containing unknown PDMS species by electrospray mass spectrometry [13]. A 90/10 solution of pentane and isopropanol containing 5 mM ammonium acetate was prepared and delivered to the electrospray ion source at a constant flow rate of 15 microliters/min using a Harvard Apparatus Model 22 syringe pump. Cationized PDMS species were admitted to a Perkin-Elmer API 300 triple quadrupole mass spectrometer and mass analyzed. Abundant ammoniated pusedomolecular ions, {M+NH4}+ with no fragmentation were observed in the mass spectrum, thereby providing a direct measure of the molecular weights of the unknown silicone species. To discern the chemical structure of these unknown PDMS species, MS-MS collisional activation at a collision energy of 25 eV using N2 collision gas was performed on selected {M+NH4}+ions to confirm the polymer end-group and repeat groups.

4. RESULTS AND DISCUSSION

Observations were made for more than 100 fluid samples exposed to fluxes ranging from 20 kW/m^2 to 70 kW/m^2 in a nitrogen environment. Using the stainless steel dish, mass loss rate measurements were conducted for 0.65 cS, 1.0 cS, 1.5 cS, 5 cS, 50 cS, 1,000 cS, 10,000 cS, and 60,000 cS PDMS-200 fluids. Simultaneous measurements of the mass loss rate and temperature profile were made using the second borosilicate glass dish for 1.5 cS, 5 cS, and 50 cS fluids at fluxes ranging from 30 kW/m^2 to 60 kW/m^2. Additional observations were made using the first prototype Borosilicate glass dish. The data record for each test consists of the mass and temperature(s) of the sample as a function of time.

Additional data were obtained from analysis of fluid residues and evolved vapors. To evaluate the gasification/volatiles sampling/analysis protocol, 50 cS fluid was subjected to an applied heat flux of 40 kW/m^2, i.e., "gasified". In two successive experiments, volatiles were sampled and collected during two identical pyrolysis intervals (Δm= 95 to 90 g. and 50 to 45 g.) in the gasification process. GPC chromatograms of the original fluid, residual fluid, and the collected volatiles for the two respective experiments are given in Figure 7. These data suggest that the gasification/sampling/analysis protocol is repeatable. Gas chromatographic analyses of the collected volatiles for the two experiments are given in Figure 8. These data suggest that the volatiles sampling/trapping is reliable since the distribution of species is virtually identical for the successive experiments. The original and residual fluids were assayed for terminal end-group content and these data along with relevant GPC data are summarized in Table 2 (Series I). Excellent repeatability is noted for the gasification method, the volatiles sampling and trapping method, and the various analytical protocols utilized (GPC, GC, end-group analysis).

4.1 General Observations

One of the unique characteristics associated with the combustion of PDMS fluids is the formation of silica ash [1,7]. Although some of this ash is transported away from the fluid, a large amount of the silica dust settles back onto the fluid surface, creating an insulating layer of ash. Although it was

believed that the formation of this silica ash was due to combustion of the fluid, one of the goals of this study was to address the possibility that silica could be formed during pyrolysis in the absence of oxygen. In addition, it has been observed that a gelatinous layer forms on the surface of some PDMS fluids during combustion [1]. This layer aids in the suspension of the silica ash that settles on the fluid surface, thus enhancing the insulating effect of the silica char layer. Although it is believed that the layer forms due to a cross-linking reaction that occurs in the presence of oxygen, one of the goals of this study was to determine whether such a gelatinous layer forms in the absence of oxygen.

It was observed that silica does not form as a result of volatilization or pyrolysis. Silica was not observed during any test, nor was silica residue found at the conclusion of any test. From this information it can be concluded that the formation of silica during the combustion of PDMS fluids is a result of the combustion process itself.

Similarly, it was observed that a gelatinous layer does not form on the surface of PDMS fluids in the absence of oxygen. To further explore this effect, a few tests were conducted in a partially oxidizing environment. Tests conducted on 50 cS and 10,000 cS fluid at a heat flux of 60 kW/m^2 in 8 volume % oxygen showed the formation of a thin gel layer on the surface of the 10,000 cS fluid; however, no gel layer was observed for the 50 cS fluid. This behavior can be attributed to two possible causes; one is the relative exposure time of the two fluids to the oxygen in the purge gas and the other is the number of methyl cleavages to form crosslinks. Upon exposure to the heat flux, the 50 cS fluid initially gasifies more rapidly than the 10,000 cS fluid; therefore, while oxygen was able to react with the surface of the 10,000 cS fluid for a substantial amount of time, the rapid gasification of the 50 cS fluid quickly purged the region above the fluid and prevented the oxygen from reaching the fluid surface. The other potential cause is based on the concept that one crosslink is required per molecule to form a gel. Consequently, because of the substantial molecular weight difference (molecular size) between the two fluids, far more methyl cleavage would be required for the 50 cS fluid to form a gel layer at the surface.

4.2 Mass Loss Rate and Temperature Measurements

Throughout this study, distinct differences were observed in the gasification behavior of the various fluids. Based on these observations, fluids can be grouped into three general separate categories according to similar properties and patterns of behavior: low viscosity fluids, intermediate viscosity fluids, and high viscosity fluids.

4.2.1 Low Viscosity Fluids

The low viscosity fluids consist of the 0.65 cS, 1.0 cS, 1.5 cS, 2.0 cS, and 5 cS PDMS-200 fluids. Also included in this category is D_4, a cyclic siloxane molecule. Although the 0.65 cS, 1.0 cS, and 1.5 cS fluids were used in the majority of tests, the 2.0 cS and D_4 were also studied on a limited basis. A description of the composition of these fluids along with relevant property data is provided in Table 1.

Due to their manufacturing process, all of these fluids (except for the 5 cS fluid) are essentially single component fluids containing more than 97% of a single siloxane oligomer. All of the fluids (up to 2 cS) have boiling points below 230 °C at one atmosphere of pressure. Because their boiling temperatures are well below temperatures required for pyrolysis (>375 °C), the gasification process for these fluids consisted solely of volatilization. Figure 9 shows the mass loss plot for a 0.65 cS fluid sample exposed to a heat flux of 70 kW/m2. This plot typifies what was observed for all of the low viscosity fluids for the range of heat fluxes studied. When the shutter is actuated to expose the fluid surface, the figure shows an initial transient period in which the mass loss rate rapidly increases. This initial transient period typically encompasses the loss of the first 5 to 10 g of fluid depending on the fluid and the heat flux. The initial transient is then followed by a long period during which a gradual increase in the mass loss rate occurs. When only about 30 g of fluid remain in the dish, a final transient period occurs in which the mass loss rate rapidly increases. This final surge in the mass loss rate, which was also observed for tests conducted with toluene and methanol, is believed to be the result of the dish's heated bottom surface enhancing the boiling process.

The gasification of these fluids by vaporization is also confirmed by the evolved gas analysis of 1.5 cS and 5 cS fluids. 1.5 cS fluid consists almost entirely of a single molecular species (MD_2M). Volatiles were sampled/collected during the mass loss interval of 30 to 15 g. GC analysis of the collected volatiles showed them to consist almost exclusively of MD_2M. Thus, gasification occurs only via volatilization of the original fluid species. No evidence for thermal degradation of the fluid was noted. That is, no new molecular species were observed within the background noise, which might arise from thermal induced rearrangement. 5 cS fluid contains a somewhat broader distribution of molecular species. Nearly all of the species in this fluid elute from a GC column. Volatiles were sampled and collected during mass loss intervals: 100 to 97 g, 55 to 50 g, and 15 to 10 g. The volatiles were analyzed via GC and GPC. The chromatographic data are given in Figures 10 [GPC] and 11 [GC]. These data clearly indicate that gasification results only from volatilization of the fluid. The volatilization is dictated by the vapor pressure of the respective species, i.e. not unlike a distillation process. In both the GPC and GC results, virtually no evidence of any cyclics is observed confirming that only volatilization is occurring during at least 90% of the fluid gasification.

The gasification behavior of these fluid samples is more easily studied when the mass loss rate data is plotted as a function of the normalized mass, where the normalized mass is defined as the remaining mass of fluid in the dish divided by the initial mass of fluid. Figure 12 shows such a plot for a 0.65 cS fluid sample exposed to different heat fluxes. The plot shows that at all fluxes, the majority of mass is lost in the period between the initial and final transients. This period, approximated as the steady-state domain, was used in calculating the average mass loss rate for these fluids. For consistency, the average mass loss rates were computed for the domain between the normalized mass values of 0.9 and 0.4. Using this domain allowed the average to be calculated over the steady-state range while omitting the transient periods from the calculation.

Throughout this paper, the reported average mass loss rates were calculated using the normalized

mass rather than time as a basis. The normalized mass was chosen as an averaging basis because it allows easy graphic comparison of the various experimental data, which had widely different time scales associated with them. Although this averaging method biases the average in favor of the higher mass loss rates, the difference between the normalized average and a traditional time based average was typically less than 10%. A larger difference between the averages occurred in those cases where the peak mass loss rate was substantially higher than the average mass loss rate. In most of these cases the tests involved an initial period of gasification in which the majority of mass was lost, followed by a long period of significantly lower mass loss rate.

During the gasification process, little bubbling of the fluid was observed until the final transient period, when the fluid rapidly volatilized. This absence of bubbling is consistent with the expectation that, because the fluids were heated rapidly, and because these fluids each have a unique boiling temperature (see Table 1), vaporization was occurring only near the surface of the fluid.

Although the gasification apparatus was designed to dilute and remove evolved products from the gasification chamber quickly, a vapor layer consistently formed above the fluid samples in these tests. The formation of this layer was due to both the high vaporization rates of the fluids and the fact that the molecular weight of the evolved PDMS molecules is substantially higher than that of the nitrogen. For the low viscosity fluids, the evolved vapors remained largely invisible due to the absence of vapor condensation in the exhaust gas; however, the vapor layer could be observed due to the strong optical distortion pattern it produced above the sample. This vapor layer, which extended several millimeters above the dish and billowed out over its edges, initially was assumed to have little effect on the gasification process. It eventually was discovered, however, that this vapor layer significantly influenced the heat transfer to the fluid surface. This effect will be discussed in greater detail in the "Vapor Absorption" section of this report.

Figure 13 shows a typical temperature distribution plot for a 1.5 cS sample exposed to a heat flux of 30 kW/m^2. The traces in the plot represent the temperature measured at different heights above the bottom of the dish as measured by 0.076 mm diameter alumel-chromel thermocouples. It should be noted that two of the thermocouples were not in contact with the fluid. The "Firebrick" thermocouple, which rested on the top surface of the Foamglas® sample holder, was pressed against the bottom surface of the borosilicate glass dish. The "20 mm from bottom" thermocouple was positioned above the surface of the fluid in order to provide a temperature measurement in the vapor layer.

For those thermocouples that were in contact with the fluid, as the surface of the fluid receded through the level of each thermocouple the temperature would decrease slightly, level off for a few seconds, and then increase once again. This occurs at a normalized mass of about 0.85 for the "14 mm from bottom" thermocouple, 0.4 for the "7 mm from bottom" thermocouple, and 0.15 for the "3 mm from bottom" thermocouple. One can observe from the plot that the fluid surface temperatures are consistent with the boiling point of the fluid. Similar results obtained at heat fluxes of 40 kW/m^2, 50 kW/m^2, and 57 kW/m^2 confirm that the gasification process for these fluids consists

of volatilization at the fluid surface. The initial overshoot of the boiling temperature as the fluid level drops through the level of the thermocouple is due to "in-depth absorption" in the fluid which results in slightly higher temperatures just below the fluid surface. The temperature spike that occurs at the end of the test is believed to be the result of accumulation of vapor in the dish. At the end of the test, the residence time of vapor in the dish increases as vapor generation at the bottom of the dish abruptly ceases. The longer residence time allows the vapors to absorb more radiation, allowing them to reach a higher temperature before finally being purged from the dish.

4.2.2 Intermediate Viscosity Fluids

The intermediate viscosity fluids consist of the 10 cS, 50 cS, and 100 cS PDMS-200 fluids. Although the 50 cS fluid was used in the majority of tests, the 10 cS and 100 cS were also studied on a limited basis. A description of the composition of these fluids is given in Table 1.

Unlike most of low viscosity fluids, the intermediate viscosity fluids do not consist of a single type of PDMS molecule; rather, these fluids are distributions of PDMS molecules. For these fluids, a higher viscosity equates to a higher average molecular weight of the PDMS molecules that compose the fluid. The gasification process for these fluids consists primarily of volatilization; however, in the later stages of gasification a significant amount of pyrolytic degradation via the rearrangement to cyclic species occurs, particularly for the 50 cS and 100 cS fluids.

While the gasification behavior of the 50 cS and 100 cS fluids represents a true intermediate between that of the low and high viscosity fluids, the behavior of the 10 cS fluid more closely resembles that of the low viscosity fluids. For this reason, a discussion of intermediate viscosity fluid behavior, referring specifically to the 50 cS and 100 cS fluids, will be followed by a separate discussion of the gasification behavior of the 10 cS fluid.

Unlike the low viscosity fluids, gasification of the intermediate viscosity fluids is not characterized by a well-defined steady-state mass loss period. In addition, the behavior of these fluids is more strongly influenced by the magnitude of the heat flux to which they are exposed. This can be observed in Figure 14 which shows the mass loss rate for a 50 cS fluid sample exposed to different heat fluxes as a function of the normalized mass. At all heat flux levels, the mass loss rate increases rapidly at first, and then increases at a more gradual rate. At fluxes above 45 kW/m^2, a significant increase in the mass loss rate then occurs further into the gasification process when about 1/2 to 2/3 of the fluid has been gasified. The point of this transition occurs further into the gasification process as the heat flux is increased. At heat fluxes of 45 kW/m^2 and less, the mass loss rate gradually increases and then decreases, with no abrupt changes in the mass loss rate.

Analyses of the residual fluids and the vapors evolved at different stages of the gasification process were conducted to determine the gasification process of these fluids. The first series of materials consisted of "residual" fluids collected at the conclusion of gasification experiments in which 50 cS fluid (100 g of fluid was initially added to the sample pan in all instances) was gasified via an

applied external heat flux of 40 kW/m^2. In this series, "residuals" ranged from 51 to 3 g depending upon the extent to which the fluid was gasified under the applied external heat flux. The "residual" fluids were analyzed by GPC and assayed for trimethylsiloxy end-group content via the EOS derivatization/GC analysis method. The EOS derivatization analysis and GPC (M_n,M_w/M_n) results are summarized in Table 2 (Series II).

GPC chromatograms for several residual fluids and the original starting fluid are given in Figure 15. The gasification process results in the preferential removal of the lightest species as evidenced by the loss of materials with the higher elution times (lower molecular weight members). It is evident from these data that gasification proceeds largely via volatilization of the most volatile molecular species in the fluid. In Table 2, further evidence for this is the reduction in polydispersity of the polymer as evidenced by the polydispersity index (M_w/M_n) for the residual fluid. M-content measured via the EOS derivatization/GC procedure are also listed along with M-content as calculated based on the number-average molecular weight (M_n) from GPC analysis. An excellent correlation is noted in Figure 16 between M-content measured via the EOS assay method and that calculated from GPC molecular weights. These data suggest that molecular species *native* to silicone fluids in this viscosity range provide the fuel necessary for ignition as well as a significant and perhaps a major component of the fuel for post-ignition burning.

Figure 17 provides a summary of the GPC data for the 50 cS fluid, residual fluid and volatile products at various stages of gasification. Observe that the initial volatiles (II) consist only of intermediate molecular weight linears which are native to the fluid. Note that the intermediate molecular weight peak shifts to progressively higher molecular weight (lower ET) throughout the gasification of the fluid. As the gasification proceeds, thermal degradation results in the formation of the expected cyclic oligomers (D_3,D_4,...), but throughout the gasification process, the major gasification mechanism is the volatilization of linear species (MD_xM) which are native to the original fluid. Mass spectral data of these same materials are given in Figure 18. These data provide unequivocal identification of the species present but do not provide quantitative information. These data demonstrate the absence of rearrangement cyclics in the early pyrolysis stage and confirm its occurrence in the later stages of the gasification of this material. Also, the formation of large cyclic structures is confirmed. Linear species are not a significant product of thermal degradation of siloxanes since end-blocking agents (e.g. OH, $(CH_3)_3Si$) are not present in sufficient quantity under these gasification conditions to provide a means for terminating the end-group sites.

These data indicate that a two stage process is occurring. Initially, gasification of these fluids is dominated by volatilization, in which the shorter chain PDMS molecules are preferentially distilled from the fluid. The later stages of gasification are dominated by pyrolysis of the remaining fluid, in which the molecular bonds of the remaining long chain PDMS molecules are rearranged, forming cyclic siloxane molecules which are then vaporized. The transition between these two processes is governed by the temperature profile within the fluid, and hence the heating rate of the sample. Because a sample exposed to a lower heat flux heats more uniformly, the majority of its fluid volume attains pyrolysis temperatures earlier in the gasification process (on a mass basis) than a sample exposed to a higher heat flux. As a result, at lower fluxes significant pyrolysis occurs

simultaneously with volatilization, producing a gradual transition between these two processes and causing the peak mass loss rate to occur earlier in the gasification process.

The average mass loss rates of the intermediate viscosity fluids were computed for the domain between the normalized mass values of 0.9 and 0.1. This domain included both the volatilization dominant and pyrolysis dominant stages of gasification in the average while omitting the initial and final transient periods from the calculation.

For these fluids, bubbling of the fluid surface was observed to occur early during the gasification process. This was followed by the inception of bubbles forming well beneath the fluid surface, which subsequently resulted in vigorous bubbling of the whole fluid. This behavior is consistent with the fact that distillation of shorter chain molecules throughout the fluid volume will produce superheated fluid that will form bubbles. In addition, pyrolysis, which also occurs throughout the fluid volume, results in the production of lower boiling point cyclic siloxanes that also will produce superheated fluid.

Another interesting aspect of the intermediate viscosity fluids is that as the fluid sample heated, it began to expand due to the corresponding density decrease of the heated fluid. As the fluid in the dish heated, its thickness would increase, reaching a maximum of 19 mm to 20 mm when only 5 g to 10 g of fluid had been gasified. After this point, the fluid layer thickness would remain relatively constant, decreasing slowly as the effect of swelling was offset by increased gasification rates. Eventually, when roughly half of the fluid had been gasified, the fluid layer thickness decreased rapidly.

As occurred for the low viscosity fluids, a vapor layer consistently formed above the fluid samples in these tests. Unlike the low viscosity fluids, the evolved vapors of the intermediate viscosity fluids tended to condense into visible vapor streams. The mass loss rate also had a significant impact on the appearance of the vapor layer. At high mass loss rates a stable vapor layer formed above the fluid surface, extending several millimeters above the dish and billowing out over its edges. At lower mass loss rates, recirculation of nitrogen above the dish provided sufficient mixing of the vapor to prevent the formation of a stable layer. Regardless of the appearance of the vapor layer, it is expected that its effect on the heat transfer to the fluid surface was significant.

Figure 19 shows a typical temperature distribution plot, as a function of normalized mass, for a 50 cS sample exposed to a heat flux of 50 kW/m^2. The traces in the plot represent the temperature measured at different heights above the bottom of the dish. It should be noted that although the fluid expanded, the "20 mm from bottom" thermocouple remained above the fluid surface throughout the tests.

For those thermocouples that were in contact with the fluid, as the surface of the fluid receded and approached the level of each thermocouple, the temperature would begin to increase more rapidly. As the surface receded past each thermocouple, an increase in noise in the thermocouple signal would appear as first the thermocouple encountered the bubbling surface and then passed into the

vapor layer. The initial overshoot and subsequent drop in the temperature that was observed for the low viscosity fluids did not occur for these fluids because of the vigorous bubbling at the fluid surface. The increase in noise in the thermocouple signal, however, was still distinct enough to allow for a rough measurement of the fluid height to be obtained at various stages of the gasification process. In Figure 19, the fluid surface passes through the "14 mm from bottom" thermocouple at a normalized mass of about 0.8 and through the "7 mm from bottom" thermocouple at a normalized mass of about 0.35. One might similarly conclude from the plot that the fluid surface passes through the "3 mm from bottom" thermocouple at a normalized mass of about 0.3; however, this conclusion would be only partially accurate. Although the thermocouple is near the fluid surface, what is actually happening is that at this stage of the gasification process the entire fluid volume is bubbling so vigorously that noise appears in the thermocouple signal even though the thermocouple is not yet at the surface of the fluid. One can observe from the plot that the fluid surface temperatures are well above those required for pyrolysis of PDMS molecules (> 650 K).

The 5 cS and 10 cS fluids are "transitional" fluids between the low and intermediate viscosity range. Like the low viscosity fluids they are composed primarily of short chain PDMS molecules that have low to moderate boiling temperatures. Accordingly they have similar mass loss profiles during the gasification of the first 70 g of fluid. This can be observed in Figure 20 which shows the mass loss rate for a 5 cS fluid sample exposed to different heat fluxes as a function of the normalized mass. As with the low viscosity fluids, the Figure shows an initial transient period in which the mass loss rate rapidly increases during the loss of the first 5 g of fluid. The initial transient is then followed by a long period during which a gradual increase in the mass loss rate occurs. As with the low viscosity fluids, this period was designated as the steady-state domain and was used in calculating the average mass loss rate. Similar to the 50 cS and 100 cS fluids, a distillation process occurs during this period in which the shorter chain PDMS molecules are more readily gasified than the longer chain molecules. When only 20 g to 30 g of fluid remain in the dish, a transient period occurs in which the mass loss rate rapidly decreases. During this phase of the gasification process, the longer chain molecules, which have boiling temperatures in excess of pyrolysis temperatures, are slowly distilled from the residual fluid. This process is combined with some pyrolysis of the remaining fluid.

The bubbling behavior for the 5 cS and 10 cS fluids was similar to that of the 50 cS and 100 cS fluids; however, it was not as vigorous. During the final stages of gasification; however, when some pyrolysis was occurring, the bubbling did increase in intensity.

As with the 50 cS and 100 cS fluids, the 5 cS and 10 cS did expand upon heating; however, the expansion was less pronounced and the duration of its effect was shorter perhaps because of the lower temperatures needed for their gasification.

The vapor layer that formed for the 5 cS and 10 cS fluids also shared characteristics in common with both the low and intermediate viscosity fluids. Although some condensation in the vapor layer occurred, a large portion of the vapor remained only visible by the distortion pattern it produced. The appearance of the vapor layer was also somewhat mass loss rate dependent; however, a stable

vapor layer eventually formed above the fluid surface at all heat flux conditions. The effect of the vapor layer on heat transfer to the fluid surface was the most significant for these fluids.

Figure 21 shows a typical temperature distribution plot, as a function of normalized mass, for a 5 cS sample exposed to a heat flux of 50 kW/m^2. As was observed for the 50 cS fluid, as the surface receded past each thermocouple, an increase in noise in the thermocouple signal would appear. Although there is no unique boiling temperature for the 5 cS fluid due to the fact that it contains a mixture of different PDMS molecules, the surface temperature of the fluid does appear to plateau at about 625 K during the steady-state period of gasification. This, coincidentally, is near the boiling temperature of MD_8M, the PDMS molecule that has a molecular weight which corresponds to the average molecular weight of the molecules contained in the 5 cS fluid. During the final stages of the gasification process, the temperature of the remaining fluid increased to levels associated with pyrolysis.

4.2.3 High Viscosity Fluids

A range of higher viscosity (higher molecular weight) polymers was investigated to provide insight into the dominant mechanisms occurring in polymers typically utilized in commercial products such as sealants, rubber, foams and gels. The polymers were fluids of the following viscosities: 10^3 cS, 10^4 cS, $6x10^4$ cS, and a "model" polymer. The "model" polymer was a specially synthesized polymer with no intermediate molecular weight species (neither cyclic or linear). This polymer was intended to provide unequivocal evidence for the formation of specific intermediate molecular weight cyclic species (macrocyclics) during the thermal pyrolysis of these silicone fluids.

Preliminary gasification experiments of 100 cS and 60,000 cS fluids illustrate the substantial differences in gasification mechanisms between the intermediate and high viscosity polymers. Residual fluids (100 cS and 60,000 cS) were characterized similar to the previous 50 cS exercise. In Table 2 (Series III), the M-content results from EOS/GC derivatization and GPC-M_n, and the GPC chromatograms in Figure 22 suggest significantly different dominant mechanisms occur during the gasification of these two materials: *Narrowing* of the molecular weight distribution and a *shift to higher* molecular weights is observed for the 100 cS fluid. These results are very similar to the earlier findings on the gasification of the 50 cS fluid. A *broadening* of the molecular weight distribution and *shift to lower* molecular weights is observed for the 60,000 cS fluid. Narrowing of the distribution results from the preferential removal of lower molecular weight species based on their slightly higher volatility (vapor pressure). Broadening results from thermal induced rearrangement and results in a shift to lower molecular weights due to the presence of excess end-block (M-content) since fluid is lost via volatilization and perhaps formation of large cyclic structures which require no end-blocker.

Good agreement is noted for the M-content values for both the original and residual 100 cS fluid. For the 60,000 cS fluid, the broadening of the polymer distribution suggests thermal induced depolymerization is dominant in the gasification of this fluid. Furthermore, a wide disparity is noted between the assayed M-content and the calculated M-content based on number-average molecular

weight (GPC). It is important to note that the assayed content (volume fraction of 2.9×10^{-3} (2900 ppm)) is far lower than the anticipated content (volume fraction of 5.4×10^{-3} (5400 ppm)) which suggests that a significant number of molecular species may be large cyclic species requiring no terminal end-groups.

Figures 23 and 24 summarize the GPC/GC characterization data on the gasification products collected at various stages of the pyrolysis of the 10,000 cS fluid. The initial gasification sample (Δm= 100 g to 98 g) consists of ~70% intermediate molecular weight species and ~30% cyclic oligomers and larger (macro) cyclics The cyclic oligomers and macrocyclics result from thermal rearrangement/degradation of the fluid. It is uncertain whether all of these macrocyclics result from degradation or are native to the fluid since the original fluid contains some small amounts of macrocyclics. The GC analysis indicates that a distribution of intermediate molecular weight linears (MD_xM) similar to that observed for the 50 cS fluid is present in these volatiles. These are native to the fluid and are not a product of rearrangement since they are observed only in the earliest stage of gasification. Thus, in this earliest stage of pyrolysis, volatilization of native species is a dominant mechanism although some depolymerization of the fluid is occurring and contributes a significant amount of oligomeric cyclics, primarily D_3 and lesser amounts of D_x ($x>3$). Note in the second and all later samplings of gasification products, the trend toward increased concentrations of small cyclic species. Also, the linears content (MD_xM) is substantially reduced whereas the prominence of macrocyclics increases and remains pretty much constant throughout the gasification of the material, further suggesting that these are in fact a product of the thermal rearrangement/degradation process. GPC analysis provided a convenient measure of the fraction of intermediate molecular weight (I-MW) species and the short chain cyclics (SC-C) (D_x, where $3 \leq x < 10$). In Table 3, the analytical (GPC) results of the gasification products are summarized for the various fluids studied. After correcting the SC-C peak for the presence of the internal standard (dodecane), the areas under the respective regions of the GPC curves provided a measure of the I-MW and SC-C components in the volatiles samples.

It is interesting to note in Table 3, that all gasification samples contain both I-MW and SC-C components. The relative concentration of these two general groups of components depends upon the fluid type (i.e. initial viscosity) and the stage of the gasification of the fluid/polymer. The SC-C component generally increases at an earlier stage in the gasification process with increasing viscosity of the original fluid and always increases as the gasification of the fluid proceeds. The I-MW component is primarily dependent upon the concentration of these species (both linear and cyclic) in the original materials. Linear volatile species almost entirely result from gasification of species native to the fluid whereas cyclic structures result both from native cyclics and are formed in the thermal rearrangement during pyrolysis. In general, the composition of gasification volatiles depends upon the volatility of species native to the fluid/polymer and the extent to which degradation via rearrangement to cyclics occurs in the pyrolysis of the material. As seen in Table 3, each material undergoes its own unique pyrolysis regime(s).

Further elucidation of the significant role of "vaporization" of materials native to the polymer in the very early stages of pyrolysis is evident from results given in Figure 25. In this experiment, 1000

cS fluid was pyrolyzed until mass losses of 2 g, 10 g, 45 g, and 80 g were achieved in successive experiments. After each of these mass losses was achieved, the pyrolysis was terminated and the remaining fluid in the sample pan was analyzed via GPC to assess which species in the material were absent as a result of their volatilization and assess what other changes had occurred in the pyrolyzing polymer. It is evident that during the initial loss of about 10% of the fluid, the lowest molecular weight species are preferentially removed via volatilization. The GPC curves for those fluids pyrolyzed for longer intervals (45 g, 80 g) clearly indicate that extensive rearrangement occurs and an overall shift of the distribution to lower molecular weights is evident and expected in view of the apparent retention of end-block species (M-content ~8700 ppm) in the material (see Table 4).

In Table 4, a summary of M- and T- structural data from EOS/derivatization analysis on the original and residual fluids is given. Note the very good agreement between M_{EOS} and M_{GPC} for those materials which pyrolyze primarily via volatilization of native species, e.g. 50 cS and 100 cS fluids. For higher molecular weight fluids in which rearrangement to cyclics is a dominant gasification regime, a wide disparity between M_{EOS} and M_{GPC} in the residual fluid occurs and an increasing trend in this disparity occurs with increasing viscosity of the original fluid. A plausible explanation is that very large cyclic structures are formed during pyrolysis and because of their molecular size do not volatilize. The T_{EOS} results in Table 4 also demonstrate an interesting trend. Methyl cleavage increases at higher temperatures and consequently increased formation of monosubstituted T-species is expected for the higher molecular weight materials wherein gasification results primarily from thermally induced rearrangement. These data also indicate that methane formation is not a significant factor in the gasification of these materials since relatively minor amounts of methyl cleavage (T-formation) occurs.

To unequivocally establish that macrocyclics are formed in the pyrolysis of these materials, a "model" polymer (trimethylsilyl end-blocked) was synthesized. The key requirement for this polymer was that it contain no intermediate molecular weight species as measured by GPC (i.e. ET= 15.7 to 18). This would provide assurance that any gasification products which elute in this range of the GPC are in fact formed during the pyrolysis/gasification process. The GPC/GC data are summarized in Figures 26 and 27. These data confirm that the I-MW species are formed in the thermal rearrangement of the fluid. Furthermore, these species are large cyclic structures (macrocyclics). The structure was inferred from GC results (Figure 27) and unequivocal confirmation of their cyclic structure was provided by mass spectral analysis, see Figure 28. Note that only very minor amounts of cyclics (D_x, where x=3,6,9...) are present in the original fluid. These species are a direct result of the polymerization of the starting material, D_3. The formation of all intervening cyclic species during pyrolysis is evident in the volatiles from all gasification samples. Also, note the enhanced concentration of all of these species even in the residual fluid at the cessation of the gasification process. Note that cyclic species with x>37 are observed in the residual fluid suggesting that the formation of substantial quantities of very large cyclic structures is a significant mode of degradation and a consequence of the thermally induced random chain scission.

As discussed above, the gasification process for these fluids consists primarily of pyrolysis;

however, significant volatilization occurs during the early stages of gasification. Like the intermediate viscosity fluids, these fluids are not characterized by a well defined steady-state mass loss period. For this reason, the average mass loss rates were calculated using the domain between the normalized mass values of 0.9 and 0.1. In addition, the high viscosity fluids are strongly influenced by the magnitude of the heat flux to which they are exposed. Figure 29 shows the mass loss rate for a 1,000 cS fluid sample exposed to different heat fluxes as a function of the normalized mass. As can be observed in the Figure, besides the fact that the mass loss rate increases with increasing heat flux, the maximum mass loss rate occurs at a lower value of the normalized mass as the heat flux increases. As with the 50 cS fluid tests, this shift in the mass loss peak is due to the fact that the entire fluid heats more uniformly as the heat flux is lowered. At lower heat fluxes, the fluid volume attains pyrolysis temperatures earlier in the gasification process (on a mass basis). As a result, at lower heat fluxes pyrolysis transitions from a surface phenomenon to a volumetric process earlier in the gasification process, thus causing the peak mass loss rate to occur earlier.

Among the high viscosity fluids, slight differences in behavior were observed. While the average mass loss rates of these fluids were essentially the same at a given flux, the 1,000 cS fluid tended to have a higher peak mass loss rate. Additionally, the mass loss rate of the 10,000 cS fluid tended to peak considerably later in the gasification process (on a time basis) than the other two fluids. This effect became more significant as the heat flux decreased.

In several ways, the gasification behavior of the high viscosity fluids resembled that of the 50 cS fluid. Although peak mass loss rates were higher for the 50 cS fluid at a given flux, the normalized average mass loss rates were roughly the same. As they were heated, the high viscosity fluids swelled in a manner similar to that observed for the intermediate viscosity fluids. The behavior of the vapors evolved from the high viscosity fluid samples also behaved as the vapors evolved from the intermediate viscosity fluids, condensing into visible vapor streams and forming a stable vapor layer above the fluid surface at high mass loss rates. In addition, the bubbling behavior of the high viscosity fluids was similar to that of the intermediate viscosity fluids with one notable exception: an interesting behavior that was observed for the 10,000 cS and 60,000 cS fluids at fluxes of 50 kW/m^2, 60 kW/m^2, and 70 kW/m^2. For these tests, as the mass loss rate peaked at a normalized mass value of 0.5 or 0.4, the fluid layer would periodically expand due to intense bubbling, and then contract as the bubbles rapidly collapsed. This phenomena, which occurred three to five times over a period of about 200 seconds, showed up in the data as a periodic oscillation in the mass loss rate. This can be observed in Figure 30 which shows the mass loss rate for a 60,000 cS fluid sample exposed to different heat fluxes as a function of the normalized mass.

Unfortunately, detailed temperature data were not obtained for any of the high viscosity fluids due to the fact that the borosilicate glass dish containing the multiple thermocouples was damaged prior to the testing of these fluids. Because this dish was extremely difficult to manufacture, a replacement was not obtained. It can be reasonably supposed, however, that the temperature profiles within these fluids are similar to those of the 50 cS fluid under similar test conditions. This conclusion is based primarily on the fact that the mass loss rates of the high viscosity fluids are essentially the same as those for the 50 cS fluid. Additionally, temperature data obtained from tests

using the first borosilicate glass dish and the temperature data obtained from the thermocouple underneath the stainless steel dish show comparable temperatures among the 50 cS and high viscosity fluids.

4.3 Average Mass Loss Rate

Figure 31 shows a plot of the average mass loss rate data obtained using the stainless steel dish for the 0.65 cS, 1.0 cS, 1.5 cS, and 5 cS fluids. A separate plot of the average mass loss rate data for the 50 cS, 1,000 cS, 10,000 cS, and 60,000 cS fluids is provided in Figure 32. In Figure 32, it can be observed that, at a given heat flux, the average mass loss rate decreases as the viscosity of the fluid increases. This behavior is consistent with the fact that as the chain length of the PDMS molecule is increased, more energy is required for it to heat to its boiling point and then vaporize (see Table 1). This energy required for gasification, commonly referred to as the global heat of gasification, will be discussed in detail in the next section of the paper. Conversely, in Figure 32, the fluid viscosity is shown to have no observable effect on the average mass loss rate. Although some differences in the behavior of these fluids were observed, their behavior is similar from the standpoint that the gasification process for these fluids consists of two processes: early distillation of short chain molecules from the fluid mixture, and pyrolysis of long chain molecules to form cyclic siloxanes which are volatilized. The result that these fluids have similar average mass loss rates appears to be an indication that pyrolysis processes for these fluids require similar amounts of energy and the mass loss by distillation is less than that by pyrolysis.

Also noteworthy in both plots is the relatively linear relationship between the mass loss rate and heat flux. This linear relationship is of particular interest for the 50 cS fluid because previous studies [2, 4] have indicated that a less regular relationship exists between these two parameters for this fluid. In these previous studies it was observed that a linear relationship exists between the mass loss rate and heat flux at low heat flux values; however, at a critical value of the heat flux, between 37 kW/m^2 and 57 kW/m^2 depending on the study, the mass loss rate of the 50 cS fluid increases dramatically with further increases in the heat flux. From Figure 32, it can be observed that no dramatic change in the mass loss rate was observed in this study for any of the fluids for the range of heat fluxes studied. Under the conditions of this experiment, however, the observed linear relationship between the mass loss rate and heat flux for all fluids is somewhat fortuitous. Although one might expect that as the heat flux is increased, the mass loss rate should increase proportionately, it should be recognized that the net heat flux to the sample may not be a linear function of the external heat flux as discussed later in this study. Such a nonlinear relationship between the net heat flux and external heat flux provides a possible explanation for the nonlinear mass loss rate behavior observed for the 50 cS fluid in the previous studies.

4.4 Global Heat of Gasification

The global heat of gasification is a defined property of a substance that represents the amount of

energy required to "gasify" a unit mass of the material. This quantity is widely used in fire calculations to determine the amount of combustible gas that would be supplied to a fire when a material is exposed to a given heat flux. For pure materials that volatilize, this quantity simply represents the sum of the heat of vaporization and the sensible heat required to raise a unit mass of the material from room temperature to its boiling point. For materials that pyrolyze, or mixtures of materials that volatilize, however, the definition of this property is not as clear. For these materials, the global heat of gasification can be highly dependent upon the conditions under which the material is gasified. Parameters such as heating rate and other environmental conditions can significantly influence the value of this property for such materials.

Because of its significance as a fire property to the fire modeling community, one of the primary goals of this investigation was to determine the global heat of gasification for the PDMS fluids studied. Of particular interest were the intermediate and high viscosity fluids, for which no consistent published values exist.

In terms of experimental measurements and its use in fire calculations, the global heat of gasification is defined mathematically as:

$$L = \frac{\dot{Q}''_{net}}{\dot{m}''} \qquad (1)$$

where L is the global heat of gasification, $\dot{Q}''_{net}$ is the net heat flux to the sample, and $\dot{m}''$ is the mass loss rate per unit surface area.

Typically, the global heat of gasification is measured and used as an average quantity; however, as Kashiwagi *et al.* [14] have shown, the instantaneous value of the global heat of gasification of any material, even solely volatilizing materials, varies with time for a given set of experimental conditions. To demonstrate this, one must first understand how the global heat of gasification is calculated from experimental measurements. Initially, as a material is heated, a large amount of the heating is dedicated to raising the temperature of the material rather than to gasifying it; therefore, the initial mass loss rate is low. This corresponds to a high instantaneous value of the global heat of gasification. As the material continues to heat, the mass loss rate eventually increases, and the corresponding value of the global heat of gasification decreases. Ideally, a steady-state will eventually be reached where the mass loss rate attains a steady or asymptotic value. This is the condition for which the global heat of gasification is typically reported. As can be seen, using this average value to estimate the mass loss rate during the initial stages of gasification may result in a significant over-estimation; therefore, care must be used in applying such average values of the global heat of gasification to a fire calculation if one does not account for the transient behavior of the gasification process.

According to equation (1), the quantities required for calculating the global heat of gasification are the mass loss rate and the net rate of heat transfer to the fluid. Determination of the net heat transfer rate requires an understanding of the energy balance for the sample. An energy balance diagram for the experimental configuration of this study is provided in Figure 33. The diagram shows that the main components which affect heat transfer to the fluid sample are the incident radiant heat flux, the absorption of radiation by the vapor layer above the fluid, the absorption of radiation by the fluid or the transmission of radiation through it, the conduction of heat to the firebrick, the radiant re-emission by the fluid, and the convective cooling of the fluid surface by the nitrogen purge gas. For the conditions under which these experiments were conducted, conduction of heat to the firebrick was minimal, and was thus neglected in calculating the net heat transfer to the fluid. Similarly, radiant transmission through the fluid sample was insignificant, and was of little consequence for the tests conducted using the stainless steel dish. The major factors in determining the net heat transfer to the fluid were the incident flux, vapor absorption, reradiation, and to a lesser extent, convective cooling.

4.4 Vapor Absorption

Initially, the vapor layer was presumed to be only weakly absorbent and therefore was considered to have little effect on the net heat transfer to the surface. However, when initial attempts failed to reconcile the measured global heat of gasification values with the calculated values (based on heat capacity and heat of vaporization data) for these fluids, the validity of this assumption was tested. Preliminary tests conducted with 1.5 cS fluid showed that the vapor absorption effect was indeed substantial, absorbing up to 35% of the incident energy. This revelation prompted a more thorough investigation of this effect.

A more controlled set of experiments was conducted to measure the vapor absorption effect for a few of the PDMS fluids at a few heat flux levels. The purpose of these tests was to provide correlations of the vapor absorption percentage (heat flux absorbed by vapor layer / incident heat flux) that could be used in conjunction with the mass loss rate data, obtained using the stainless steel dish, to calculate the global heat of gasification for the various fluids. The tests were conducted using a specially designed borosilicate glass dish that allowed simultaneous measurement of the vapor absorption effect and the mass loss rate. This dish was constructed to mimic, as closely as possible, the experimental conditions of the standard mass loss rate experiments. The dish, which was configured like a donut, was manufactured from a standard borosilicate glass petri dish and a segment of thin walled borosilicate glass tubing. The tubing, which protruded through the center of the dish, created a cylindrical hole inside which a heat flux gauge could be inserted. The top of the cylinder was positioned at a level of 8 mm below the lip of the dish in order to allow sufficient space for the vapor layer to form above the heat flux gauge.

A sketch of the dish and sample holder is provided in Figure 34. Using this dish, each measurement of the vapor absorption effect required three separate tests. The first test measured the baseline heat

flux at the level of the heat flux gauge. The second test measured the absorption effect of a window, designed to shield the heat flux gauge from direct exposure to the PDMS vapors, that was placed on top of the interior cylinder. For these first two tests, no fluid was placed inside the dish. The third test measured the absorption of the vapor layer with the window in place.

For these tests, the empty dish was placed on top of a specially designed Foamglas® that had a hole through its center to accommodate the heat flux gauge. The level of the dish was set according to the desired heat flux at the level of the fluid surface. The heat flux gauge was then threaded through the sample support hardware and placed inside the dish so that its surface was 3 mm -10 mm below the top of the inside cylinder. This level, which depended on the heat flux, was chosen to minimize the view factor between the heat flux gauge and the surfaces of the dish, while maintaining sufficient distance from the top of the cylinder, where a window would later be added, in order to minimize condensation of fluid vapor on the window's surface because if a cooled heat flux gauge was too close to the window, it would cool the window. For the first test, this assembly was inserted into the gasification chamber, and the baseline heat flux at the level of the heat flux gauge was measured. For the second test, a 3 mm thick KBr window was placed on top of the inside cylinder. KBr was chosen because of its low absorptivity in the infrared and near visible range where the majority of the incident radiant energy was concentrated. The empty dish with the window in place was then inserted into the gasification chamber, and the heat flux was measured to determine the absorption effect of the window. Lastly, heat flux measurements were conducted with 100 g of fluid in the dish.

A composite heat flux plot of these tests for a 1.5 cS sample exposed to a heat flux of 40 kW/m^2 is provided in Figure 35. In the Figure, the magnitude of the vapor absorption effect is indicated by the difference between the "heat flux with fluid" and the "heat flux with window only" traces. The Figure shows that once significant gasification begins, the heat flux level drops dramatically. This initial drop is followed by a slow but steady decrease in heat flux as the mass loss rate gradually increases. As expected, the heat flux reaches a minimum value when the mass loss rate reaches its maximum; however, the dramatic increase in mass loss rate does not produce a corresponding large decrease in the heat flux. A probable explanation for this behavior is that the vapor layer has a maximum thickness and density for a given set of experimental conditions. This maximum thickness and density is the result of the fluid dynamics dictated by the geometry of the dish, the mass loss rate, the properties of the vapor, and the flow field of the nitrogen purge gas.

Tests were conducted at heat fluxes of 40 kW/m^2, 55 kW/m^2, and 64 kW/m^2 for the 1.5 cS, 5 cS, and 50 cS fluids. The experimental conditions were limited to this set due to the time-consuming nature of the experiments. Multiple tests conducted for each test condition showed reasonably repeatable results with respect to qualitative behavior; however, significant quantitative variability was observed in some cases as discussed later. The tests revealed a strong relationship between the mass loss rate and the vapor absorption percentage at low mass loss rates. With the exception of the 50 cS fluid, at high mass loss rates the vapor absorption percentage was only weakly dependent on the mass loss rate. The tests also revealed a significant heat flux dependence of the results. This heat flux dependence is believed to be due to flow geometry changes related to the position of the sample

dish with respect to the heater.

In order to establish a correlation that could be used to estimate the vapor absorption effect, plots of the percentage absorption as a function of the mass loss rate were constructed for each test condition and then compared. The plots revealed correlations for each test condition; however, the limited number of test conditions used did not provide sufficient data to allow the vapor absorption effect to be neatly correlated as a function of heat flux. As a result, the patterns observed from the data had to be used to make educated estimates of the vapor absorption effect for the full range of test conditions for which the standard mass loss rate measurements were made.

For the 1.5 cS fluid, it was observed that the vapor absorption percentage would increase steadily with increasing mass loss rate until it reached a value of the mass loss rate at which point the vapor absorption percentage would increase only slowly with further increases in the mass loss rate. The value of the mass loss rate at which this transitional behavior occurred increased with increasing heat flux. This behavior can be observed in Figure 36 which shows the vapor absorption data obtained at all three heat flux conditions. In the Figure, the data for each heat flux condition represents a compilation of the data from three separate tests. For the 55 kW/m^2 and 64 kW/m^2 tests, the vapor absorption percentage rose to a value of between 25% and 30% at a mass loss rate of about 0.2 g/s, at which point the vapor absorption percentage held steady with further increases in the mass loss rate. For the 40 kW/m^2 case, the vapor absorption percentage rose to a value of 15% at a mass loss rate of 0.1 g/s, and then slowly increased to a value of 25% at a mass loss rate of 0.6 g/s. Figure 36 shows that at all three heat flux conditions tested, the vapor absorption percentage had a relatively constant value of about 25% ± 5% for mass loss rates in excess of 0.4 g/s. The fact that at all three heat flux conditions the vapor absorption percentage attained a maximum asymptotic value is consistent with the explanation discussed above regarding the existence of a maximum vapor layer thickness. Because the average mass loss rates measured for the 1.5 cS fluid using the stainless steel dish were all near or above 0.4 g/s, a vapor absorption percentage of 25% was used for the purposes of calculating the global heat of gasification values. This vapor absorption percentage value was also used for the calculations involving the 0.65 cS and 1.0 cS fluids.

Figure 37 shows a composite of the vapor absorption data obtained for the 5 cS fluid. In the figure, the data for each heat flux condition represents a compilation of the data from three separate tests for the 55 kW/m^2 and 64 kW/m^2 conditions and from two tests for the 40 kW/m^2 condition. The vapor absorption behavior of the 5 cS fluid was observed to be similar to that of the 1.5 cS data at heat fluxes of 55 kW/m^2 and 64 kW/m^2, i.e., the vapor absorption percentage would increase steadily with increasing mass loss rate until it reached an asymptotic value. At 40 kW/m^2, however, the vapor absorption effect never attains this asymptotic condition due to the lower mass loss rates. It reasonably can be assumed that if higher mass loss rates had been achieved at this heat flux level, the vapor absorption effect would have also reached an asymptotic value similar to that for the higher heat flux tests. Using this assumption, a reasonable estimate of 35% ±5% for the vapor absorption can be used at mass loss rate values above 0.18 g/s. For mass loss rates below 0.18 g/s, a linear scaling law can be used to estimate the vapor absorption percentage. These estimates of the

vapor absorption percentage were used in calculating the global heat of gasification values for the 5 cS fluid.

A composite of all the percentage absorption vs. mass loss rate plots for the 50 cS fluid is shown in Figure 38. The data in the Figure represent two tests at 40 kW/m^2, three tests at 55 kW/m^2, and four tests at 64 kW/m^2. The Figure shows that the percentage absorption is confined to a range of values bounded by two lines passing through the origin, one representing the maximum vapor absorption effect and the other representing the minimum. The maximum absorption limit is primarily established by the data from the 40 kW/m^2 test condition while the minimum limit is primarily established by the 64 kW/m^2 data. The 55 kW/m^2 data falls throughout the range with a slight bias toward the maximum limit. The slope of the upper limit line is 22% per 0.1 g/s while the slope of the lower limit is 9 % per 0.1 g/s.

In accordance with the observation that the data tend toward the higher limit at the lower flux and toward the lower limit at the higher flux, the following correlation for estimating the vapor absorption percentage as a function of heat flux was established. At fluxes of 45 kW/m^2 and lower, the maximum value was used while at fluxes of 65 kW/m^2 and higher, the minimum value was used. For fluxes between 45 kW/m^2 and 65 kW/m^2, the percentage absorption varied proportionately from the maximum to the minimum value. Because of the large difference between the maximum and minimum percentage absorption values, particularly at high mass loss rates, the potential error in estimating the vapor absorption effect is significant; however, the actual error associated with these estimates is believed to be ±5%. The above correlation was used in the global heat of gasification calculations for the 50 cS fluid. The similar gasification behavior of the 50 cS and high viscosity fluids justified the use of this correlation for the 1,000 cS, 10,000 cS and 60,000 cS fluids as well.

4.5 Reradiation

For the low viscosity fluids, reradiation from the fluids was not significant due to the low boiling temperatures of these fluids. The reradiation for these fluids was on the order of 1 kW/m^2; therefore, accurate estimation of the reradiation from the fluids was not critical. For these fluids a sufficient estimate of the reradiation could be obtained by assuming each fluid sample emitted as a gray body at its boiling temperature, having an emissivity of 0.9. For the high and intermediate viscosity fluids, however, reradiation was substantial, having values on the order of 1/3 of the incident heat flux. For these fluids, accurate estimation of the reradiation was of more concern, and therefore prompted development of a more sophisticated method to estimate these losses.

Calculation of the reradiation for these fluids was complicated by the fact that reradiation occurs throughout the entire fluid layer. Energy radiated within the fluid layer is partially absorbed by the surrounding fluid, and the remainder escapes to the environment. Therefore, to calculate the reradiation by the entire fluid, each layer of fluid must be treated as a separate emitter. Calculation requires knowledge of the temperature as a function of depth within the fluid layer. In addition, the

absorption coefficient of the fluid as a function of frequency must be known in order to account for the attenuation of re-emitted energy by the surrounding fluid. Although some absorbance data for these fluids were found in the literature, the data were more qualitative than quantitative in nature. The published data did reveal, however, that these fluids weakly absorbed over several frequency ranges in the visible and infrared spectrum. This confirmed the need for a computer model to calculate the reradiation for these fluids, as well as the need for quantitative measurements of the absorption coefficient.

Measurements of the absorbance as a function of frequency were made using a Fourier Transform Infrared Spectrometer (FTIR) that had a operating wavelength range of 2.3 μm to 13 μm. An adjustable thickness, sealed liquid cell with calcium fluoride windows was used for the measurements. Absorbance measurements were made for the operating range of the FTIR using 100 cS fluid samples having thicknesses of 0.5 mm and 0.1 mm. The absorbance data was then converted into values of the absorption coefficient. Because of the large path length used in these tests, this data was only useful in quantifying the absorption coefficient for the weakly absorbing frequency ranges. For the strongly absorbing ranges, estimates of the absorption coefficient were made from the published data and compiled with the above measured values. A plot of this composite data set, showing the absorption coefficient as a function of frequency, is provided in Figure 39.

Using the absorption coefficient data and temperature data from the borosilicate glass dish tests, a computer model was used to calculate the reradiation for the various experimental conditions. The model divided the fluid into thin layers that were each assumed to emit as blackbodies at their respective temperature. The amount of energy emitted by each layer, that was not absorbed by the fluid layers above it, was then calculated. The sum of the emitted energies from all of the layers provided the total re-emitted energy.

Calculations were performed for each set of temperature data obtained for the 5 cS and 50 cS fluids using the borosilicate glass dish. The thermocouple data were used to estimate the temperature profiles and fluid layer thickness as a function of normalized mass for each test. Calculations were performed at normalized mass increments of 0.1 and then averaged to obtain an average value of the reradiation for each test. These reradiation values were then plotted as a function of heat flux to yield a correlation that could be used for the full range of heat fluxes tested using the stainless steel dish. Figure 40 shows that the calculated re-emission values ranged from 16 kW/m^2 to 23 kW/m^2 for the 50 cS tests, and ranged from 7.8 kW/m^2 to 8.7 kW/m^2 for the 5 cS tests. Because no temperature data were obtained for the higher viscosity fluids, the correlation obtained using the 50 cS temperature data was used in the global heat of gasification calculations for the 50 cS as well as the high viscosity fluids. As discussed earlier, this is believed to be a reasonable approximation due to the similar mass loss rate behavior among the 50 cS and high viscosity fluids. The correlation obtained using the 5 cS temperature data was used only in the global heat of gasification calculations for the 5 cS fluid.

For the majority of tests conducted with the stainless steel dish, heat losses due to convective cooling of the fluid surface were insignificant. For these tests, the vapor layer, which absorbed a significant fraction of the incident heat flux, also shielded the fluid surface from the cooler nitrogen purge gas. In those tests which had mass loss rates that were less than about .05 g/s, however, the vapor layer was unable to prevent convective cooling of the fluid. Under these conditions, encountered with high and intermediate viscosity fluids at low heat fluxes, nitrogen was able to circulate above the fluid surface and thus provide a cooling effect. This effect was evidenced by the significantly lower fluid temperatures measured when the mass loss rate was less than .05 g/s. Even under conditions where the mass loss rate was greater than .05 g/s for the majority of the test, when the mass loss rate fell below this threshold, a more rapid decrease in the fluid temperature and mass loss rate was observed.

Although convective cooling was observed to be significant under some circumstances, an attempt to accurately measure this effect was not pursued due to the complex nature of the gas flow above the fluid sample. Instead, the temperature data from the borosilicate glass dish tests was used to estimate the convective cooling. Assuming thermal equilibrium existed at the end of each test, the estimates were obtained by calculating the radiant heat flux from the surface beneath the dish, by using the measured temperature, and then subtracting this value from the incident heat flux. These calculations provided an estimated convective cooling value of 8 kW/m^2 when the mass loss rate was less than .05 g/s. For those tests that had mass loss rates less than .05 g/s during part of their gasification process, the fraction of the period between normalized mass values of 0.9 and 0.1 for which their rates were less than .05 g/s was multiplied by 8 kW/m^2 to obtain the average convective cooling estimate.

4.6 Global Heat of Gasification Values

Using the above estimates of the various heat losses, global heat of gasification values were calculated using the measured average mass loss rate for each experiment. The values from all of the experiments with a particular fluid were then averaged to obtain an average global heat of gasification value. Figure 41 shows the calculated global heat of gasification values for the eight PDMS-200 fluids for which mass loss rate data were reported in Figures 31 and 32. Figure 41 also shows a graphical comparison of the calculated and theoretical values of the global heat of gasification for the low viscosity fluids. The Figure shows reasonable agreement between the experimental and theoretical values for these low viscosity fluids, a result which validates the method used to calculate the global heat of gasification from the experimental data.

Figure 41 also shows that an average value of 630 J/g was calculated for the 5 cS fluid. Although there is no defined theoretical value of the global heat of gasification for the 5 cS fluid, it is an interesting result that the measured global heat of gasification is near that of MD_8M (710 J/g), the PDMS molecule having a molecular weight that corresponds to the average molecular weight of the molecules contained in the 5 cS fluid.

The 50 cS and high viscosity fluids all had similar global heat of gasification values in the range of 1200 J/g to 1300 J/g. The fact that heat of gasification values for these fluids were similar should be expected due to their similar average mass loss rates and the fact that the 50 cS data was used to estimate the heat losses for the high viscosity fluids. In any case, one would expect that the global heat of gasification values of the high viscosity fluids should be similar due to their similar structure and gasification behavior. As alluded to previously, however, the similarity between the heat of gasification values for the 50 cS and high viscosity fluids indicates that both the distillation and pyrolysis processes for these fluids require similar amounts of energy.

As has been shown in the above paragraphs, one cannot simply determine the global heat of gasification for these fluids by dividing the incident heat flux by the mass loss rate; rather, the net heat flux to the sample must be determined. Similarly, when applying the global heat of gasification values reported in this study to a fire calculation, one must account for the effects of reradiation from the sample, absorption of radiant energy by the vapor layer, as well as other phenomena that will affect the heat transfer to the fluid.

5. Experimental Sensitivities

In the process of developing the experimental method for these tests, several complications were encountered that affected the measurement of the mass loss rate and the calculation of the global heat of gasification. Where it was possible, these problems were resolved through modifications of the experimental hardware; however, the nature of the experiment prevented resolution of some of these problems. The experience gained through this problem resolution exercise demonstrated that mass loss rate and global heat of gasification measurements of the type conducted in this study can be significantly influenced by the experimental design; therefore, care must be exercised in identifying and accounting for experimental sensitivities when conducting these types of measurements.

One of the major complications encountered in this study involved the condensation of fluid vapor, primarily for the low viscosity fluids. Although condensation of the fluid vapor did not occur in the exhaust for the low viscosity fluids, condensation did occur on the colder surfaces inside the gasification chamber. This presented a problem when condensation occurred on the surfaces of the sample holder and its support structure. Although several attempts to minimize this effect were attempted, they were only partially successful. Because the vapor layer that formed above the sample tended to flow over the sides of the dish, the vapor would penetrate the pores of the Foamglas® sample holder and saturate it. This resulted in the retention of less than 10 g of gasified fluid per test. Accordingly, this resulted in small errors in the mass loss rate measurements. For the 5 cS and 10 cS fluids, condensation of the fluid vapor on the sample support hardware was somewhat less of a problem than for the low viscosity fluids. For the 50 cS, 100 cS, and high viscosity fluids, although condensation of the fluid vapor did occur in the exhaust, condensation on the sample support hardware was typically not a problem for these fluids due to their lower mass loss rates.

Several other aspects of the experimental design impacted the mass loss rate measurements. Among them, the design of the sample dish had the most significant influence on the results. The effects of the dish's design can be separated into two categories: effects due to the geometry of the dish, and effects due to the properties of the dish material. The influential geometric properties were the height, diameter, and wall thickness of the dish. The primary material properties that affected the mass loss rate were the density and specific heat. Although the thermal conductivity of the dish can significantly influence the rate of heat loss from the dish via conduction, the design of the sample holder in these tests provided sufficient insulation to minimize this effect. Similarly, differences in the emissivity and transmission of the various dish materials can effect the mass loss rate in these types of tests; however, such differences for the various dishes used in these experiments were not significant due to the relatively high absorptivity of the PDMS fluids.

Together, the wall thickness, density, and specific heat determined the thermal mass of the dish, a property of the dish that had a significant effect on the mass loss rate of the fluid contained within. Tests conducted with standard borosilicate glass petri dishes, which were thicker than the specially-made lightweight borosilicate glass dishes, demonstrated this effect. Due to the extra energy required to raise the temperature of the dish, mass loss rates were delayed for the standard borosilicate glass dishes in comparison to the mass loss rate profiles of the lightweight dishes. In addition, average mass loss rates were somewhat lower for the standard dishes. Similar observations were made when comparing the mass loss rate data obtained using the first lightweight borosilicate glass dish with that obtained using the lighter weight second borosilicate glass dish.

Due to the observation that the thermal mass of the dish had a significant effect on the mass loss rate, an effort was made to minimize thermal mass of the stainless steel dish when it was designed. Although stainless steel has a much higher product of its density with its specific heat than borosilicate glass, the thermal mass of the stainless steel dish was kept at a lower value by reducing its wall thickness. As a result of its lower thermal mass, tests conducted using the stainless steel dish for the low viscosity and 5 cS fluids had average mass loss rates that were consistently higher than those conducted using the borosilicate glass dish. For the intermediate and high viscosity fluids, however, the average mass loss rates were similar for all of the dishes.

Although the average mass loss rates of the intermediate and high viscosity fluids were similar for the borosilicate glass and stainless steel dishes, differences in the transient mass loss rate behavior were observed. The most significant difference that was observed was the appearance of a bimodal peak in the mass loss rate for the tests conducted with the borosilicate glass dishes. This bimodal peak replaced the single broad peak observed in the mass loss rate tests conducted with the stainless steel dish. As with the stainless steel dish data (see Figure 14), tests conducted with the 50 cS fluid showed that this twin peak shifted toward lower normalized mass values and broadened with decreasing heat flux. It is believed that this difference in behavior could be due to the different surface roughness qualities of the two types of dishes, which affect surface boiling characteristics of the fluids when the fluids are heated.

One other behavioral difference between the borosilicate glass and stainless steel dish tests that was significant was the observation that the borosilicate glass initially had a catalytic effect on the mass loss rate of the intermediate and high viscosity fluids. The first indicator of this effect was the observation that the mass loss rates measured during the first few tests conducted with the new borosilicate glass dishes were considerably higher than those measured later. The peak mass loss rates for the initial tests were also observed to be significantly higher. Using the stainless steel dish with a borosilicate glass fragment inside, a few tests were conducted using 50 cS fluid to investigate this catalytic effect. Tests conducted with fresh borosilicate glass fragments had average mass loss rates that were almost twice as high as tests conducted without the borosilicate glass fragments. Additionally, peak mass loss rates were nearly three times higher than their non-catalyzed counterparts. After the borosilicate glass fragments had been used once, their effect on subsequent tests was minimal. This result indicates that the catalyzing agent associated with the borosilicate glass is removed during the gasification process. It is believed that the catalyzing agent for these tests is sodium which is present in the borosilicate glass. Sodium is known to be a strong catalyst for PDMS pyrolytic degradation via siloxane bond rearrangement..

Toluene, which was used to clean the dishes after each test, was also observed to have a slight catalytic effect on the pyrolysis process of the intermediate and high viscosity fluids. This minor effect, although similar to that of the new borosilicate glass, was not as severe. As a result of this observation, however, care was exercised to remove all residual toluene from the dish prior to each test by careful wiping and heating the dishes.

The dish height and nitrogen purge flow rate together also significantly influenced the flow pattern surrounding the dish, in turn, produced two effects: (1) the thickness of the vapor layer that formed above the fluid surface and consequently amount of blocking of the incident radiant flux, and (2) changed convecting cooling of the hot fluid surface by the room temperature nitrogen flow.

Despite the existence of all of the experimental sensitivities described in this report, experiments conducted under the same experimental conditions in this study were remarkably repeatable. Methods used to correct for these sensitivities are believed to have produced reliable measurements of the mass loss rate from which reasonable estimates of the global heat of gasification were made.

6. CONCLUSIONS

1. Silica particles are not formed during the gasification and the degradation of the siloxane fluids.

2. The gasification of siloxanes occurs via two modes or combinations thereof: 1) volatilization of molecular species native to the polymer, and 2) volatilization of cyclic molecules which result from the thermally induced degradation of the polymer via siloxane bond rearrangement. The former process dominates for low molecular weight siloxanes (< 10 cS) and the latter process dominates

for high molecular weight siloxanes (> 1,000 cS). For the intermediate molecular weight siloxanes, both volatilization and degradation processes occur.

3. The average gasification rate of all siloxanes studied in this work increases linearly with an increase in external radiant flux. The global heat of vaporization of unit mass of siloxanes increases with an increase in the molecular weight of the siloxanes up to a 50 cS fluid and its value remains constant at about 1,200 J/g for all higher molecular weight dimethylsiloxanes.

4. Extreme care is necessary measuring the global heat of vaporization due to effects of: (1) absorption of external radiation by the gasification products, (2) heat sink and loss of heat through a sample container, (3) reradiation loss and convective heat loss from the sample surface during the gasification period.

5. The volatility of siloxanes contrasts sharply with that for organic molecules in that the energy associated with gasification (heat capacity and heat of vaporization) is markedly lower for siloxanes than for organics of equivalent molecular weight. The dominant gasification regime or combination of regimes depends upon the molecular sizes of species in the original polymer and the stage of the gasification. Based on these findings, improved fire resistant silicones will result from: 1) the elimination and/or minimization of low molecular weight species (<5000 g/mol) in the polymer, and 2) enhanced thermal stability to forestall thermally induced degradation and formation of volatile cyclics.

ACKNOWLEDGMENTS: This work was conducted under a CRADA between NIST and Dow Corning Corporation. We would like to acknowledge technical assistance of Mr. Ken Steckler and Dr. Steve Ritchie of BFRL/NIST and Ms. Cynthia Gould (GLC), Mr. Mark Reiter (GPC), Drs. Ron Tecklenburg (MS) and Michael Lee (model polymer) of Dow Corning Corporation.

References:

1. Buch, R.R., *Fire Safety J.*, 17:1(1991).

2. Hemstreet, R.A., "Flammability Tests of Askarel Replacement Transformer Fluids," prepared for National Electrical Manufacturers Association, 2102 L Street N.W., Suite 300, Washington, D.C. 20037, FMRC Serial No. 1A7R3.RC, FMRC No. RC78-T-43, August, 1978.

3. Kanakia, M., Characterization of transformer fluid pool fires by heat release rate calorimetry. Presented at the 4th Int. Conf. Fire Safety, Univ. of San Francisco, 1979.

4. Tewarson, A., Lee, J. L., and Pion, R. F., "Fire Behavior of Transformer Dielectric Inslating

Fluids," prepared for US Department of Transportation, Kendall Square, Cambridge, MA 02142, Report # FRA/ORD-80/08, January, 1980.

5. Buch, R.R., Hamins, A., Konishi, K., Mattingly, D., and Kashiwagi, T., *Comb. Flame*, 108:118-126(1997).

6. Lipowitz, J., *J. Fire Flamm.*, 7:482(1976).

7. Lipowitz, J. and Ziemelis, M.J., *J. Fire Flamm*, 7:504(1976).

8. Johannson, O. K. and Lee, C. L., "Cyclic Siloxanes and Silazanes," Chapter 6, High Polymers, Frisch, H. C. editor, Volume XXVI, Wiley-Interscience, 1972.

9. Grassie, N. and Macfarlane, I G., *Europ. Pol. Jour.* 14: 875-884(1978).

10. Zeldin, M., Kang, D. W., Rajendran, G. P., Qian, B., and Choi, S. J., *The Science of the Total Environment*, 73:71-85(1988).

11. Siloxane Polymers, edited by Clarson, S. J. and Semlyen, J. A., Chapters 3 and 5, P T R Prentice-Hall, 1993.

12. Steciak, J. and Tewarson, A., "Flammability Characteristics of Dielectric Insulating Fluids and Resins," prepared for Dow Corning Corporation, Midland MI, Report No. FMRC J.I.0M2R2.RC, April, 1992.

13. Tecklenburg, R. E., "The Use of Atmospheric Pressure Ionization Mass Spectrometry for the Rapid and Reliable Structural Identification of Silicones," 52nd Annual ACS Fall Scientific Meeting, Delta College, University Center, MI, October 26, 1996.

14. Kashiwagi, T., Omori, A. and Nanbu, H, *Comb. Flame,* 81:188-201 (1990).

TABLE 1.

FLUID-POLYMER PROPERTIES

FLUID	COMP'N. (1)	MW	BP(C)	Q[kJ/kg]	ΔH_v [kJ/kg]	G_f [kJ/kg] (2)
0.65cS	MD_0M	162	100	158	193	351
1.0 cS	MD_1M	237	153	250	153	403
1.5 cS	MD_2M	311	194	324	130	454
2.0 cS	MD_3M	385	230	391	115	506
2.3 cS	D_4	296	176	286	130	416
	D_5	370	211		113	
	D_6	444	245		101	
	D_7	518	276		92	
	D_8	592	303		84	
	D_9	666	326		79	
	MD_4M	459	260	447	104	550
	MD_5M	533	287	494	96	590
	MD_6M	607	311	547	89	636
	MD_7M	681	334	589	83	672
	MD_8M	755	355	635	77	712
5 cS	MD_8M		(3)			
10 cS	$MD_{15}M$		(3)			
20 cS	$MD_{28}M$		~375(4)			~3300
50 cS	$MD_{58}M$		~375(4)			~3300

(1) $M=(CH_3)_3SiO_{1/2}$, $D=(CH_3)_2SiO$

(2) $G_f = \Delta H_v + Q$, where $Q = \int c_p(T)dT$, and ΔH_v is the heat of vaporization at BP.

(3) Does not exhibit a characteristic boiling point.

(4) Approximate onset temperature for thermal degradation (reversion) to volatile cyclics (D_3, D_4, ..., D_n); $\Delta H_{DEPOL'N.} \approx$ 170-210 kJ/mole

(5) MMA = methylmethacrylate

TABLE 2

TERMINAL END-GROUP ANALYSIS-ORIGINAL AND RESIDUAL FLUIDS
REPEATABILITY-GASIFICATION/SAMPLING/TRAPPING/ANALYSIS

FLUID	%RESIDUAL	M_N(GPC)	M_W/M_N	M^1 [Calc'd.]	M^2 [Meas'd.]	T^3 [Meas'd.]
SERIES I						
50 cS	100	3,540	1.44	45,800	43,500	230
" "	37	5,590	1.26	29,000	29,300	319
" "	37	5,550	1.26	29,200	30,000	466
SERIES II						
50 cS	100	3,540	1.4	45,800	43,500	230
" "	51	6,130	1.2	26,400	25,200	
" "	49	5,400	1.3	30,000	28,700	311
" "	4	17,350	1.4	9,300	8,700	430
" "	25	6,800	1.3	23,800	23,500	366
" "	22	4,650	1.4	34,900	33,500	416
" "	3	14,500	1.3	11,200	10,800	
" "	5	12,500	1.2	13,000	12,900	
SERIES III						
100 cS	100	5,060	1.6	32,000	26,300	125
" "	23	11,700	1.2	13,800	13,900	1,063

60,000 cS	100	55,600	1.9	2,900	2,400	183
" " "	5	30,000	2.1	5,400	2,960	4,400

---

1. $M[ppm] = [2x81 \div M_n(GPC)]x10^6$

2. M[ppm]= M-content as measured analytically via "EOS Derivatization Method"

3. T[ppm]= T-content as measured analytically via "EOS Derivatization Method"

TABLE 3

VOLATILES ANALYSIS/CHARACTERIZATION-GPC

POLYMER	50 cS		10^3 cS		10^4 cS		$6x10^4$ cS		MODEL	
Mass Loss Range	POLY	CYC	POLY	CYC	POLY	CYC	POLY	CYC	POLY	CYC
100-->98	90	10	62	38	70	30	20	80	7	93
			49	51						
95-->90	-	-	35	65	-	-	14	86	7	93
			32	68						
75-->70	56	44	-	-	21	79	12	88	-	-
55-->50	-	-	12	88	9	91	-	-	9	91
			9	91						
35-->30	26	74	-	-	-	-	-	-	-	-
20-->15	18	82	32	68	18	82	25	75	9	91

TABLE 4

EOS ANALYSIS SUMMARY(M- & T-CONTENT)

FLUID	M_{EOS} (ppm)	M_{GPC} (ppm)	T_{EOS} (ppm)
50 cS			
Original	43,500	45,800	230
Residual (30 g)	27,100	27,900	400
" " (15 g)	23,100	23,800	570
1000 cS			
Original	8,700	12,300	5,200
100-98 Residual	8,750	11,450	5,200
95-90 Residual	8,500	10,900	5,100
50-45 Residual	8,700	12,500	6,100
Residual (20 g)	9,200	14,900	6,900
10,000 cS			

Original	4,300	4,600	180
Residual (7 g)	5,660	9,050	4,100
60,000 cS			
Original	2,550	2,500	200
Residual (15 g)	4,030	7,150	3,550
Model Fluid			
Original	3,150	5,370	n.d.
Residual (15 g)	6,960	13,300	1,120

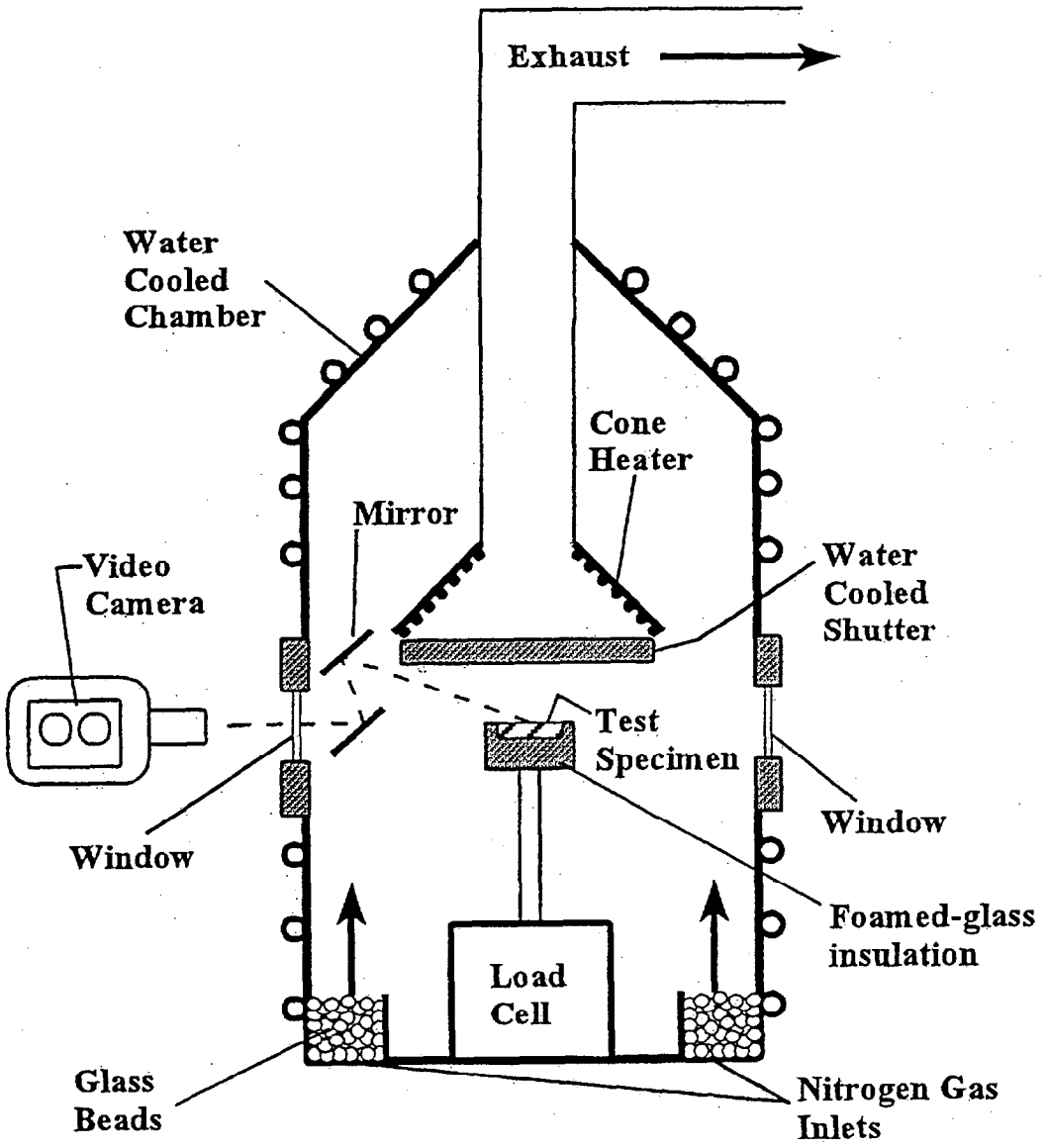

Figure 1. Schematic of Gasification Apparatus.

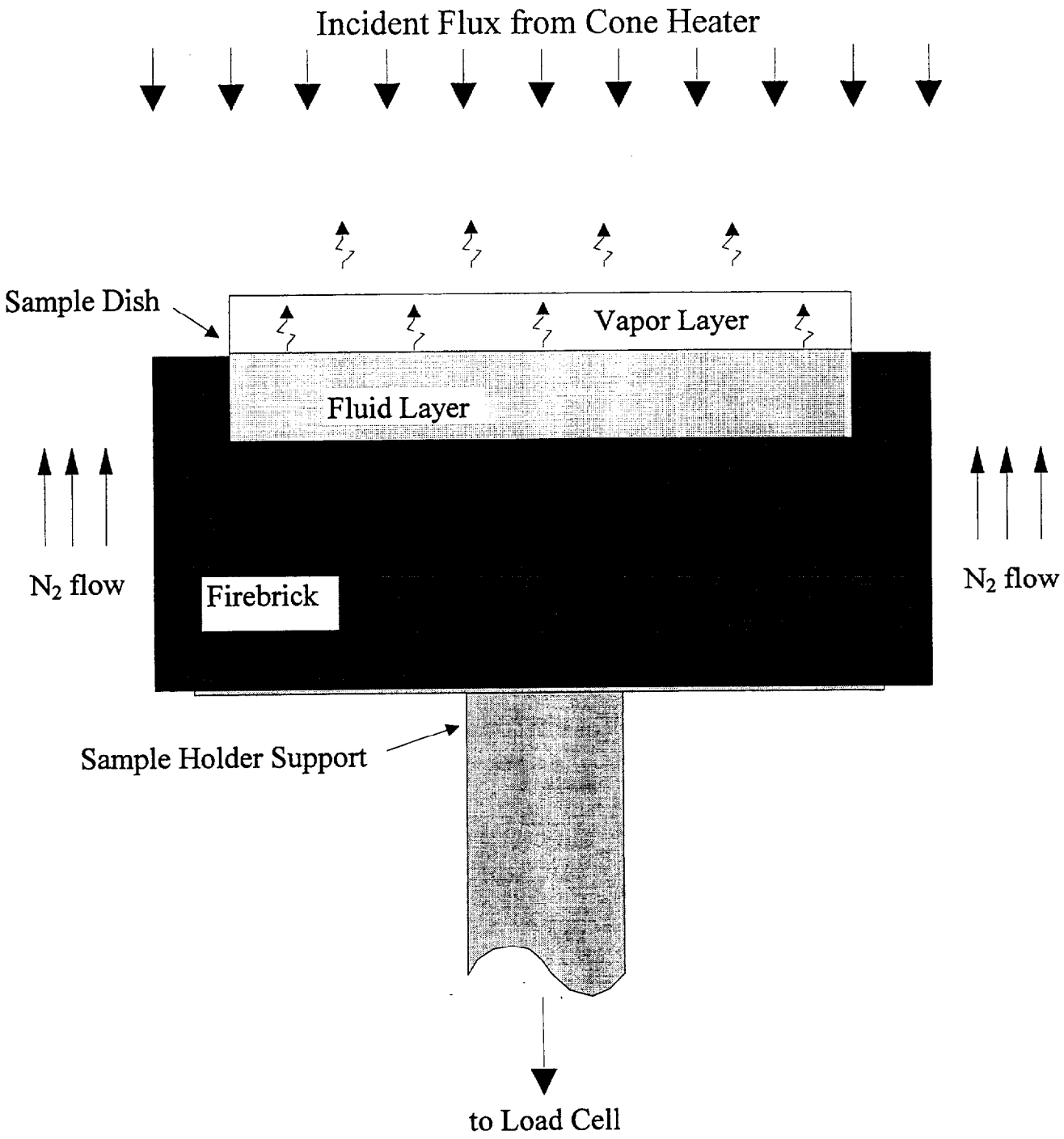

Fig.2 Cross-sectional View of Sample in Holding Apparatus

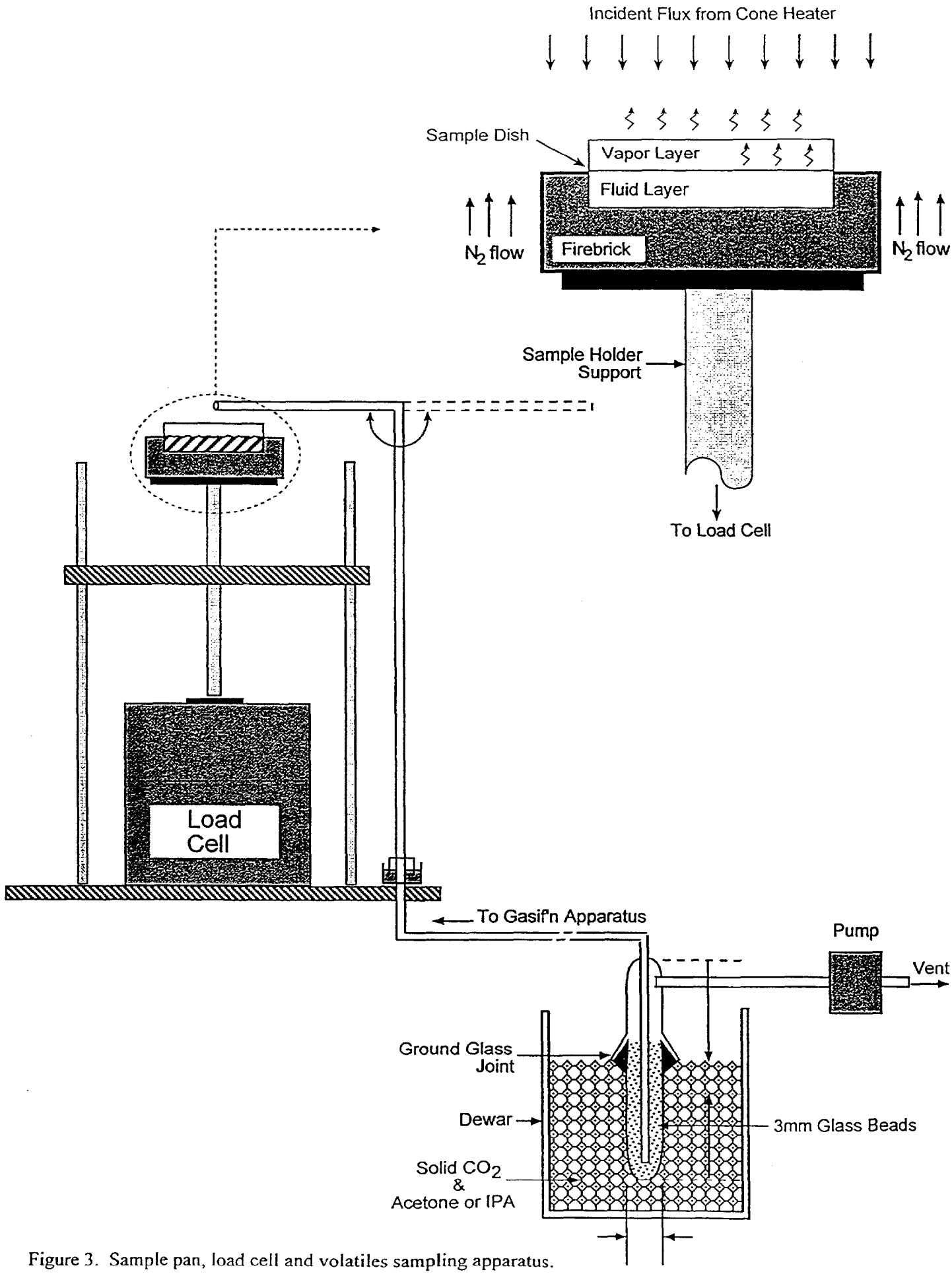

Figure 3. Sample pan, load cell and volatiles sampling apparatus.

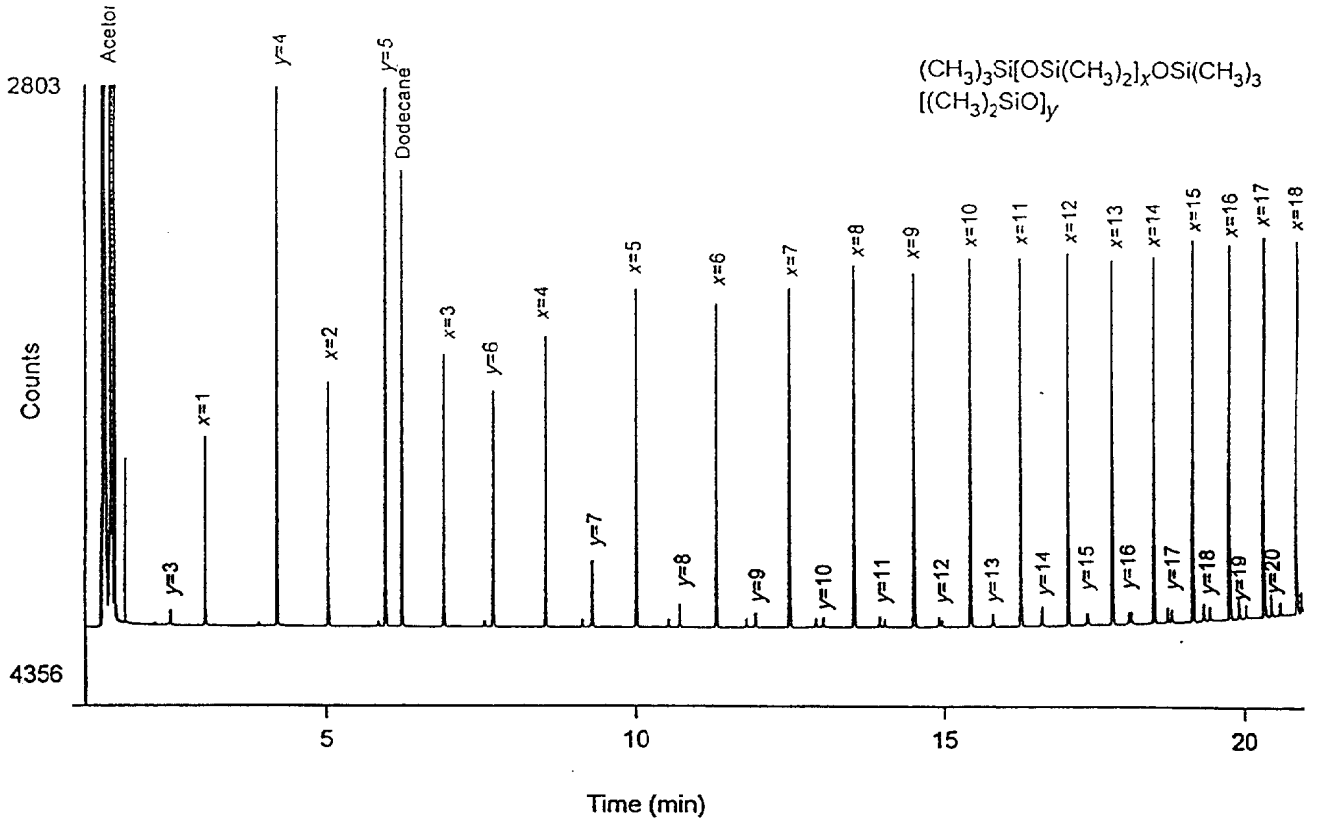

Figure 4. Typical gas chromatogram of "acetone extractables".

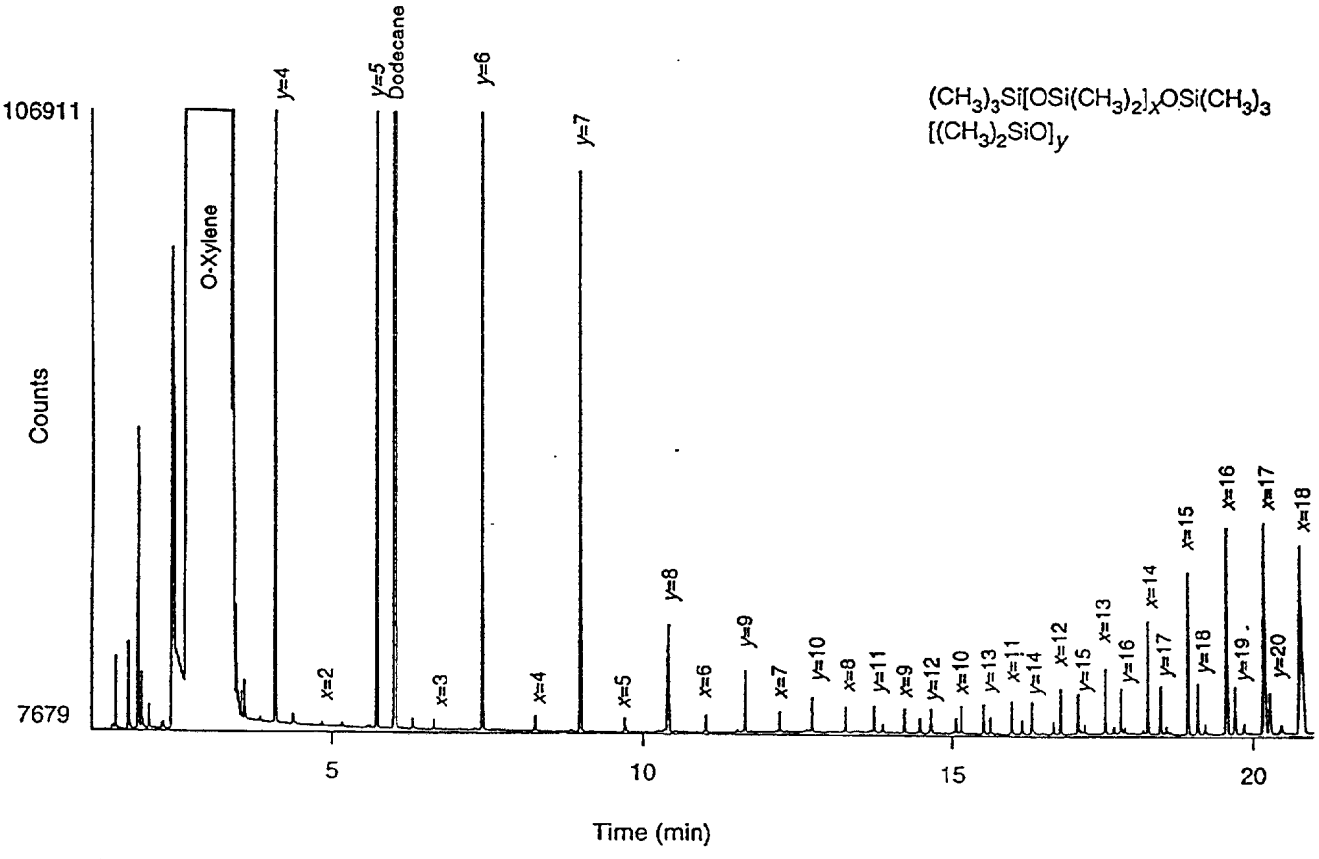

Figure 5. Gas chromatogram of cyclics (D_x, $x \leq 20$) and linears (MD_xM, $x \leq 18$).

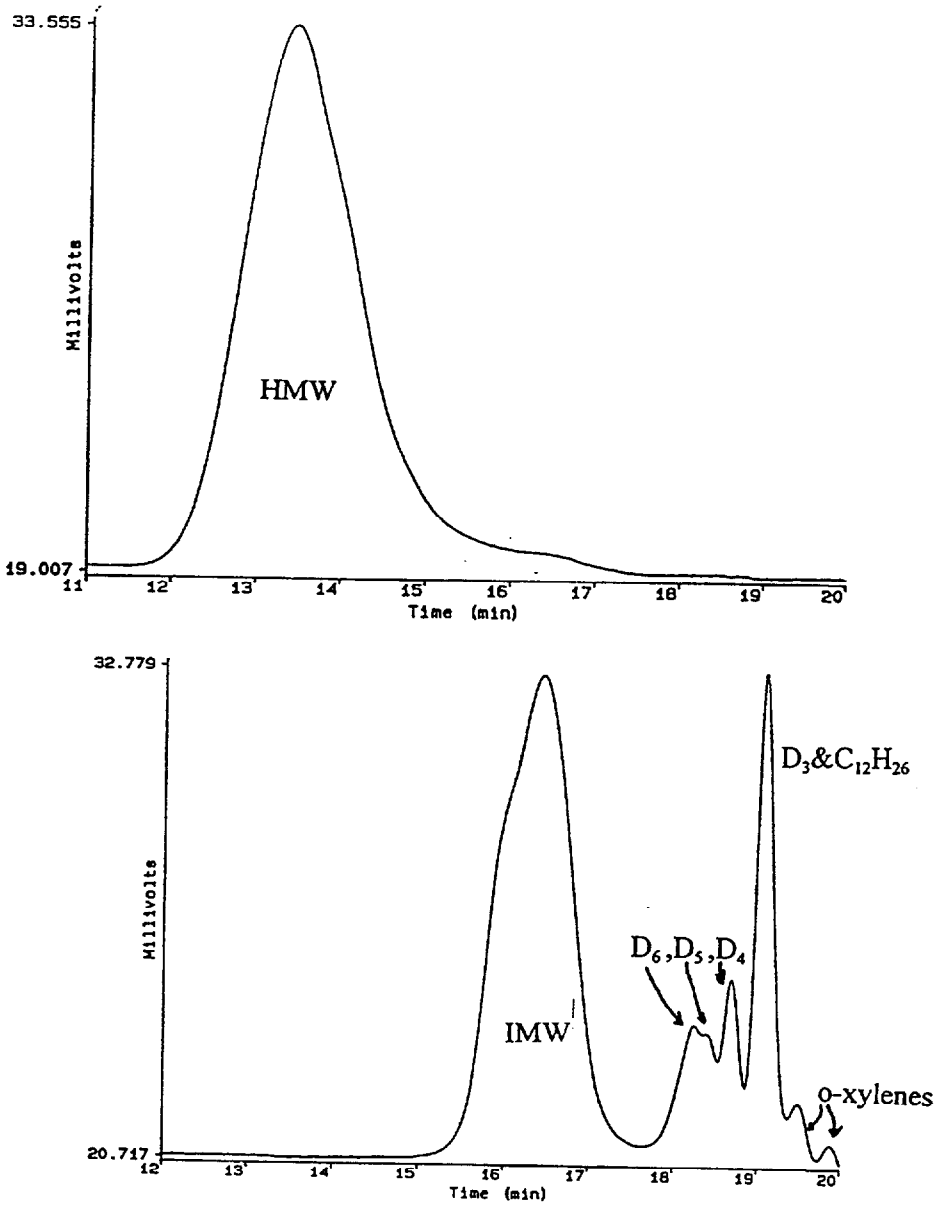

Figure 6. GPC chromatograms of high polymer (HMW); intermediate molecular weight polymer (IMW); 0ligomeric cyclics ($D_{3,.....,6}$), docedane ($C_{12}H_{26}$)-glc internal standard; and o-xylenes (solvent).

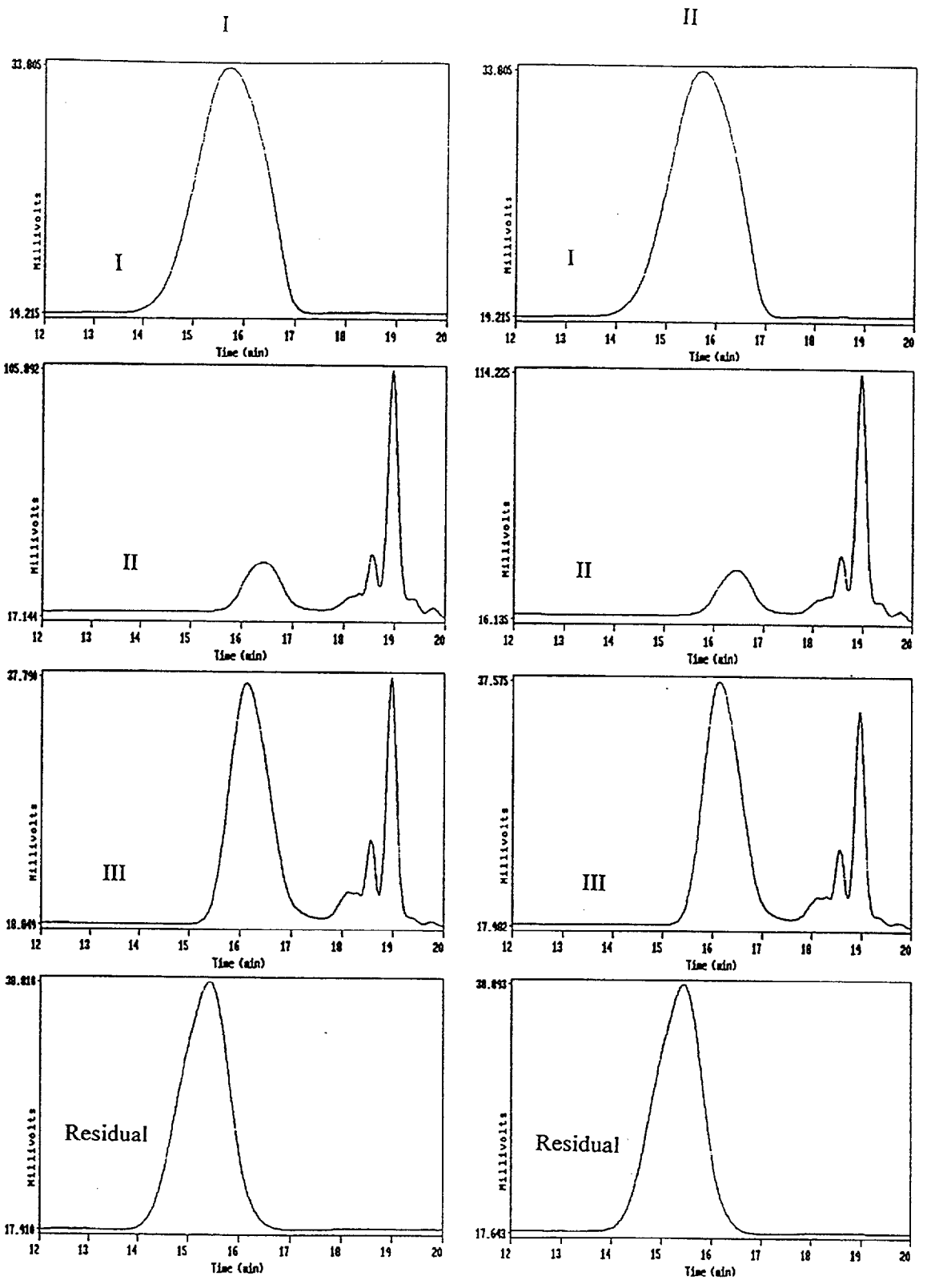

Figure 7. GPC chromatograms of the 50 cs fluid (I), 95-90 g mass loss volatiles (II), 50-45 g mass loss volatiles (III), and residual fluid at termination of the gasification for two successive gasification experiments.

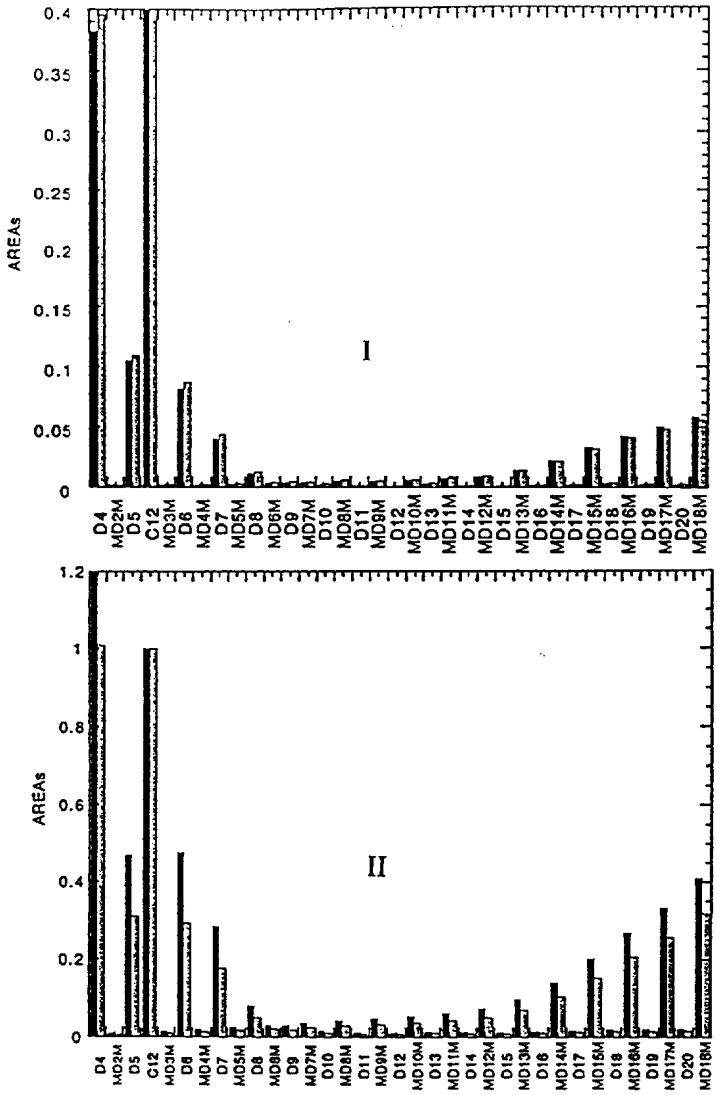

Figure 8. Gas chromatographic analyses of the: 95-90 g. mass loss volatiles(I) and the 50-45 g. mass loss volatiles (II) for two successive gasification experiments of 50 cS fluid.

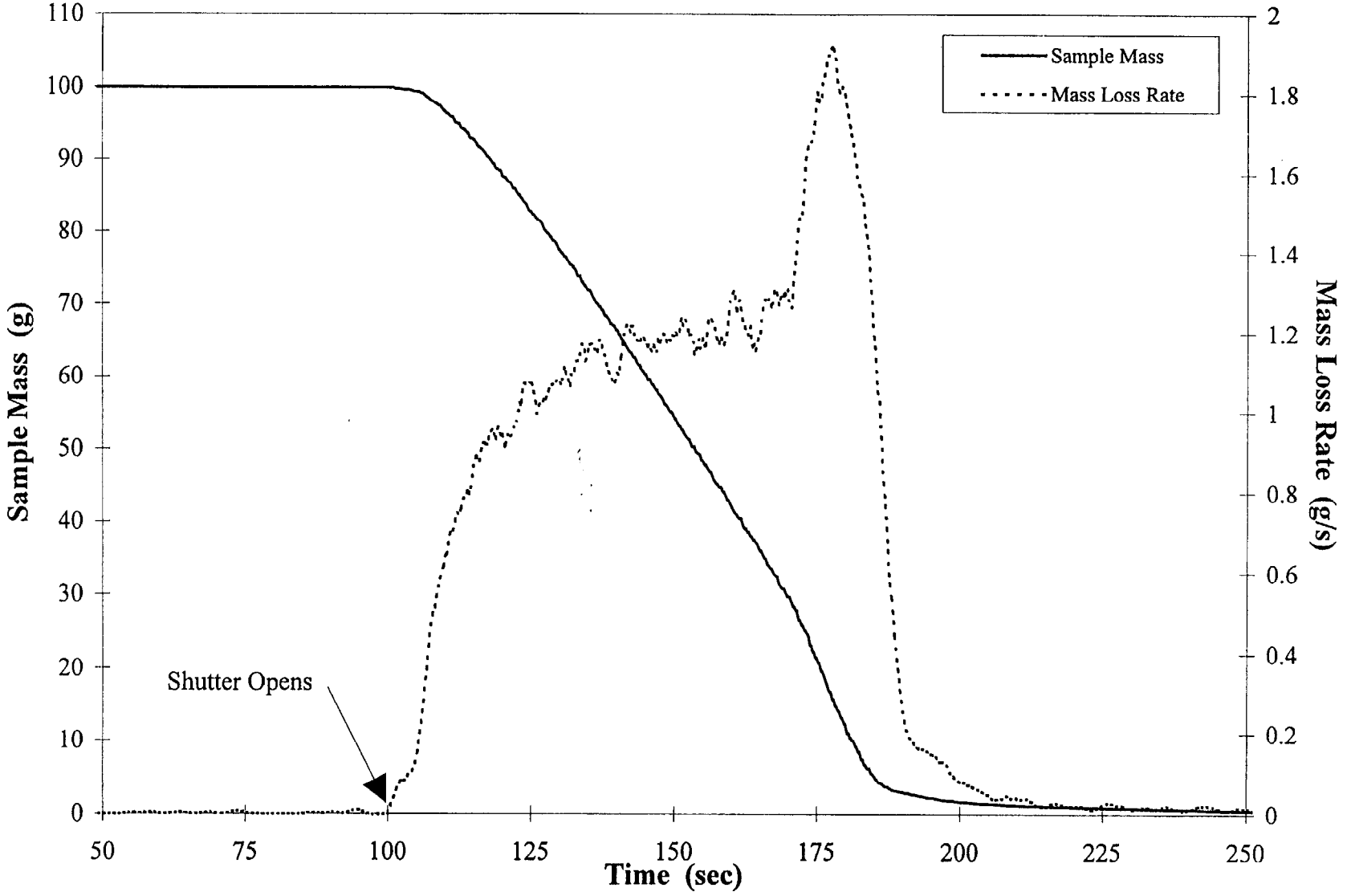

Fig. 9 Sample Mass and Mass Loss Rate as a Function of Elapsed Time for 0.65cs. PDMS 200 Sample Exposed to a Radiant Heat Flux of 70 kW/m^2 in Nitrogen

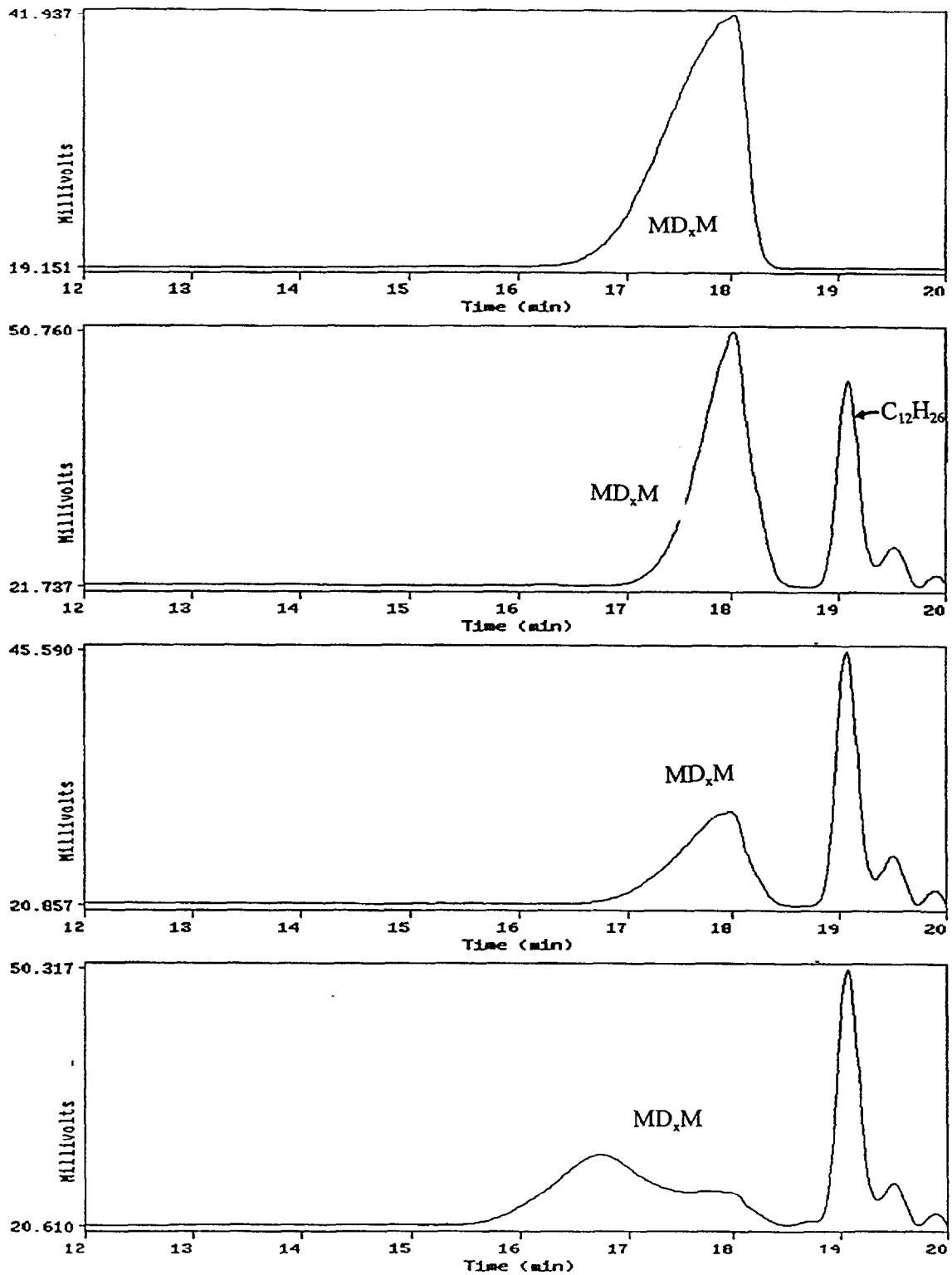

Figure 10. GPC chromatograms of volatiles from 5 cs fluid: 5 cs fluid (I), 100-97 g volatiles (II), 55-50 g volatiles (III), 15-10 g volatiles (IV).

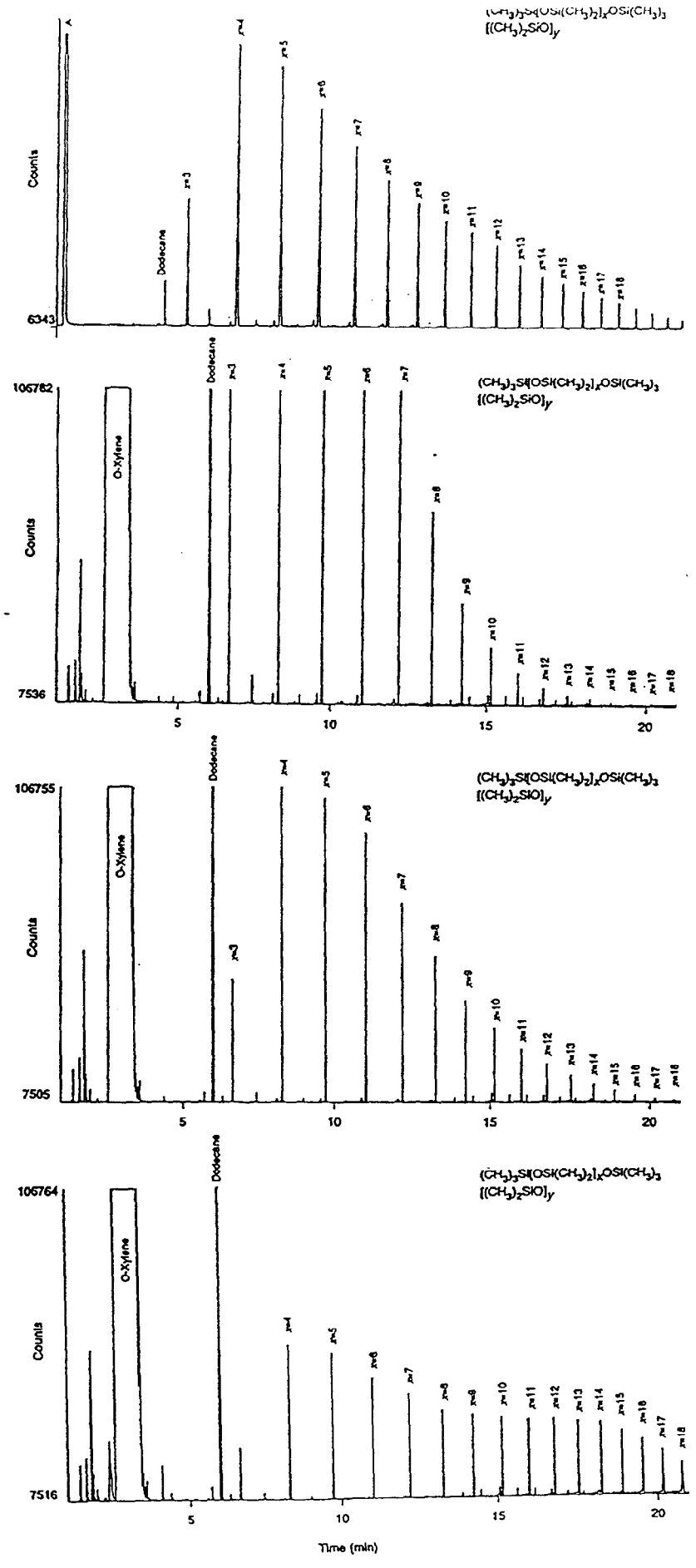

(I)-5 cS Fluid-Original

(II)-100 to 97 g. volatiles

(III)-55 to 50 g. volatiles

(IV)-15 to 10 g. volatiles

Figure 11. Gas chromatographic analysis of volatiles from 5 cS Fluid: I(5cS Fluid), II(100-97)g. volatiles, III(55-50)g. volatiles, IV(15-10)g. volatiles.

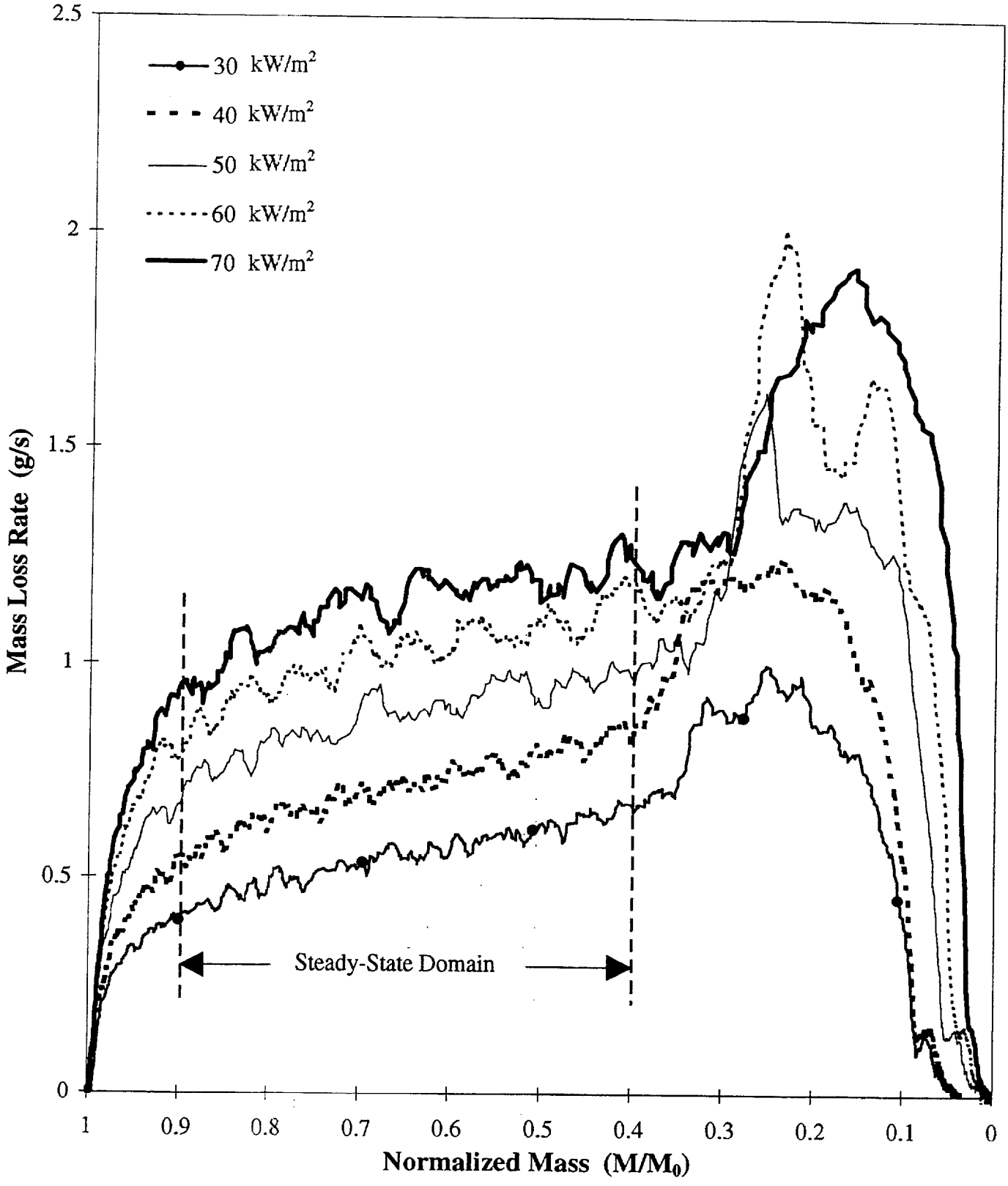

Fig. 12 Sample Mass Loss Rate as a Function of Normalized Mass and Heat Flux for 0.65cs. PDMS-200 Samples in Nitrogen

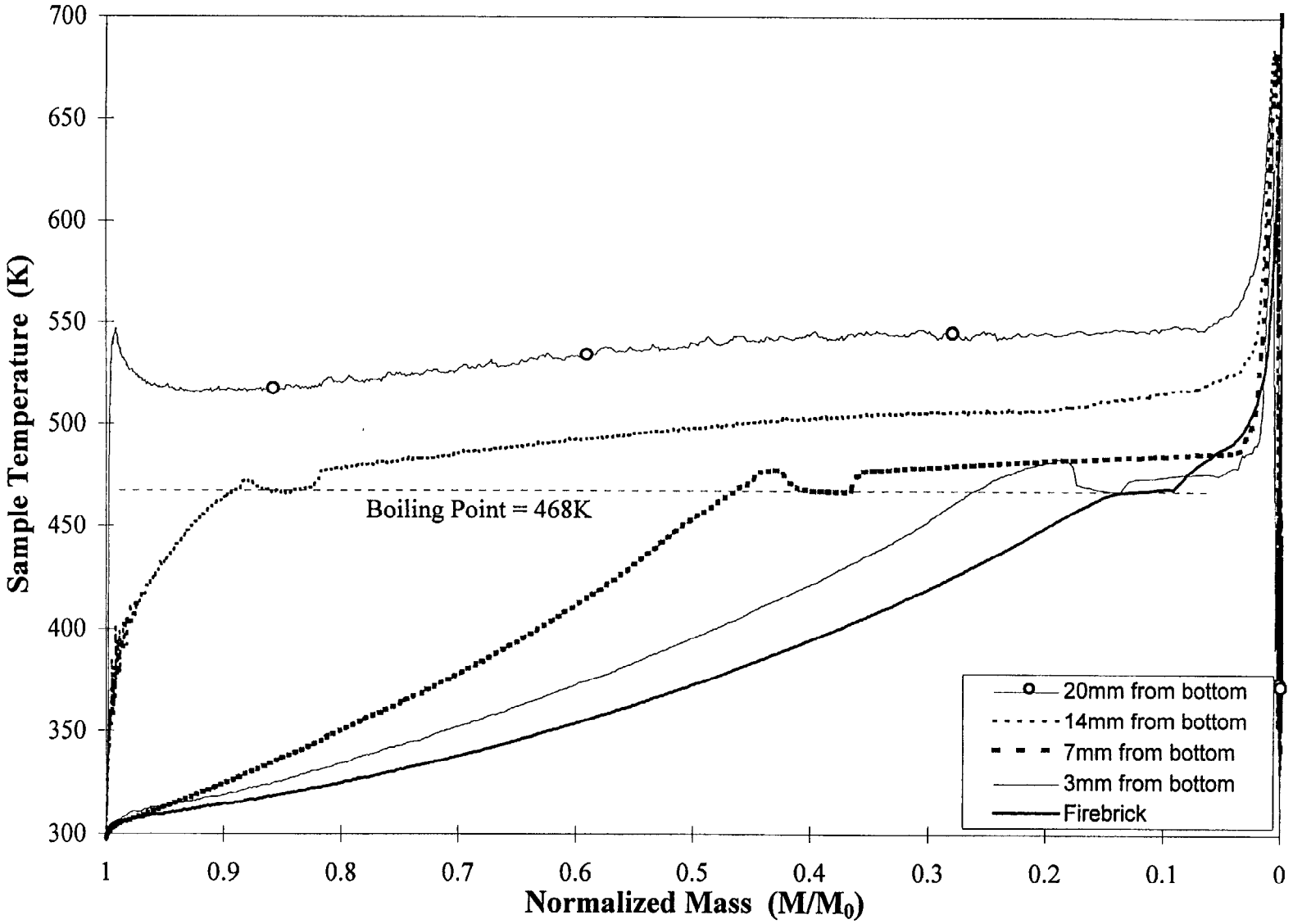

Fig. 13 Sample Temperature as a Function of Normalized Mass and Distance from the Bottom of the Dish for a 1.5cs. PDMS-200 Sample Exposed to a Radiant Heat Flux of 30 kW/m^2 in Nitrogen

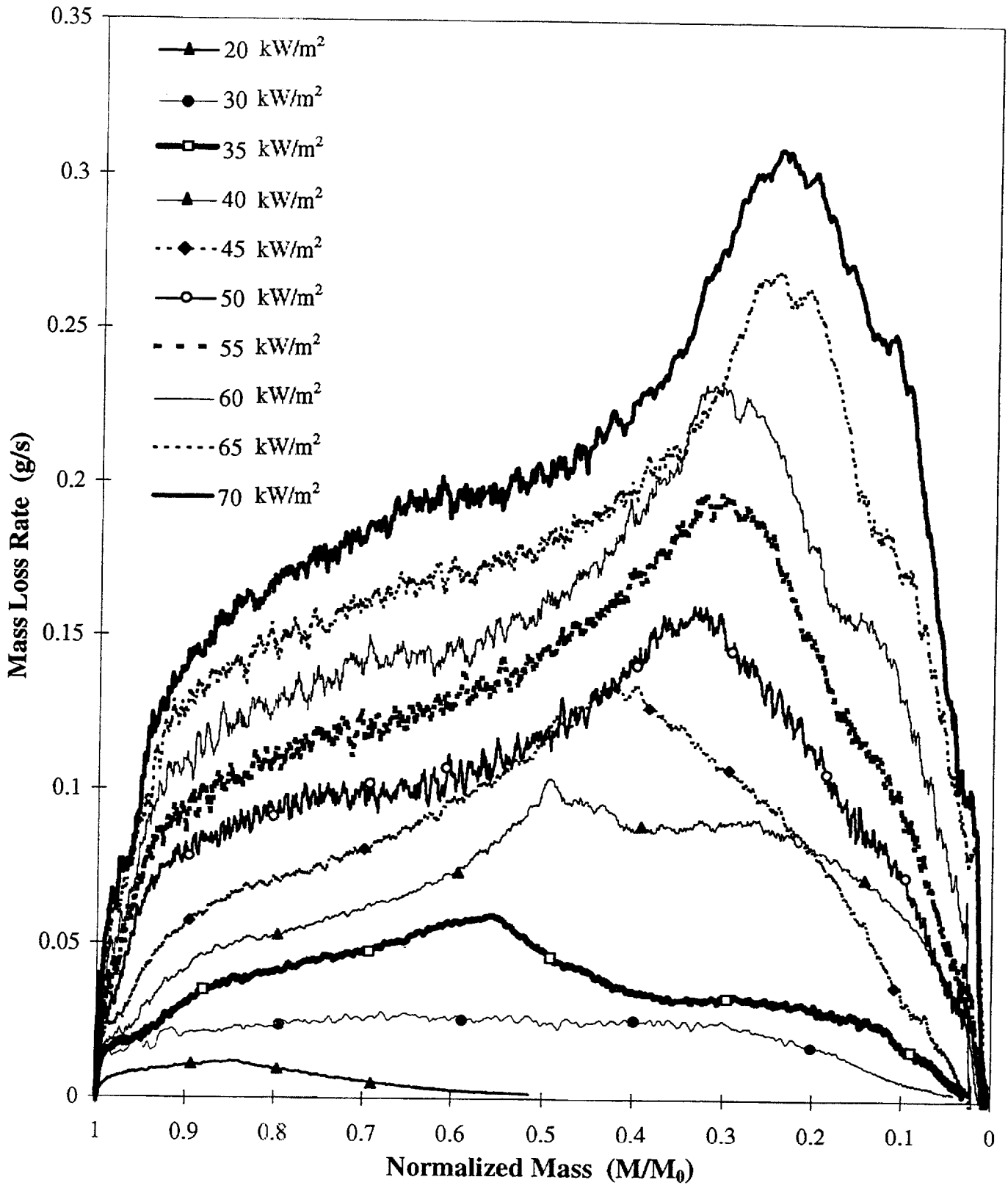

Fig. 14 Sample Mass Loss Rate as a Function of Normalized Mass and Heat Flux for 50cs. PDMS-200 Samples in Nitrogen

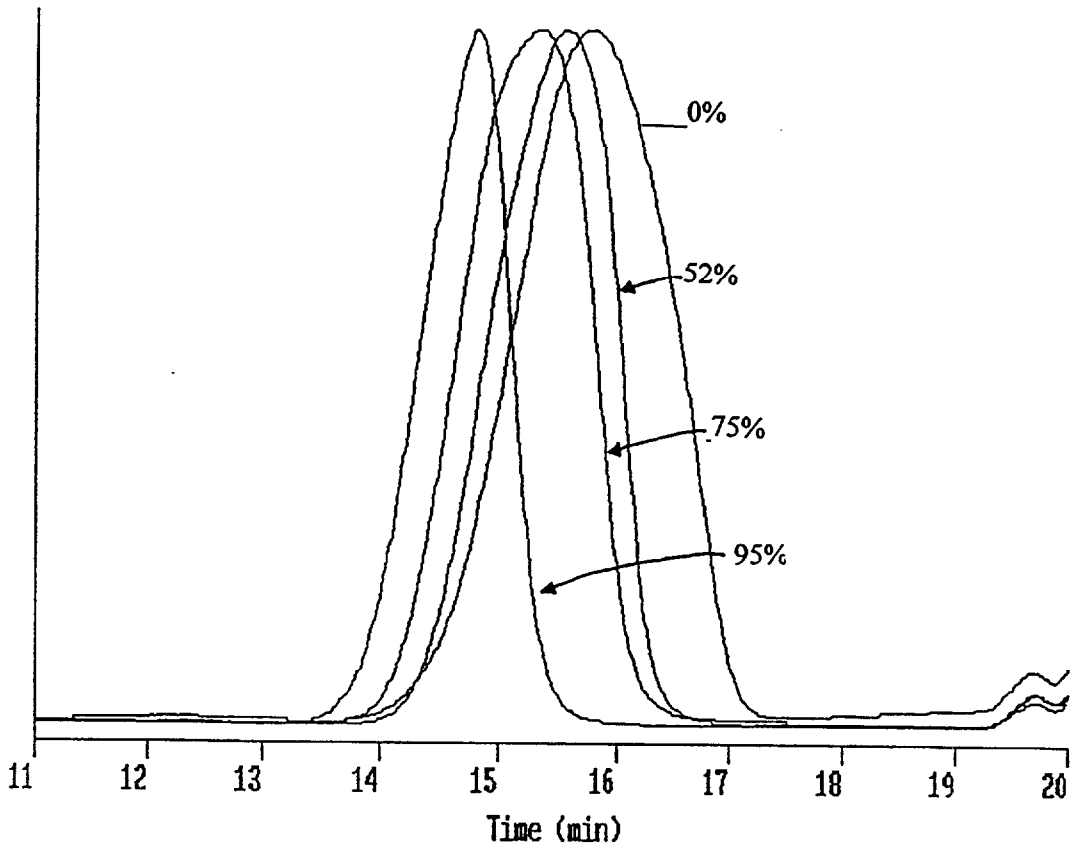

Figure 15. GPC chromatograms of 50 cs *residual fluids* at various stages of gasification (0 %, 52 %, 75 %, 95 %).

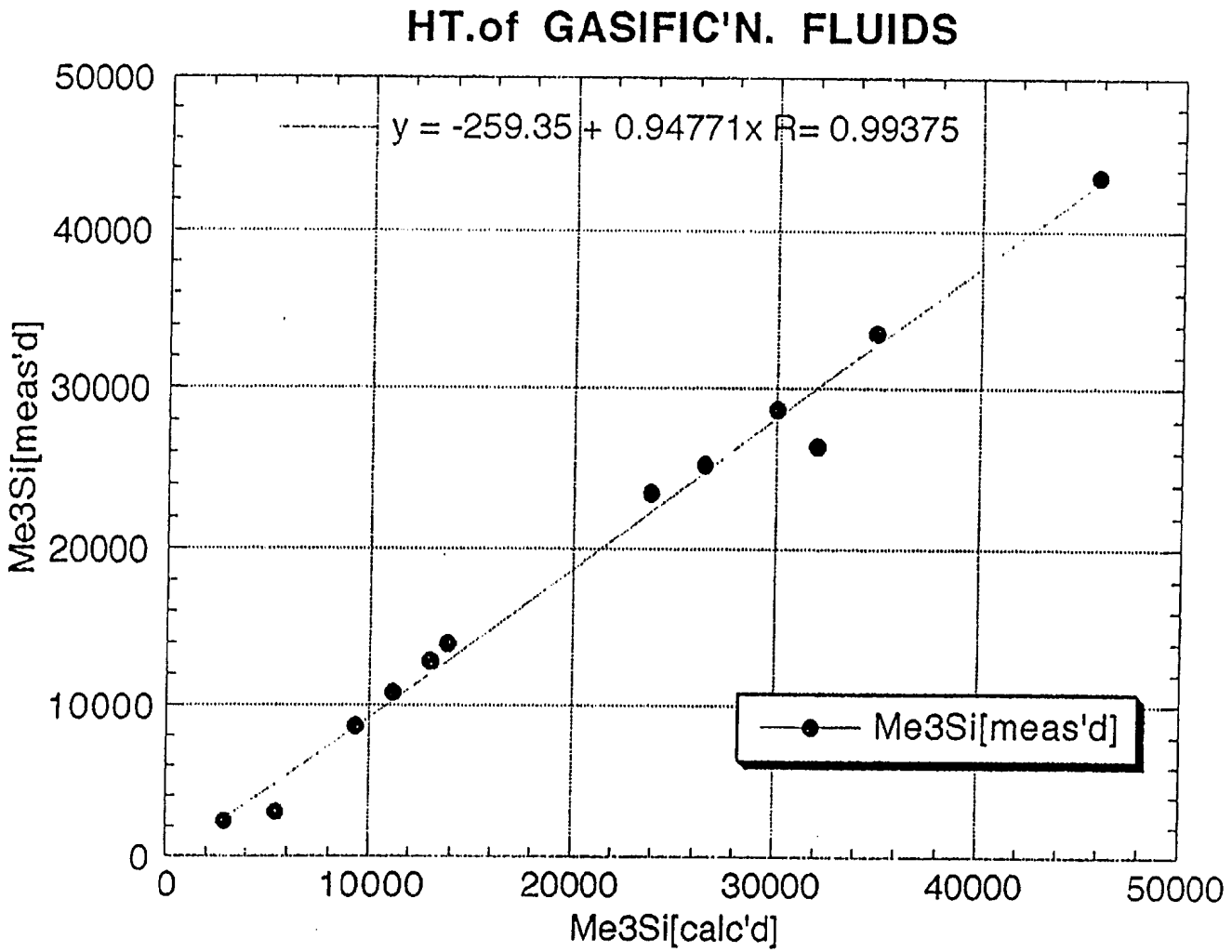

Figure 16. M-content [ppm] measured via EOS derivatization versus M-content [ppm] calculated based on GPC number-average molecular weight.

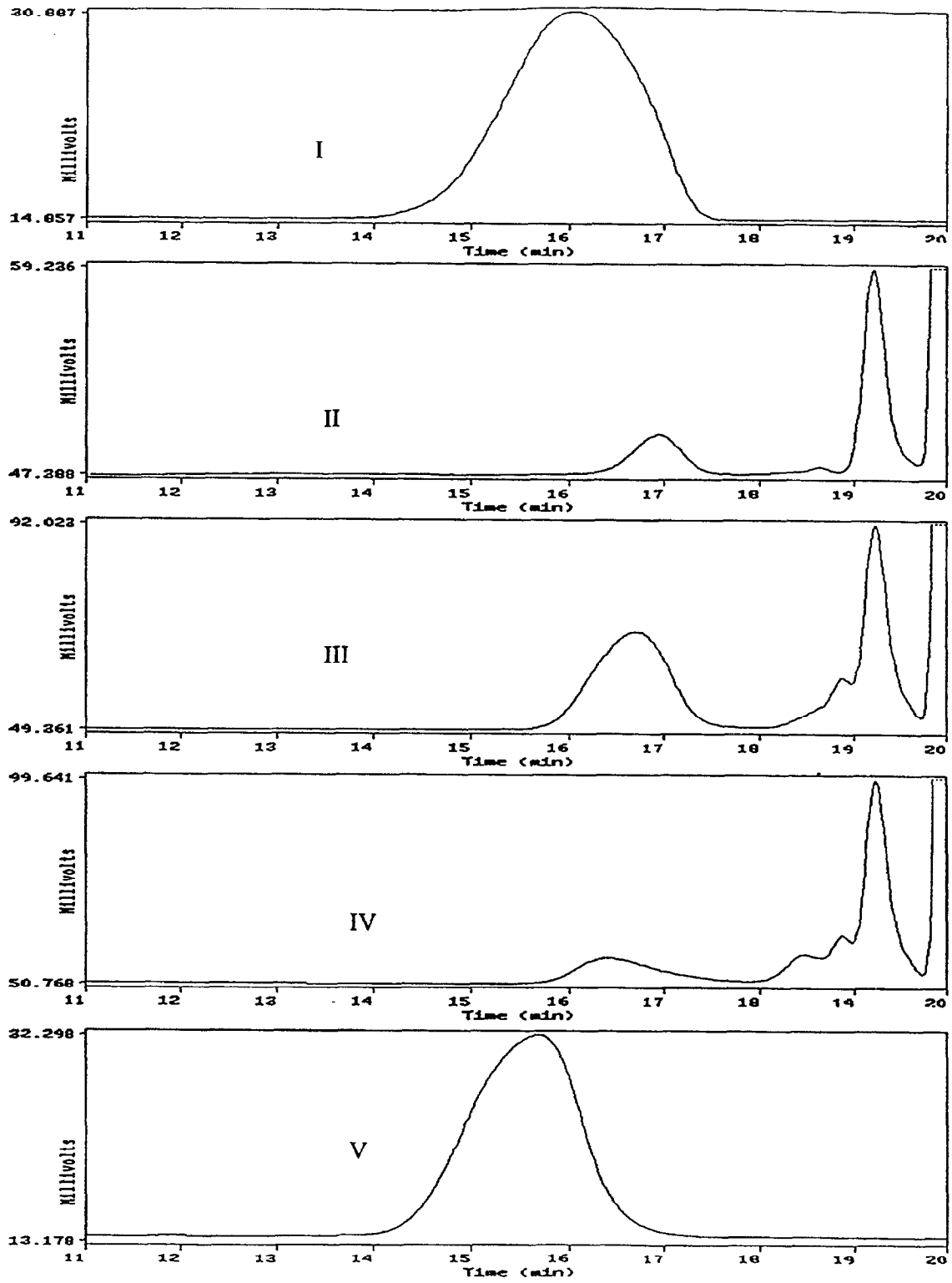

Figure 17. GPC chromatograms of 50 cs (I=original fluid), samples of volatiles at: 100-99 g (II), 75-70 g (III), 35-30 g (IV) and the residual (30 g) fluid (V).

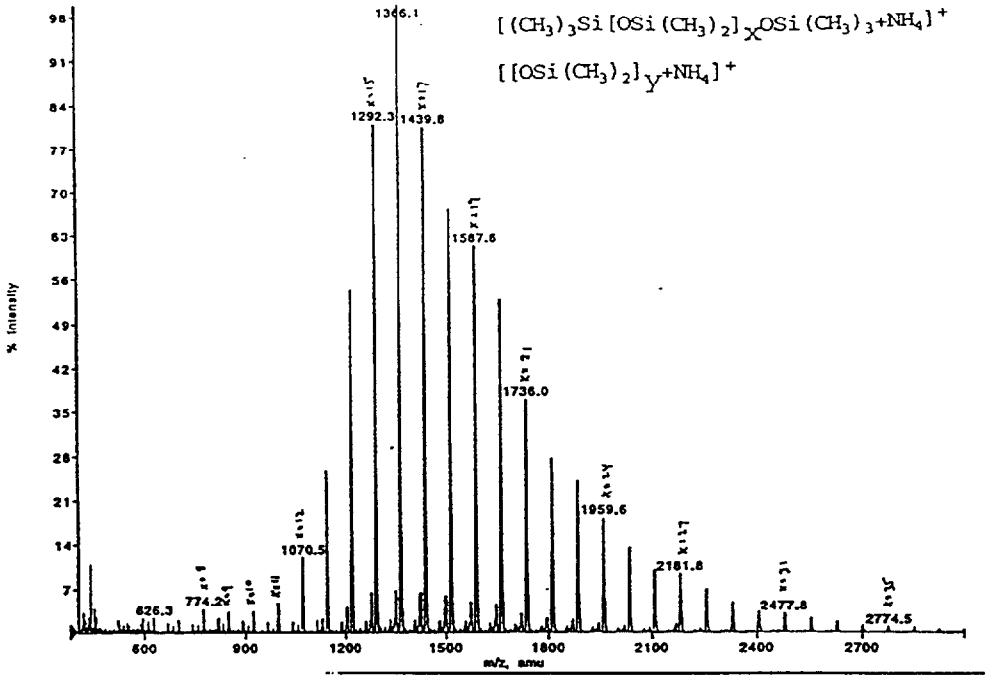

I- 50 cS Original

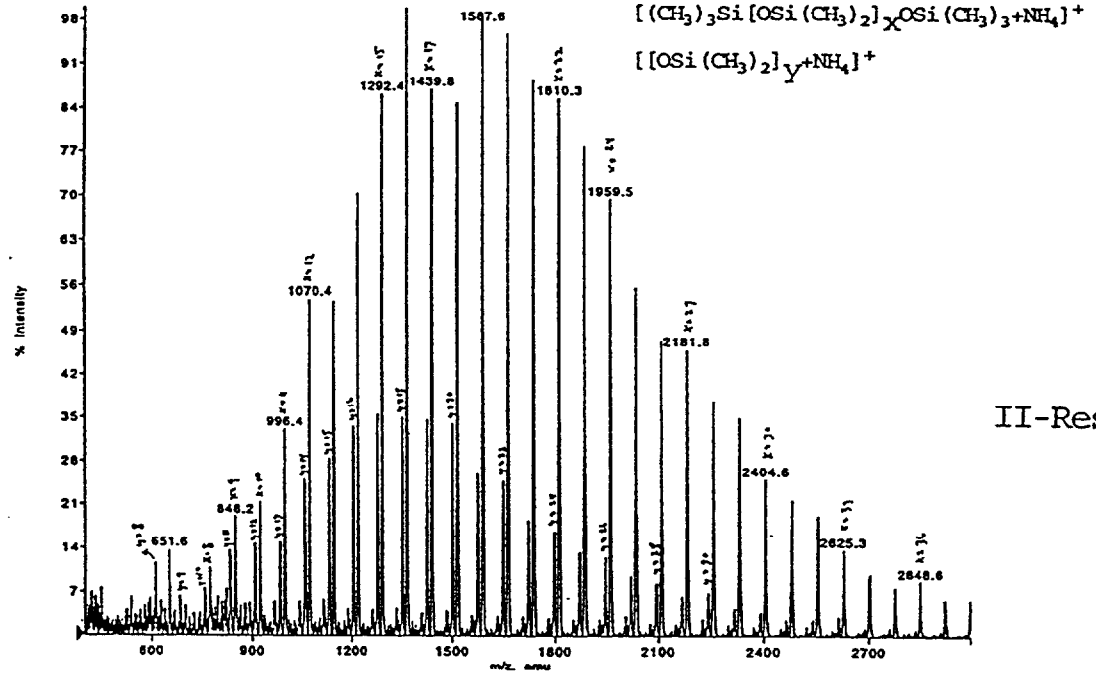

II-Residual Fluid

Figure 18. Mass spectra of 50 cS (I=original fluid), the residual (30 g.) fluid (V), and samples of volatiles{*see next page*} at: 100-99 g. (II), 75-70 g. (III), and 35-30 g. (IV).

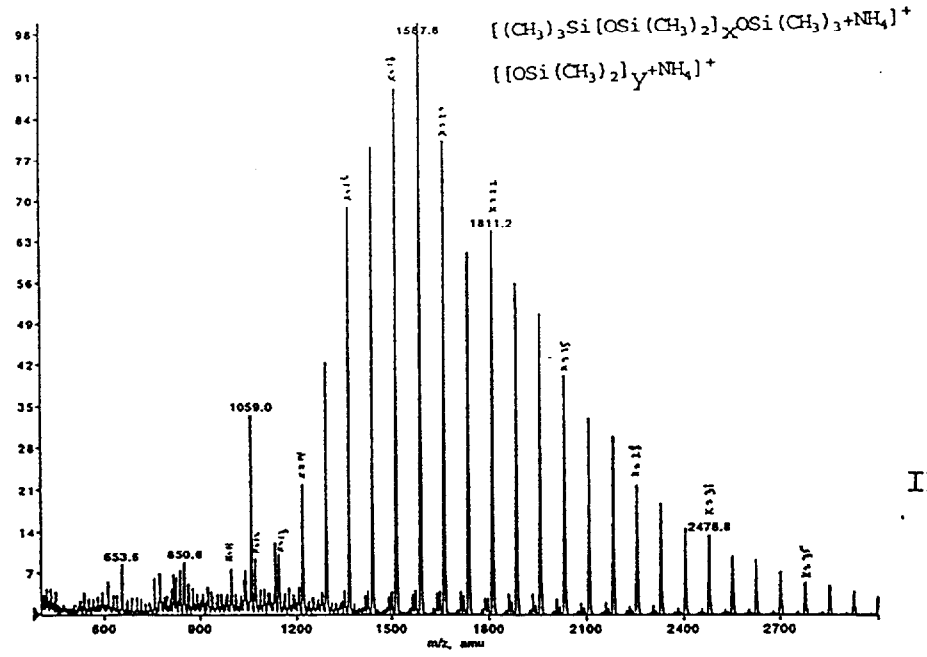

II-100 to 99 g. volatiles

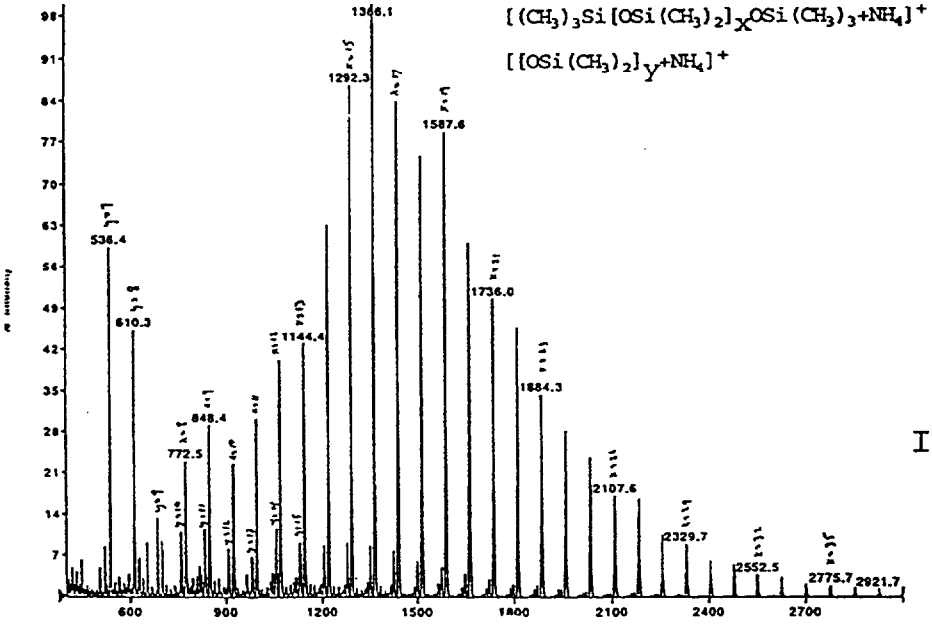

III-75 to 70 g. volatiles

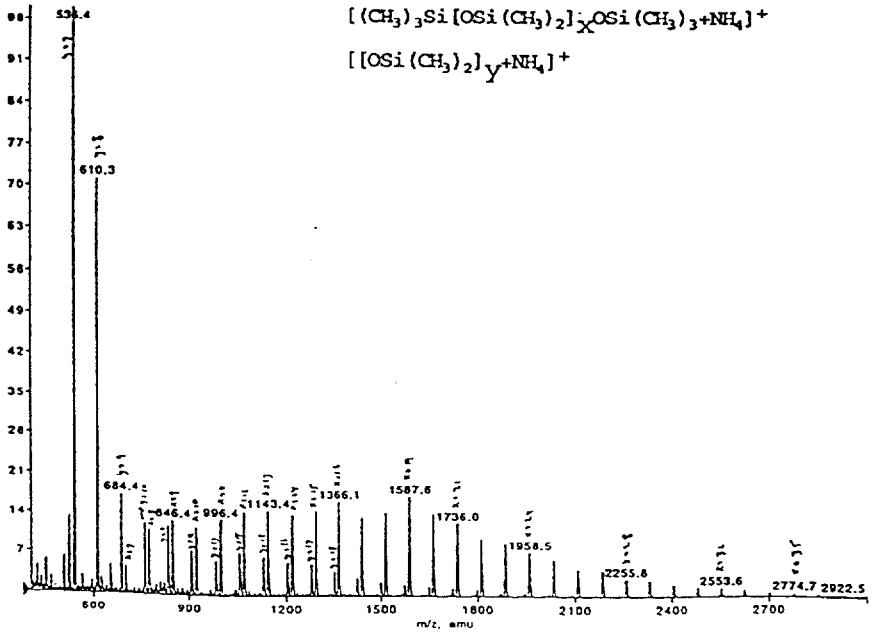

IV-35 to 30 g. volatiles

Figure 18. (cont'd.)

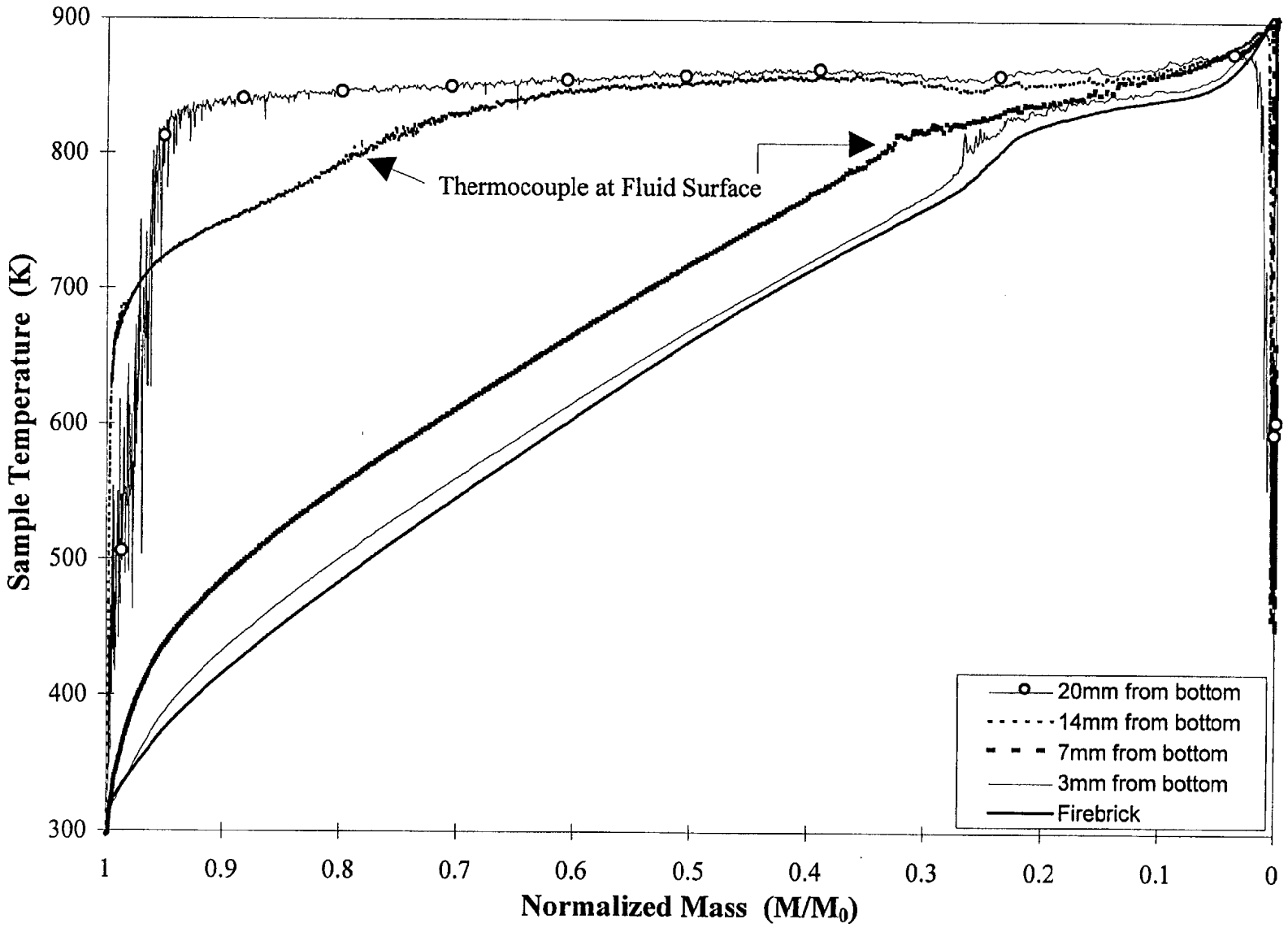

Fig. 19 Sample Temperature as a Function of Normalized Mass and Distance from the Bottom of the Dish for a 50cs. PDMS-200 Sample Exposed to a Radiant Heat Flux of 50 kW/m^2 in Nitrogen

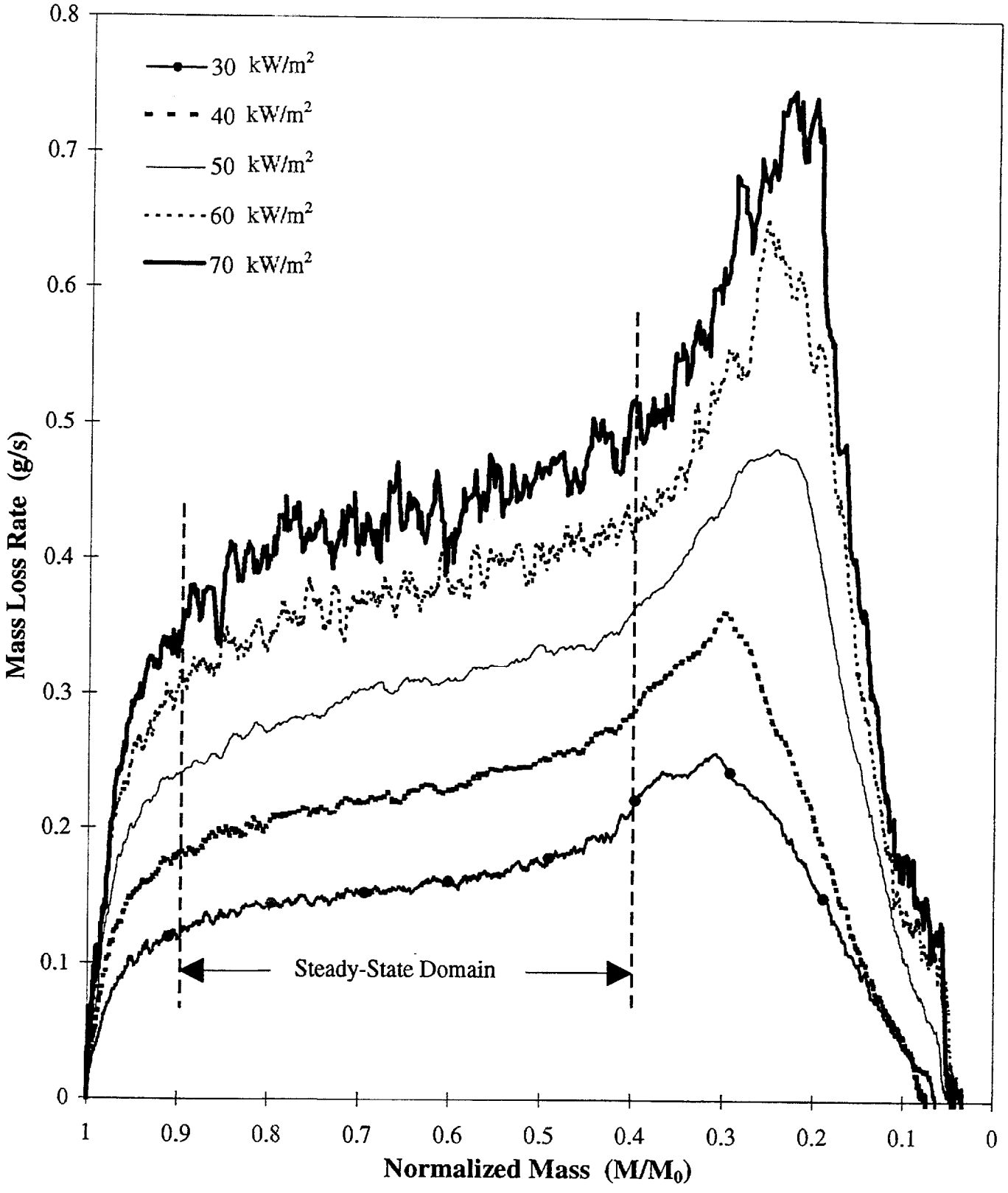

Fig. 20 Sample Mass Loss Rate as a Function of Normalized Mass and Heat Flux for 5cs. PDMS-200 Samples in Nitrogen

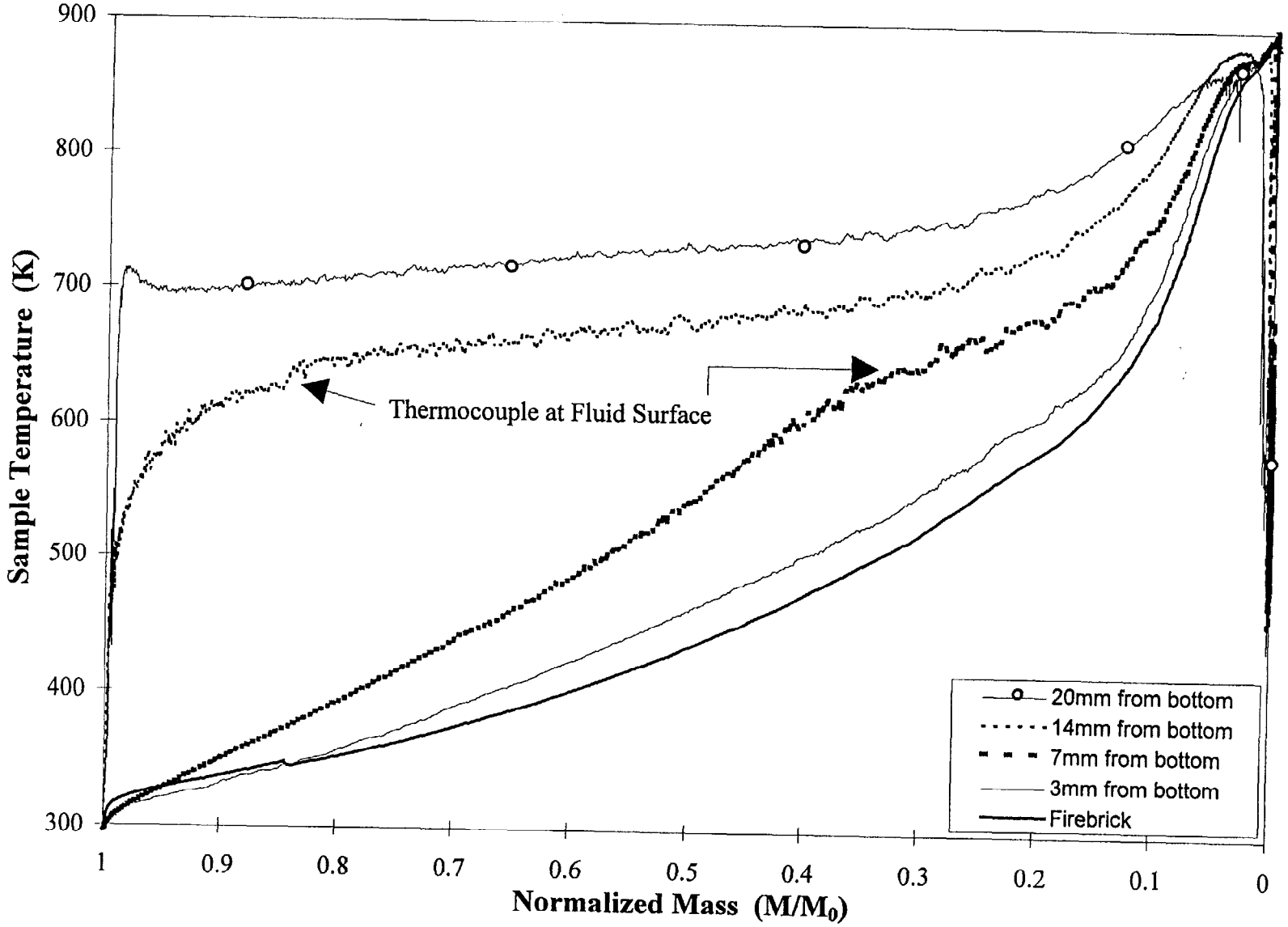

Fig, 21 Sample Temperature as a Function of Normalized Mass and Distance from the Bottom of the Dish for a 5cs. PDMS-200 Sample Exposed to a Radiant Heat Flux of 50 kW/m^2 in Nitrogen

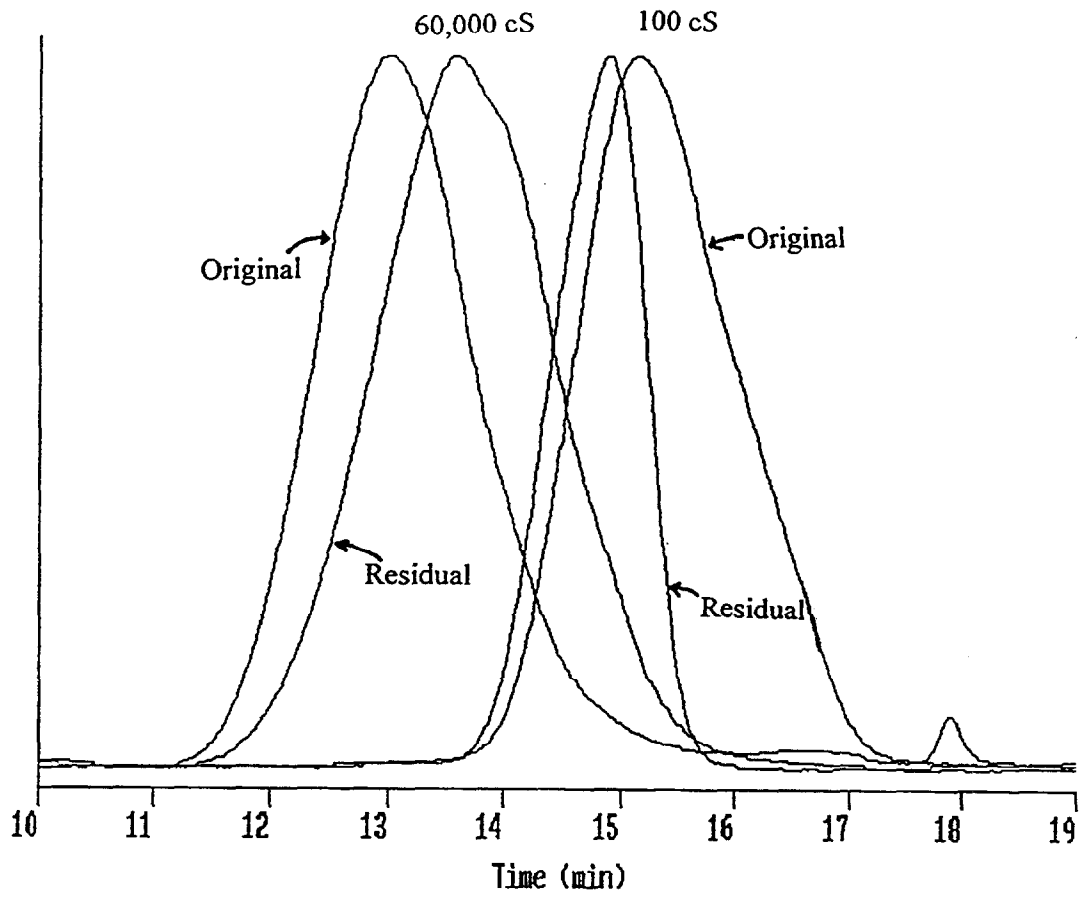

Figure 22. GPC chromatograms of original and residual fluids for 100 cs and 60, 000 cs fluids.

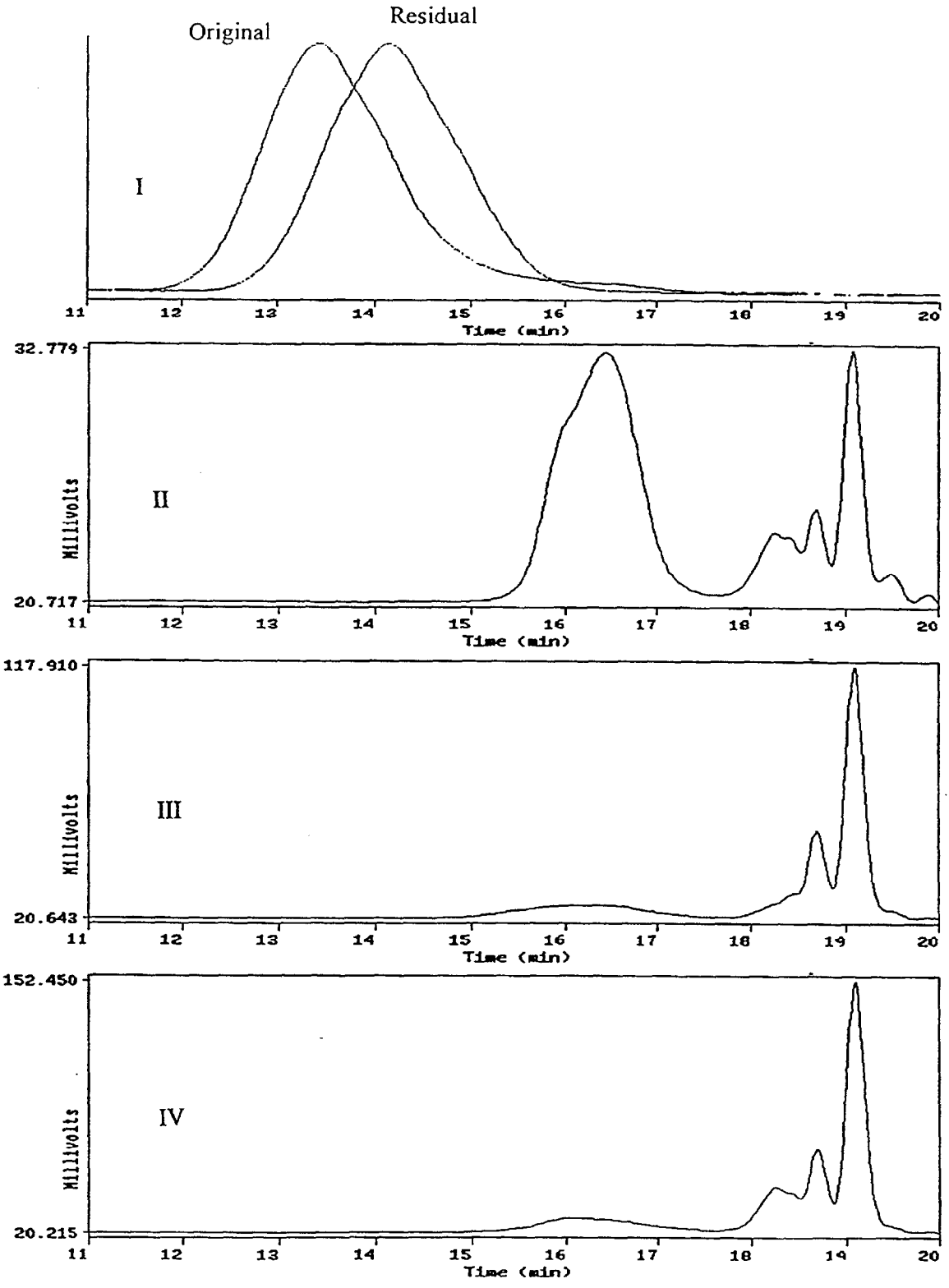

Figure 23. GPC chromatograms of 10^4 cs fluid: (I) - original and residual fluid (7 g), (II) - 100 to 99 g volatiles, (III) - 75 to 70 g volatiles, (IV) - 12 to 7 g volatiles.

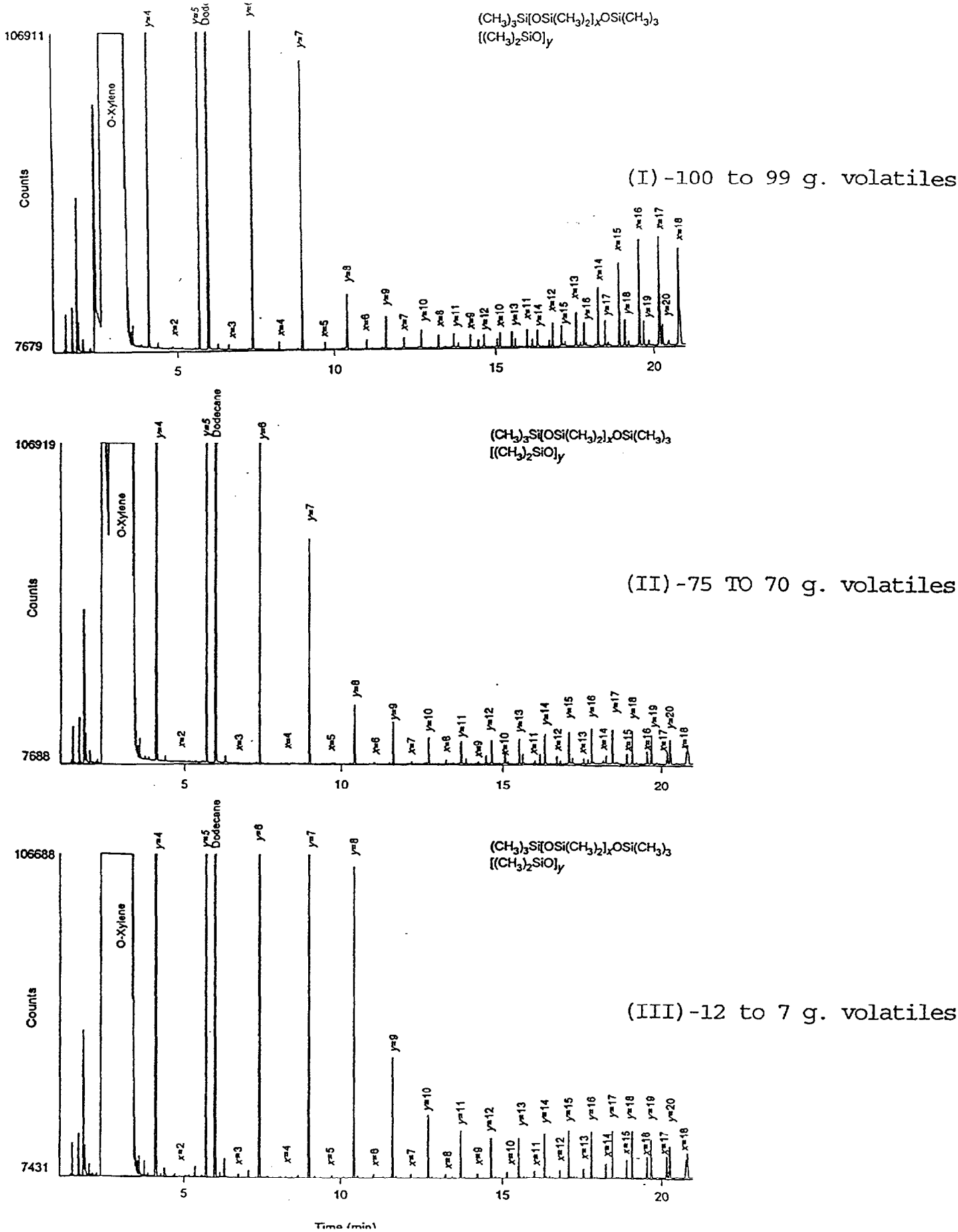

Figure 24. Gas chromatographic analysis of 10^4 cS Fluid volatiles samples: 100-99 g. (I), 75-70 g.(II), and 12-7 g.(III).

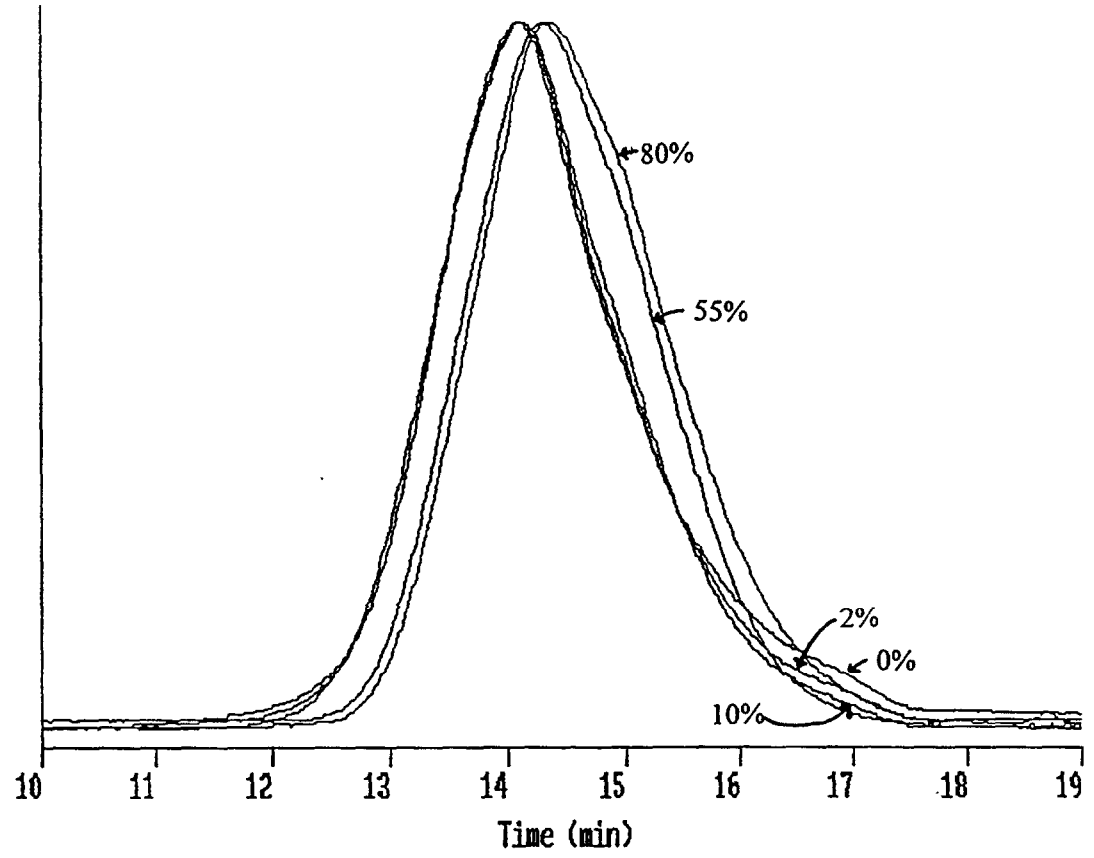

Figure 25. GPC chromatograms of the original and *residual* fluids from various stages of 1000 cs fluid gasification: 0, 2, 10, 55 and 80 % gasification.

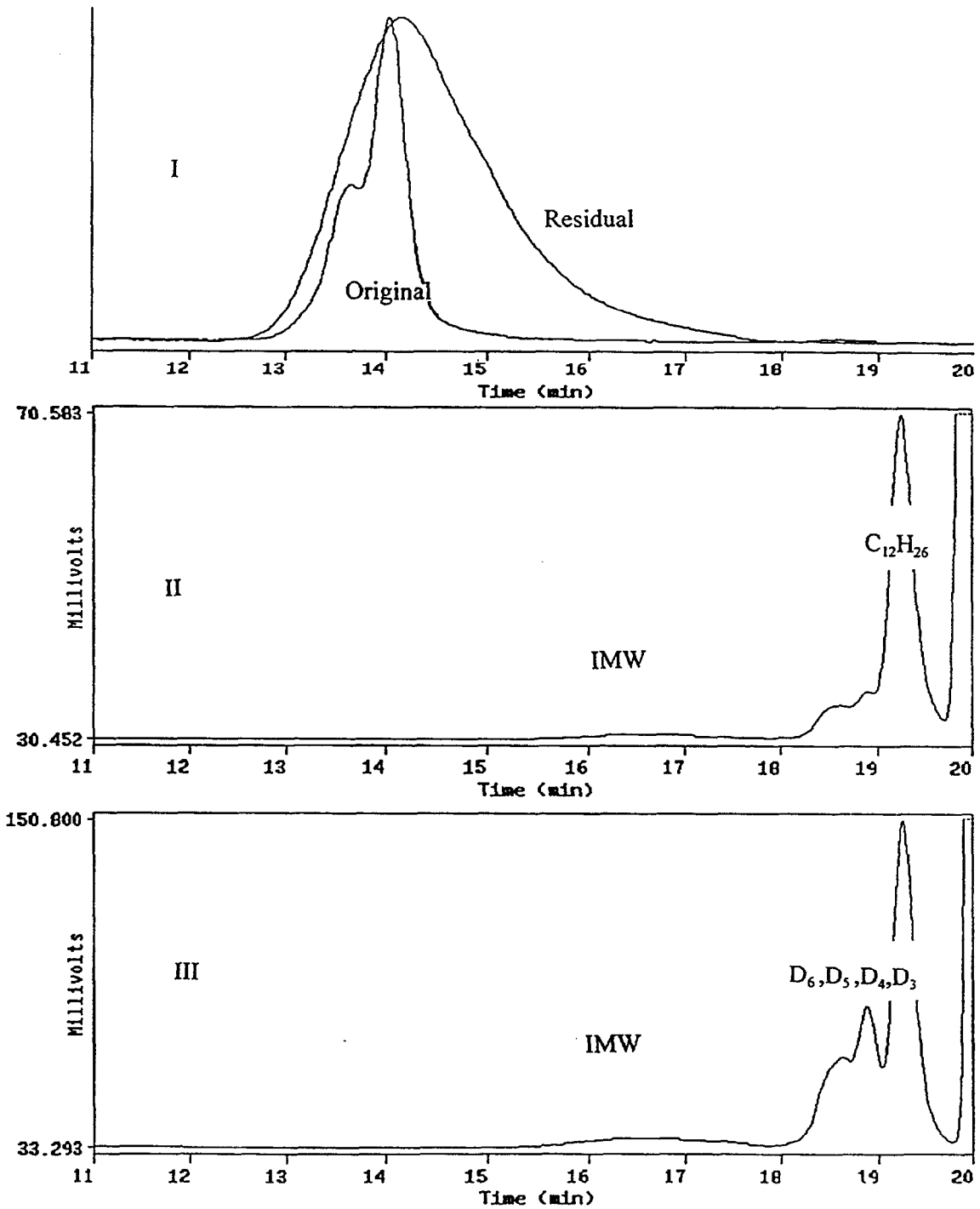

Figure 26. GPC chromatograms of "Model Fluid": (I) - original and residual fluid (15 g), (II) - 100 to 99 g volatiles, (III) - 20 to 15 g volatiles.

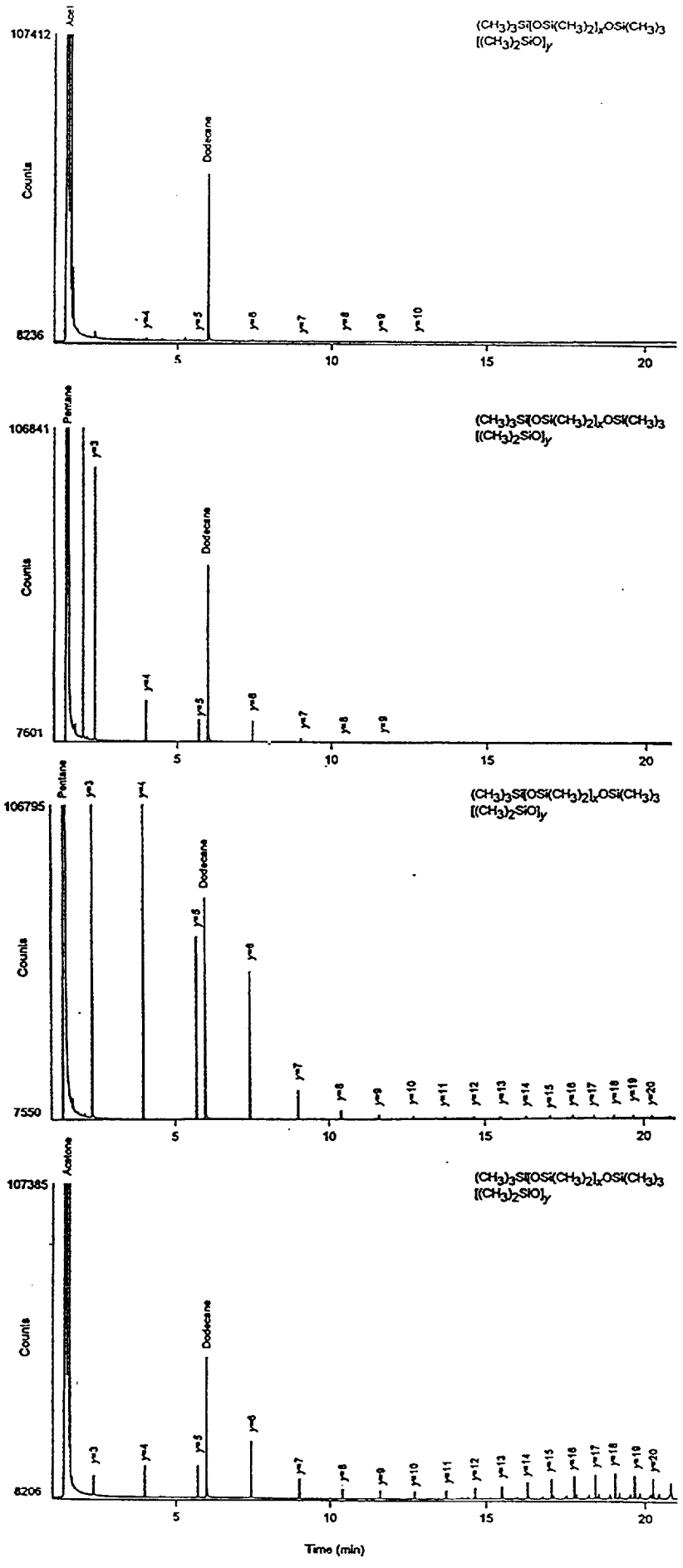

Figure 27. Gas chromatographic analysis of "Model Fluid": (I)-original and (IV)-residual fluid (15 g.), II-100 to 99 g. volatiles, III- 95 to 90 g. volatiles.

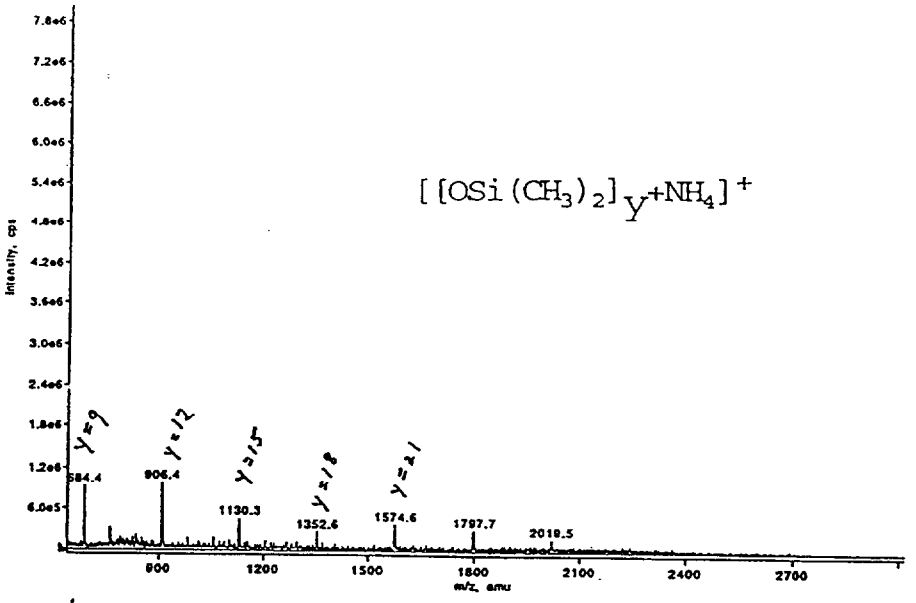

(I)-Model Fluid-Original

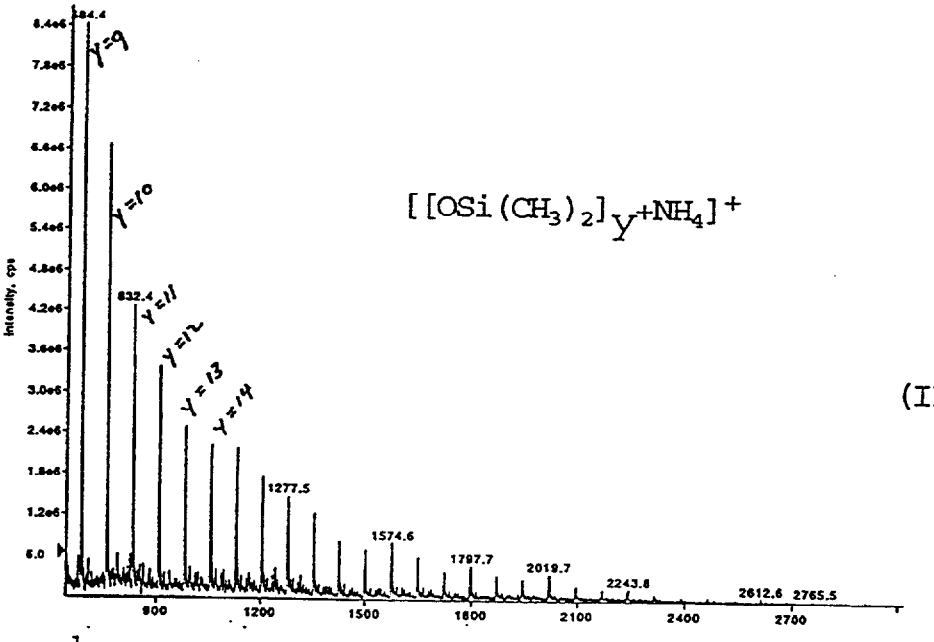

(II)-95 to 90 g. volatiles

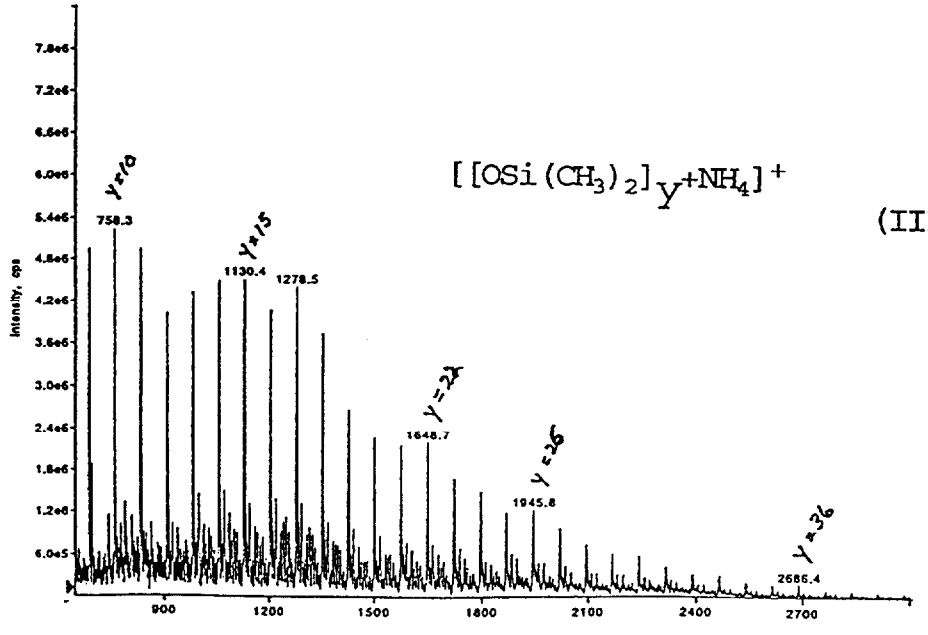

(III)-Residual Fluid (15g.)

Figure 28. Mass spectral analysis of "Model Fluid": (I)-original and (III)-residual fluid (15 g.), and II-95 to 90 g. volatiles.

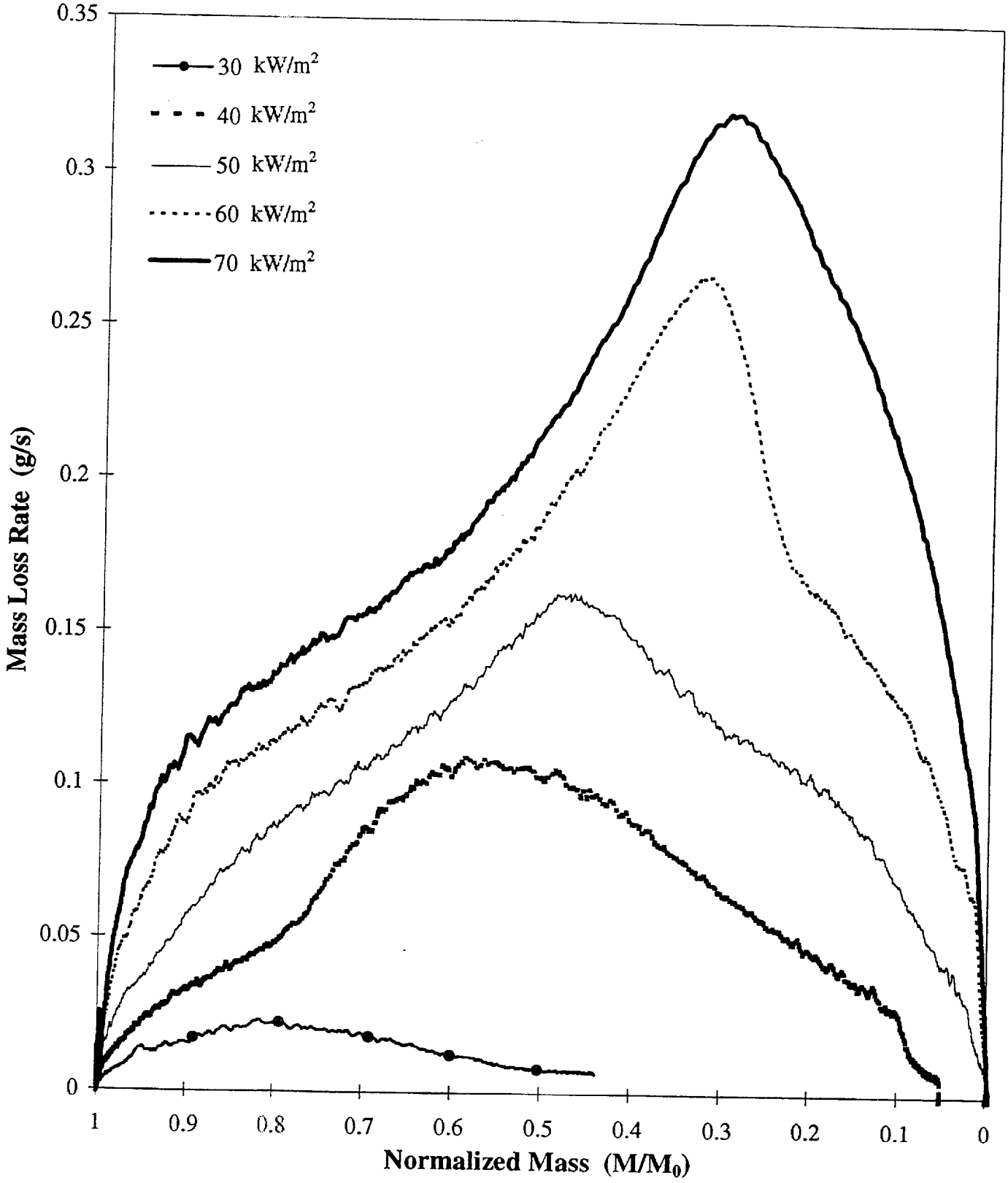

Fig. 29 Sample Mass Loss Rate as a Function of Normalized Mass and Heat Flux for 1,000cs. PDMS-200 Samples in Nitrogen

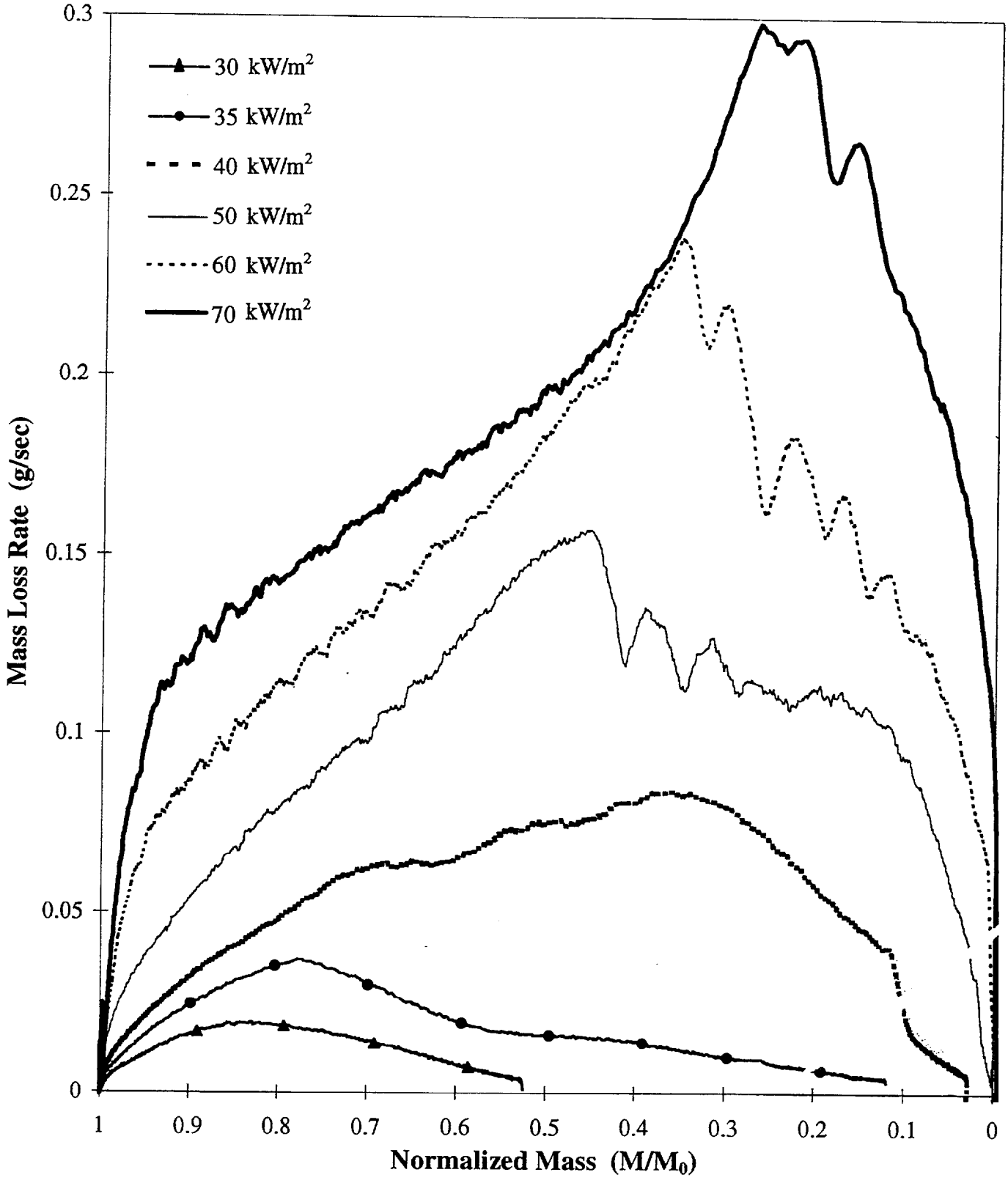

Fig. 30 Sample Mass Loss Rate as a Function of Normalized Mass and Heat Flux for 60,000cs. PDMS-200 Samples in Nitrogen

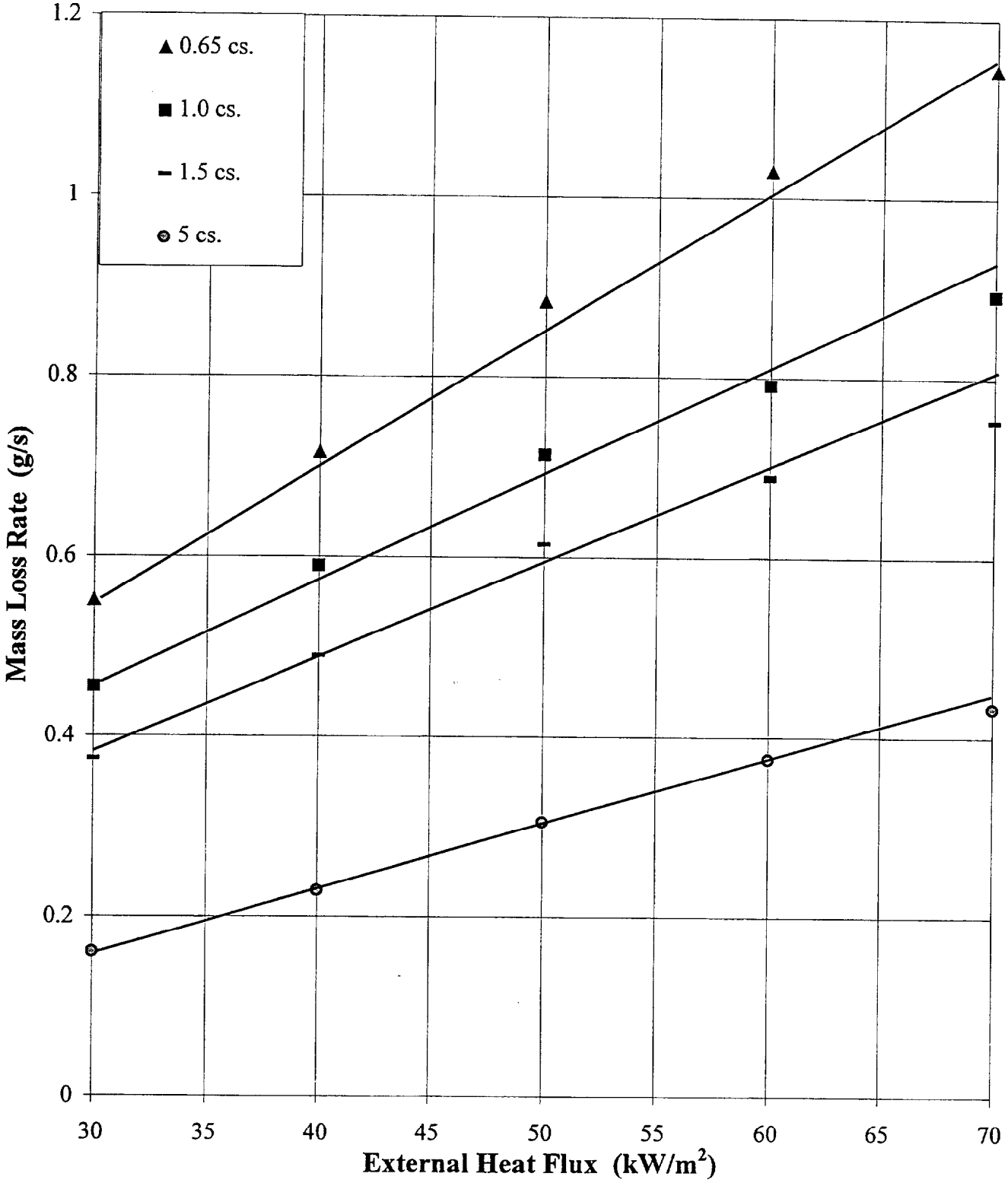

Fig. 31 Normalized Average Mass Loss Rate as a Function of Heat Flux for PDMS-200 Samples in Nitrogen

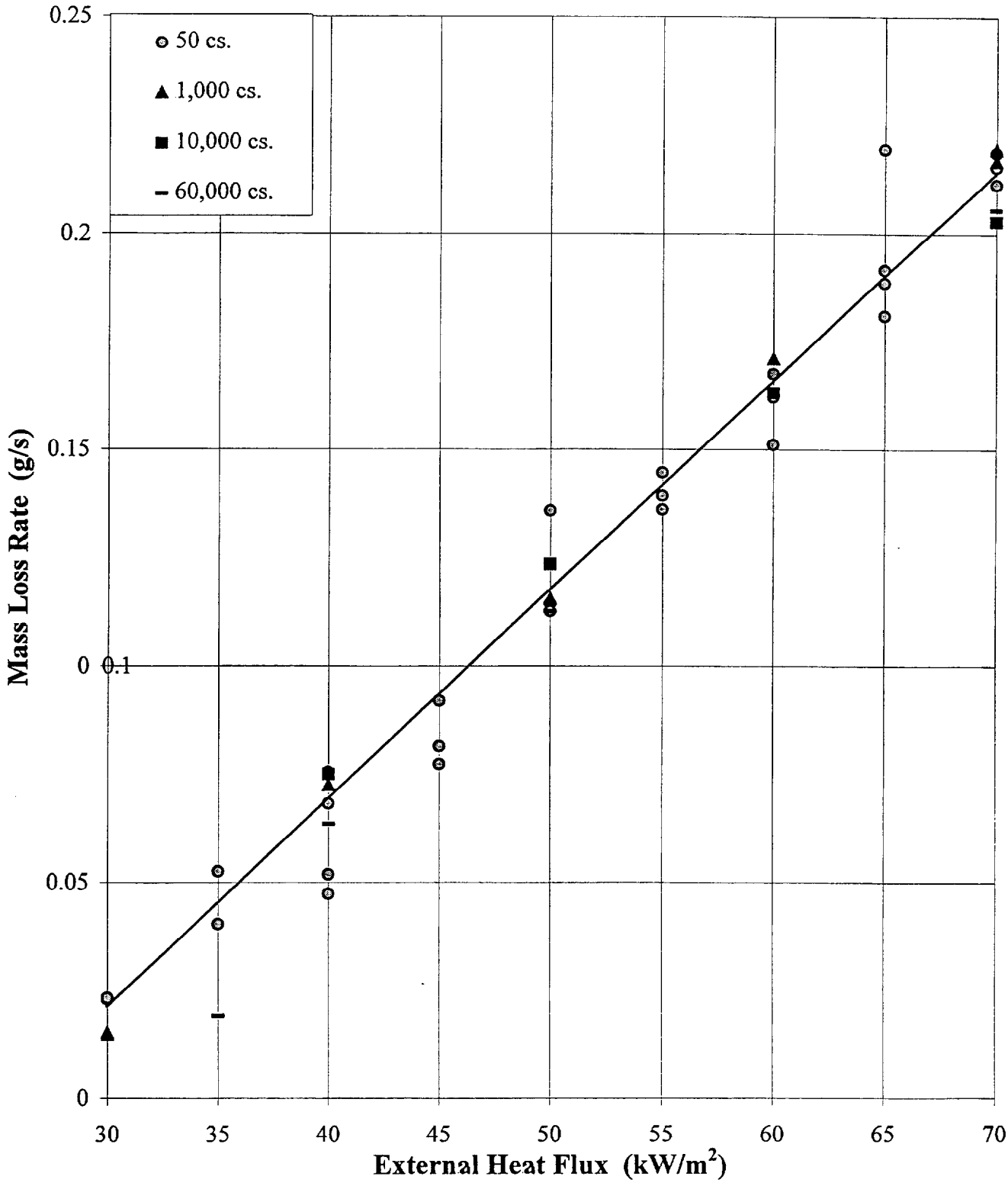

Fig. 32 Normalized Average Mass Loss Rate as a Function of Heat Flux for PDMS-200 Samples in Nitrogen

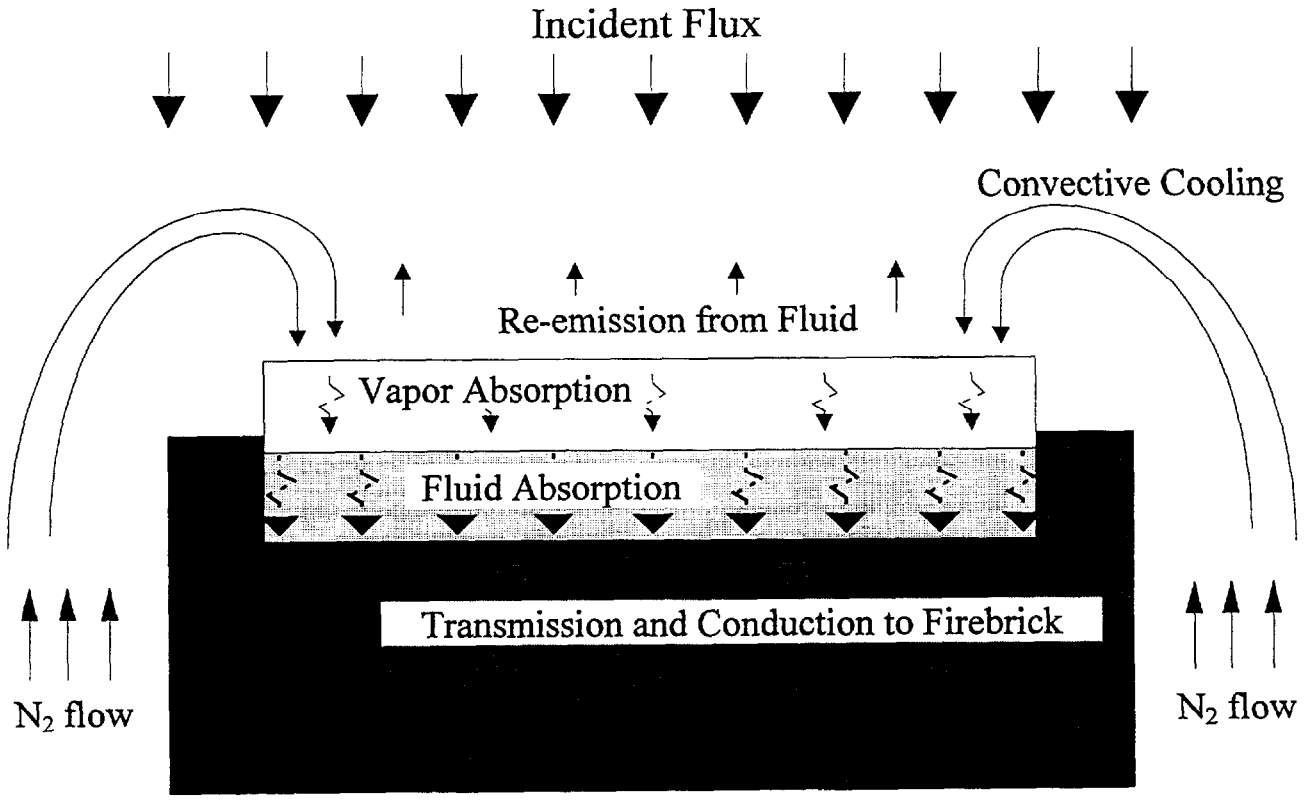

Fig. 33 Energy Balance Diagram

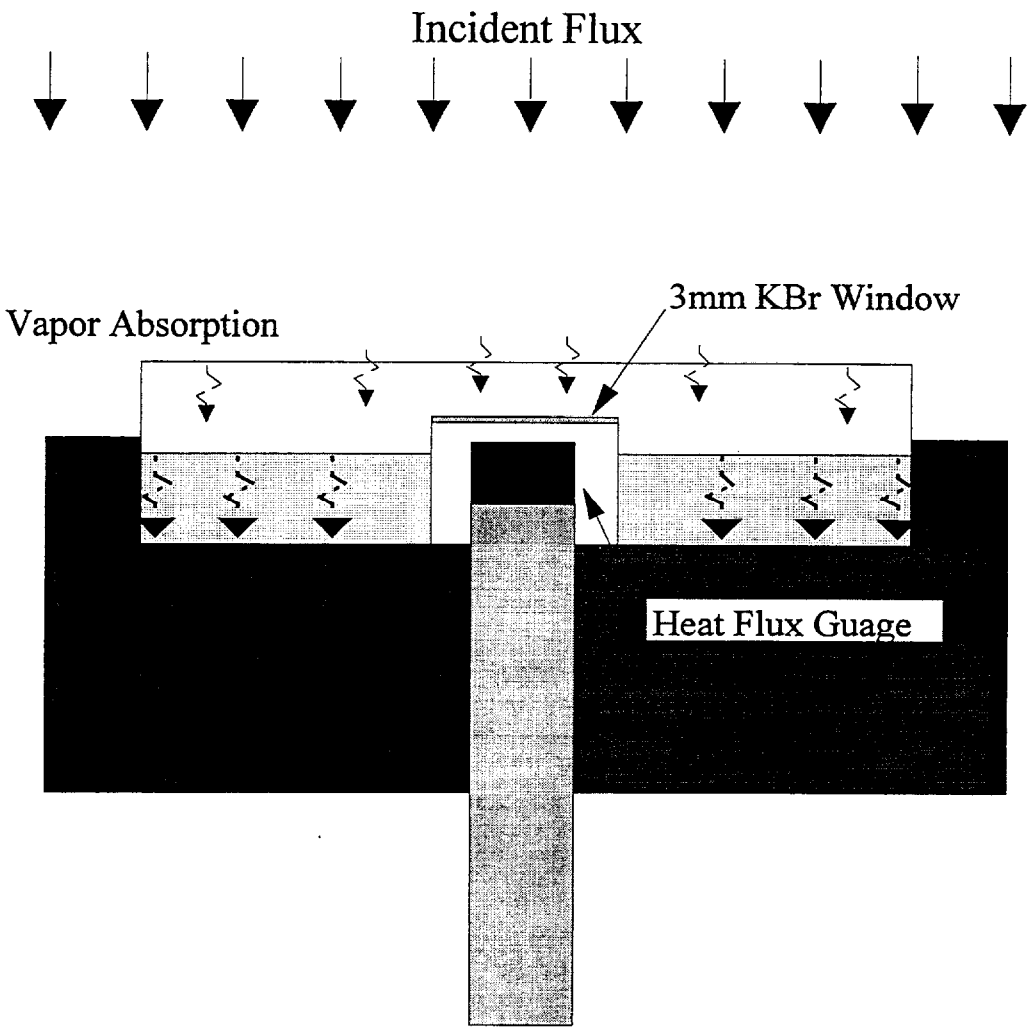

Fig. 34 Technique Used to Measure Absorption by Vapor Layer

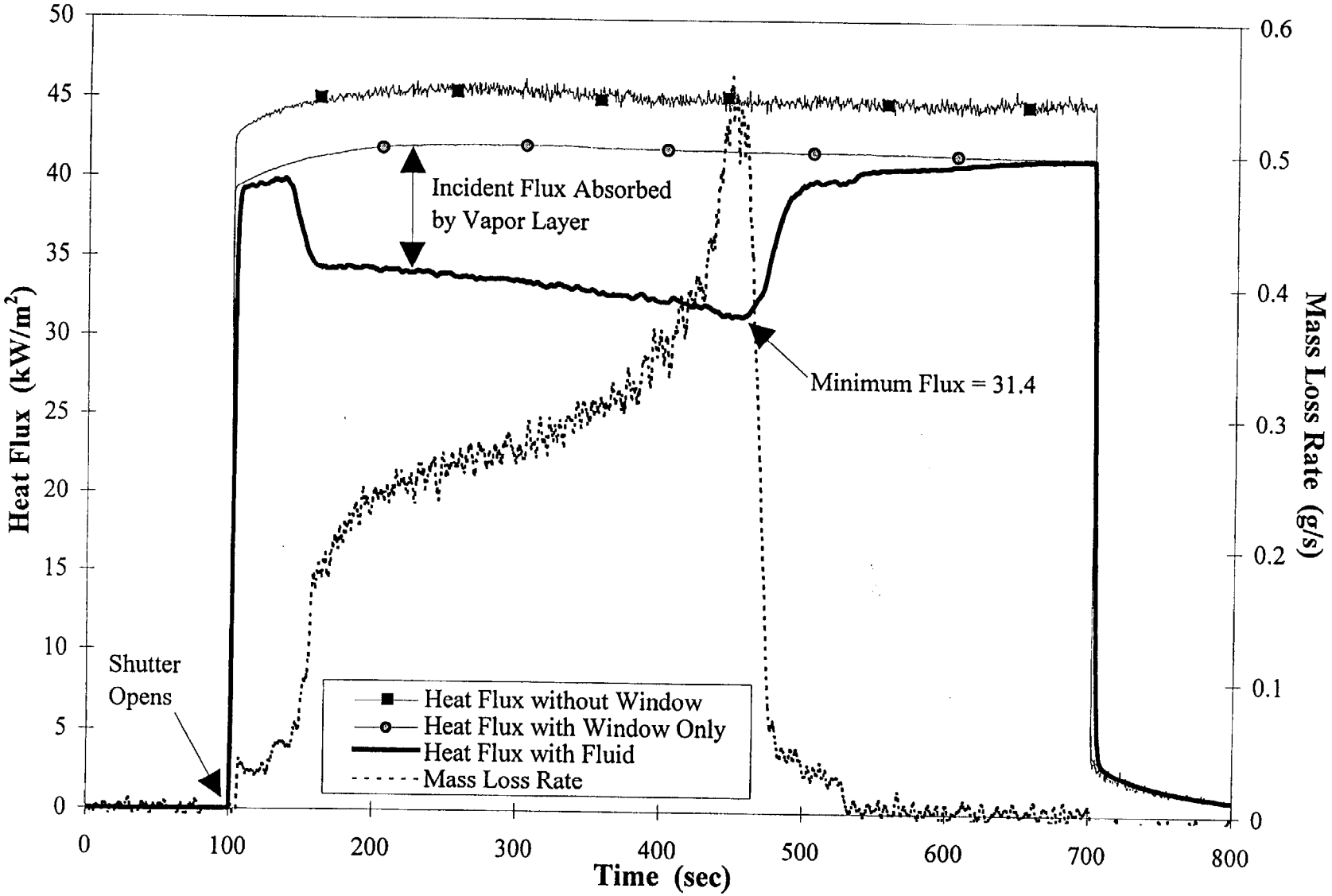

Fig. 35 Heat Flux and Mass Loss Rate as a Function of Elapsed Time for a 1.5cs. PDMS-200 Sample Exposed to a Radiant Heat Flux of 40 kW/m^2 in Nitrogen in Vapor Absorption Measurement Dish

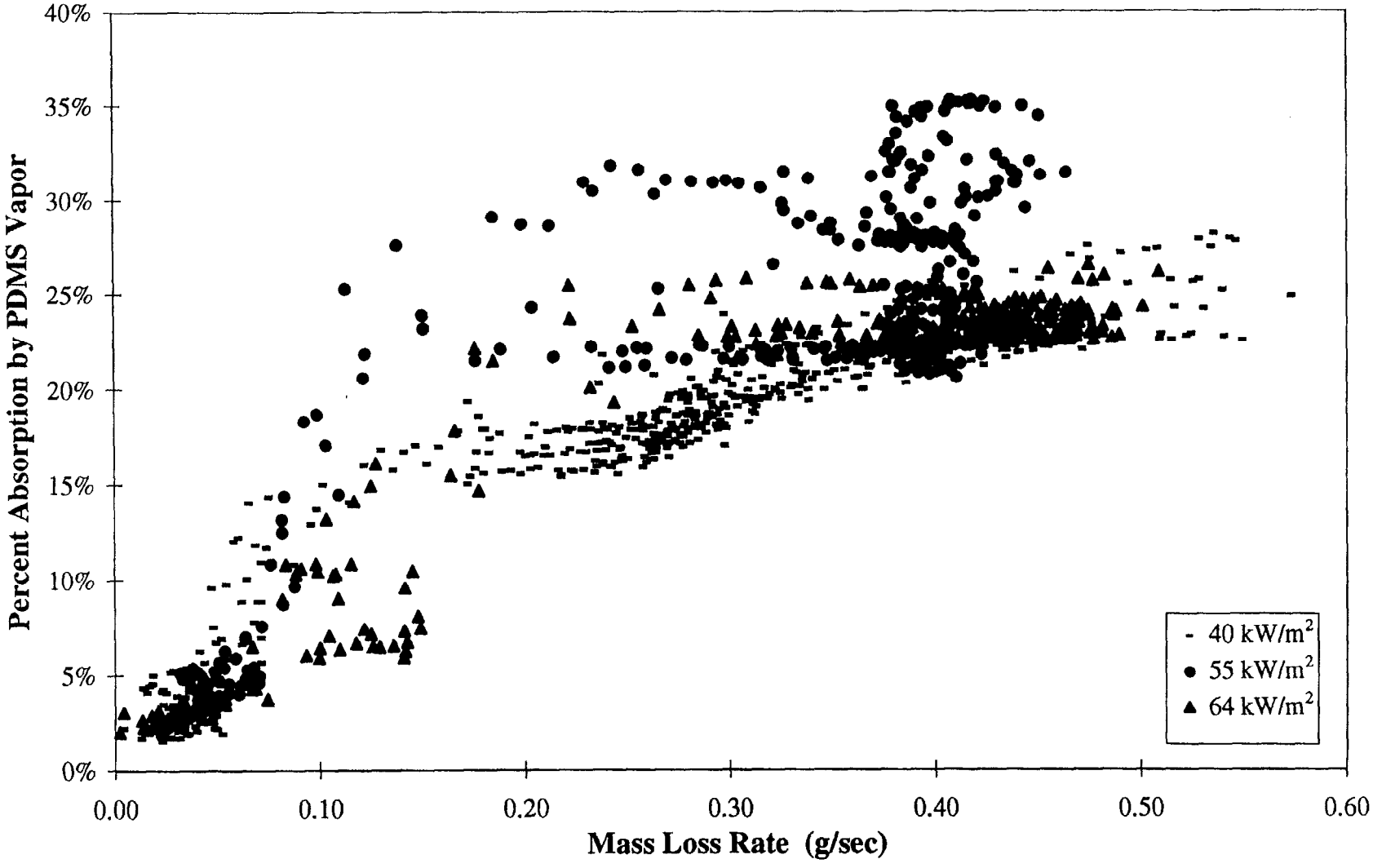

Fig. 36 Vapor Absorption as a Function of Mass Loss Rate and Heat Flux for 1.5cs. PDMS-200 Samples in Nitrogen in Vapor Absorption Measurement Dish

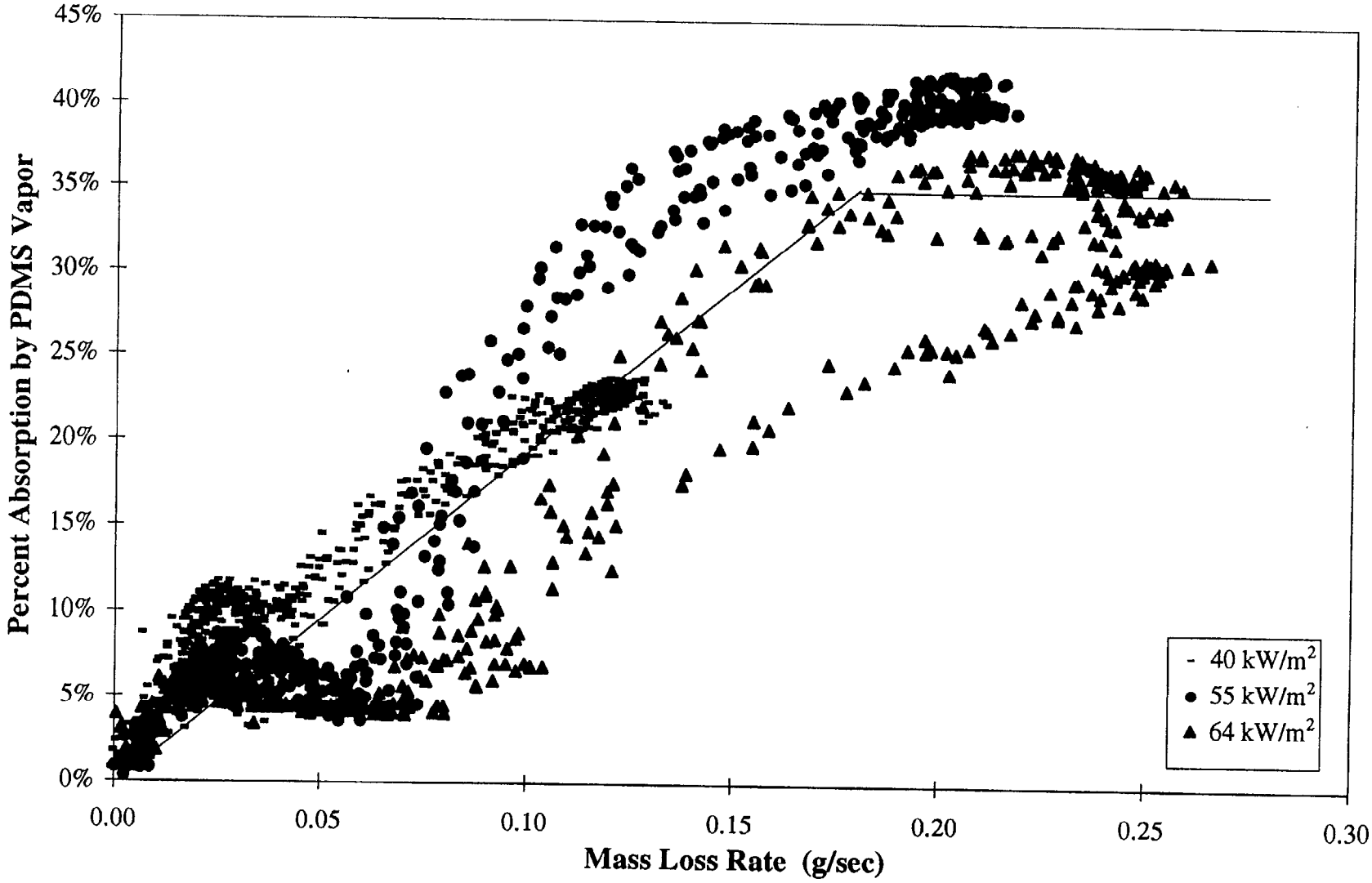

Fig. 37 Vapor Absorption as a Function of Mass Loss Rate and Heat Flux for 5cs. PDMS-200 Samples in Nitrogen in Vapor Absorption Measurement Dish

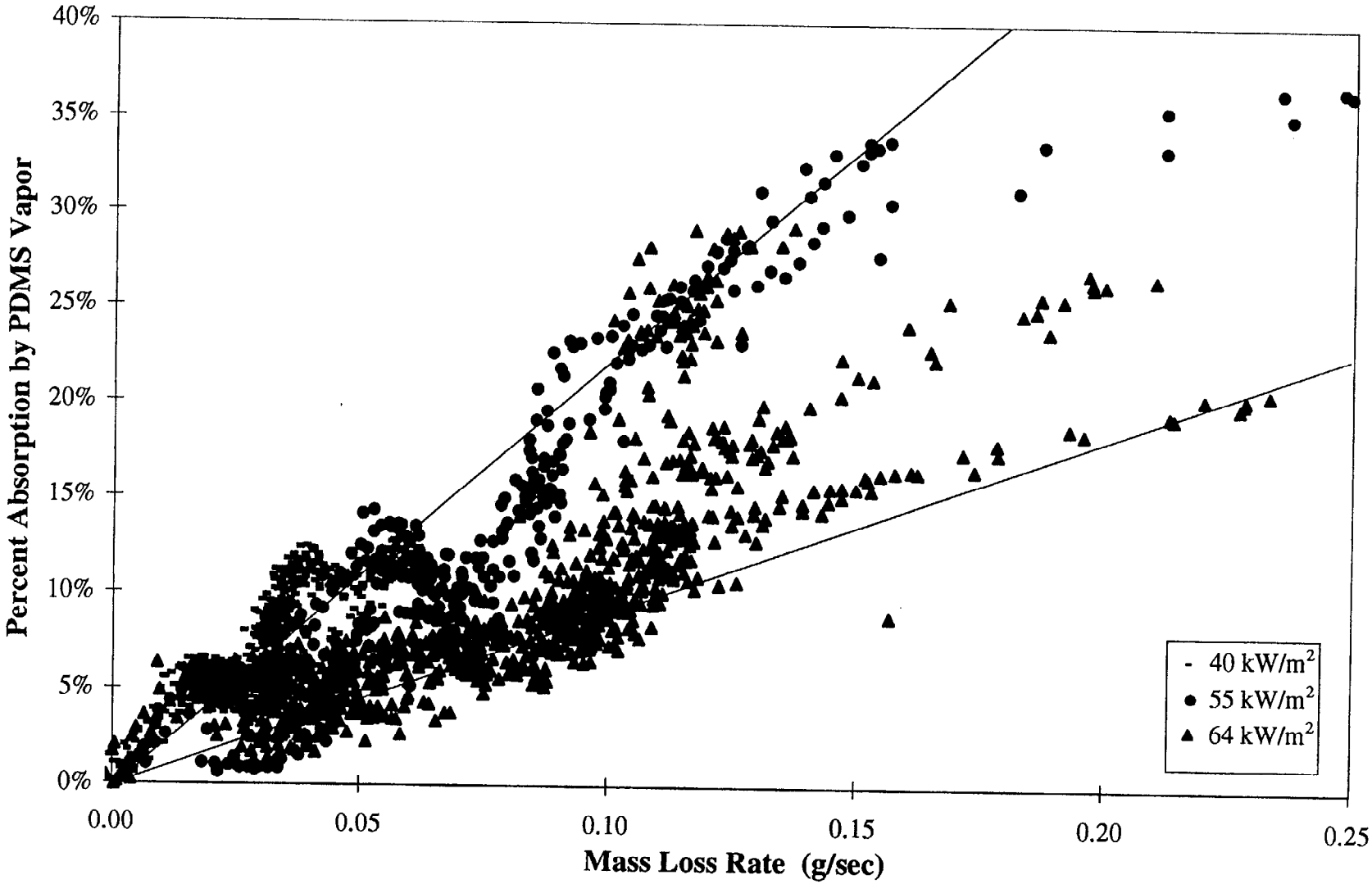

Fig. 38 Vapor Absorption as a Function of Mass Loss Rate and Heat Flux for 50cs. PDMS· 200 Samples in Nitrogen in Vapor Absorption Measurement Dish

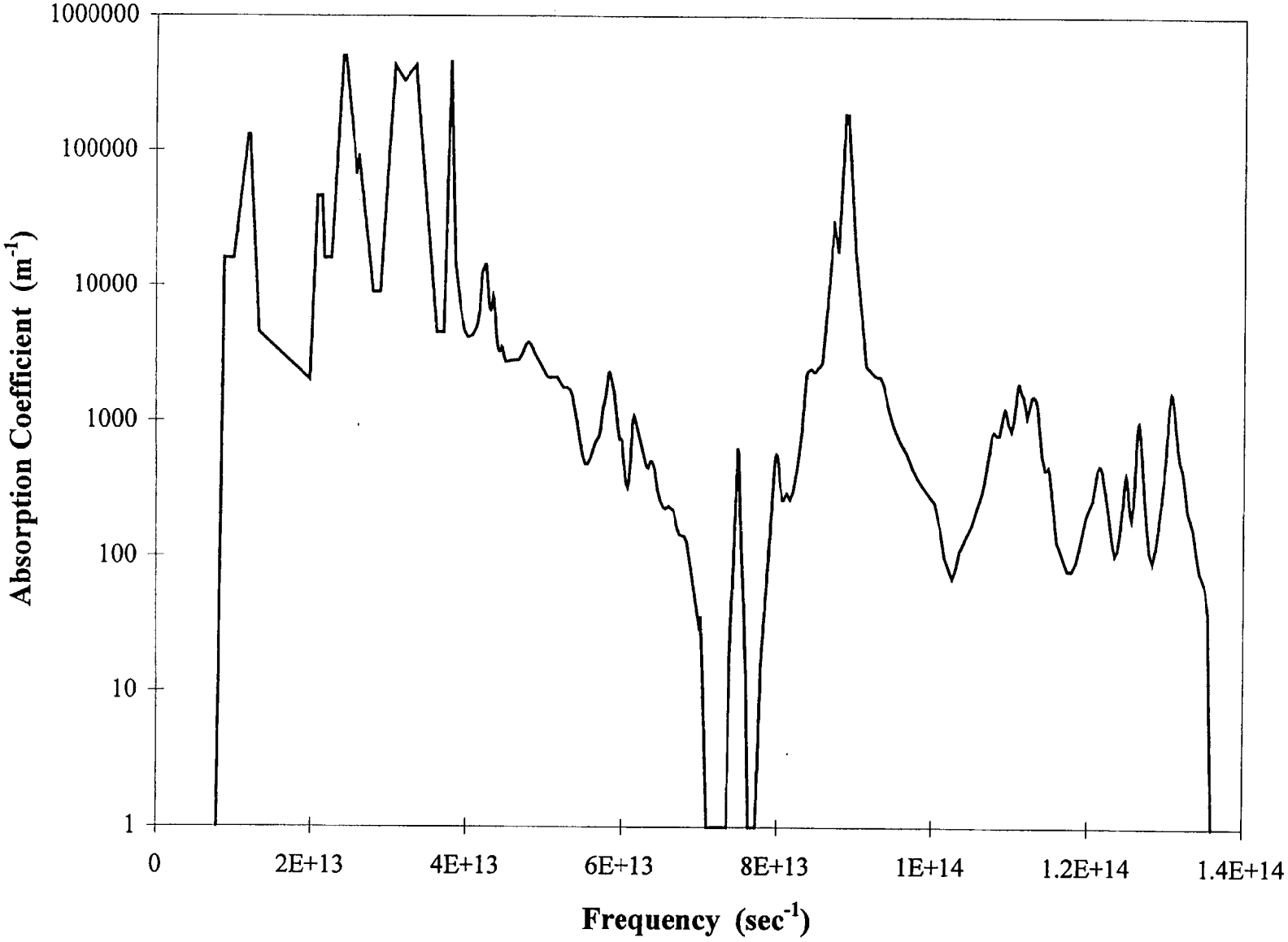

Fig. 39 Absorption Coefficient Plot for 100cs. PDMS-200

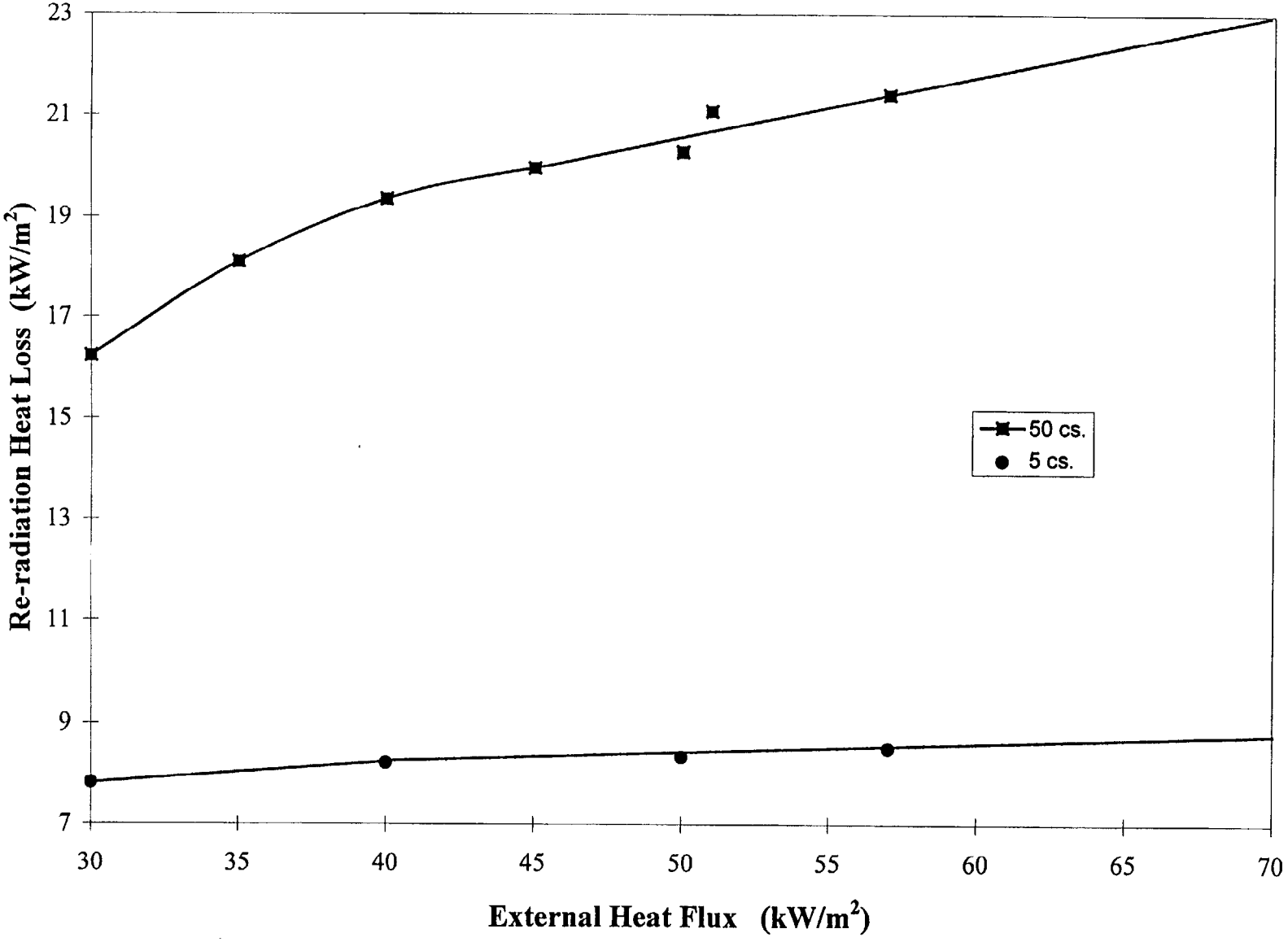

Fig. 40 Re-radiation Heat Loss from Fluid as a Function of External Heat Flux for 5cs. and 50cs. PDMS-200 Samples in Nitrogen

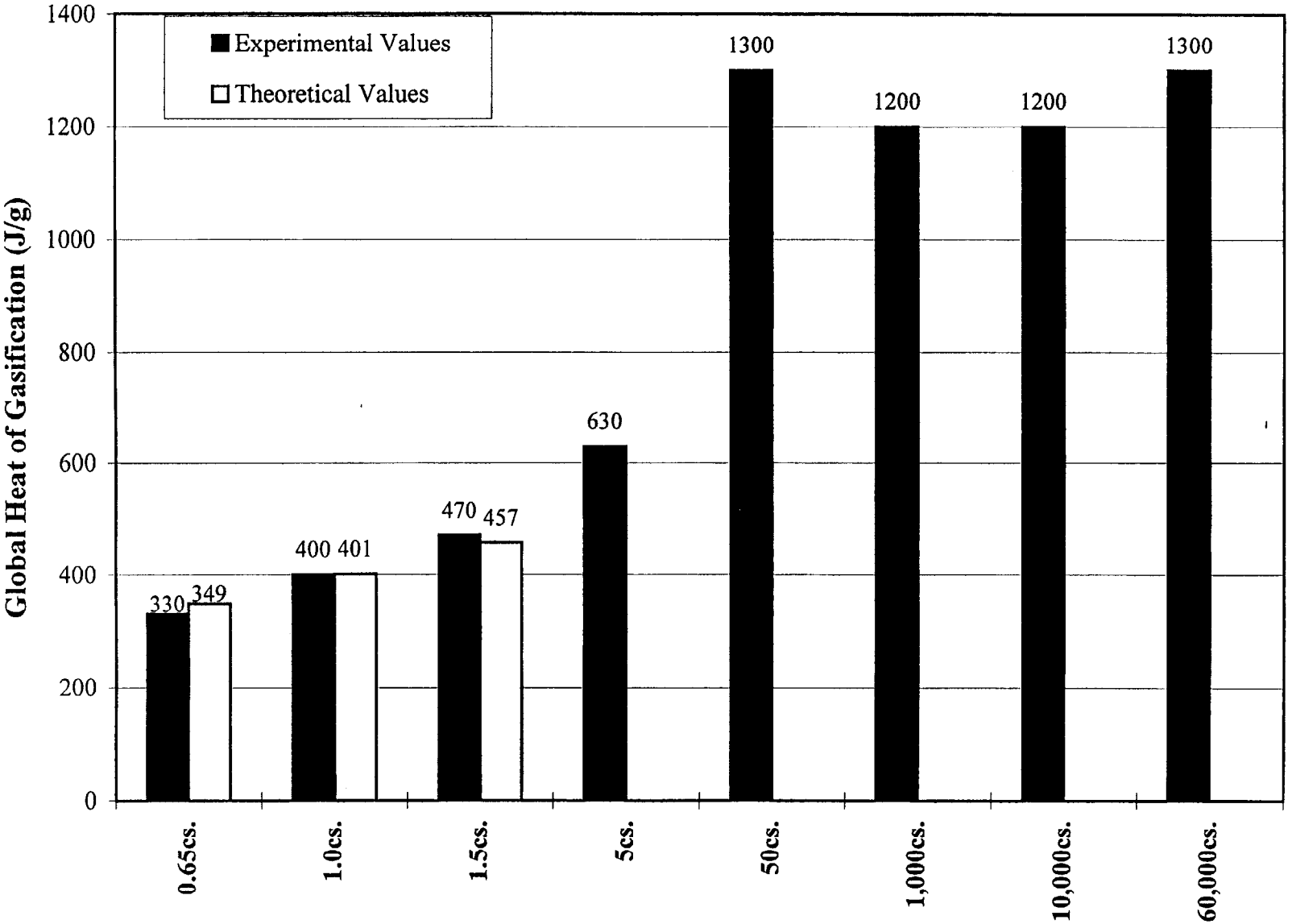

Fig. 41 Global Heat of Gasification for PDMS-200 Fluids

NIST-114
(REV. 11-94)
ADMAN 4.09

U.S. DEPARTMENT OF COMMERCE
NATIONAL INSTITUTE OF STANDARDS AND TECHNOLOGY

(ERB USE ONLY)
ERB CONTROL NUMBER | DIVISION
PUBLICATION REPORT NUMBER | CATEGORY CODE
NISTIR 6041
PUBLICATION DATE | NUMBER PRINTED PAGES
July 1997

MANUSCRIPT REVIEW AND APPROVAL

INSTRUCTIONS: ATTACH ORIGINAL OF THIS FORM TO ONE (1) COPY OF MANUSCRIPT AND SEND TO THE SECRETARY, APPROPRIATE EDITORIAL REVIEW BOARD.

TITLE AND SUBTITLE (CITE IN FULL)

Gasification of Silicone Fluids Under External Thermal Radiation

CONTRACT OR GRANT NUMBER

TYPE OF REPORT AND/OR PERIOD COVERED

AUTHOR(S) (LAST NAME, FIRST INITIAL, SECOND INITIAL)

Austin, P.J., Buch, R.B., and Kashiwagi, T.

PERFORMING ORGANIZATION (CHECK (X) ONE BLOCK)
☒ NIST/GAITHERSBURG
☐ NIST/BOULDER
☐ JILA/BOULDER

LABORATORY AND DIVISION NAMES (FIRST NIST AUTHOR ONLY)

Building and Fire Research Laboratory/Fire Science Division

SPONSORING ORGANIZATION NAME AND COMPLETE ADDRESS (STREET, CITY, STATE, ZIP)

PROPOSED FOR NIST PUBLICATION

☐ JOURNAL OF RESEARCH (NIST JRES)
☐ J. PHYS. & CHEM. REF. DATA (JPCRD)
☐ HANDBOOK (NIST HB)
☐ SPECIAL PUBLICATION (NIST SP)
☐ TECHNICAL NOTE (NIST TN)
☐ MONOGRAPH (NIST MN)
☐ NATL. STD. REF. DATA SERIES (NIST NSRDS)
☐ FEDERAL INF. PROCESS. STDS. (NIST FIPS)
☐ LIST OF PUBLICATIONS (NIST LP)
☒ NIST INTERAGENCY/INTERNAL REPORT (NISTIR)
☐ LETTER CIRCULAR
☐ BUILDING SCIENCE SERIES
☐ PRODUCT STANDARDS
☐ OTHER

PROPOSED FOR NON-NIST PUBLICATION (CITE FULLY) ☐ U.S. ☐ FOREIGN

PUBLISHING MEDIUM
☒ PAPER ☐ CD-ROM
☐ DISKETTE (SPECIFY)
☐ OTHER (SPECIFY)

SUPPLEMENTARY NOTES

ABSTRACT (A 2000-CHARACTER OR LESS FACTUAL SUMMARY OF MOST SIGNIFICANT INFORMATION. IF DOCUMENT INCLUDES A SIGNIFICANT BIBLIOGRAPHY OR LITERATURE SURVEY, CITE IT HERE. SPELL OUT ACRONYMS ON FIRST REFERENCE.) (CONTINUE ON SEPARATE PAGE, IF NECESSARY.)

Transient gasification rate and fluid temperatures were measured for polydimethylsiloxanes having fluid viscosity from 0.65 cS to 60,000 cS in a nitrogen atmosphere at external radiant fluxes from 20 kW/m^2 to 70 kW/m^2. Trapped volatile products and fluid residues collected at different gasification stages were analyzed to determine their chemical structure using various analytical methods. Detailed energy balance of fluid samples was conducted to determine global heat of vaporization including absorption of incident radiation by the volatile products, reradiation loss from heated fluids and heat loss to the substrate. The measured average gasification rate of all siloxanes studied in this work increases linearly with an increase in external radiant flux. The global heat of vaporation per unit mass of siloxanes increase with an increase in the molecular weight of the siloxanes up to a 50 cS fluid and its value remains constant at about 1,200 J/g for all higher molecular weight dimethylsiloxanes. The gasification of siloxanes occurs via two modes or regimens or combinations thereof: 1) volatilization of molecular species native to the polymer, and 2) volatilization of cyclic molecules which result from the thermally induced degradation of the polymer via siloxane bond rearrangement. The former process dominates for low molecular weight siloxanes (<10 cS) and the latter process dominates for high molecular weight siloxanes (>1,000 cS). For the intermediate molecular weight siloxanes, both volatilization and degradation processes occur.

KEY WORDS (MAXIMUM OF 9; 28 CHARACTERS AND SPACES EACH; SEPARATE WITH SEMICOLONS; ALPHABETIC ORDER; CAPITALIZE ONLY PROPER NAMES)

degradation products; gasification; heat of vaporization; silicone; thermal degradation

AVAILABILITY
☒ UNLIMITED ☐ FOR OFFICIAL DISTRIBUTION - DO NOT RELEASE TO NTIS
☐ ORDER FROM SUPERINTENDENT OF DOCUMENTS, U.S. GPO, WASHINGTON, DC 20402
☒ ORDER FROM NTIS, SPRINGFIELD, VA 22161

NOTE TO AUTHOR(S): IF YOU DO NOT WISH THIS MANUSCRIPT ANNOUNCED BEFORE PUBLICATION, PLEASE CHECK HERE. ☐

ELECTRONIC INFORMS